Development of carbon-based catalysts for small molecule activation

DOCTORAL THESIS

SINCHEM - Sustainable Industrial Chemistry
Erasmus Mundus - Joint Doctoral Research program

Dottorato di XXXI ciclo in

Ingegneria e Chimica dei Materiali e delle Costruzioni

Coordinator: Prof. Signorino Galvagno

SSD: Chim04

Supervisor (HOME): Prof.ssa Siglinda PERATHONER

Supervisor (HOST): Prof. Dr. Walter LEITNER

Shiming CHEN

September 2018

University of Messina

Departement of Engineering

RWTH Aachen University

ITMC

“Entwicklung von kohlenstoffbasierten Katalysatoren für die Aktivierung kleiner Moleküle”

Der Fakultät für Mathematik, Informatik und Naturwissenschaften der RWTH Aachen University vorgelegte Dissertation zur Erlangung des akademischen Grades eines Doktors der Naturwissenschaften

von

M.Sc. Shiming Chen

aus. ***China***

The research presented in this Ph.D. thesis was carried out at the University of Messina, Department of Engineering, Laboratory of Catalysis for Sustainable Productions and Energy (CASPE/INSTM) and RWTH Aachen, ITMC.

This work was co-funded through a SINCHEM Grant. SINCHEM is a Joint Doctorate programme selected under the Erasmus Mundus Action 1 Programme (FPA 2013-0037),

ACKNOWLEDGEMENT

Firstly, I would like to express my sincere gratitude to my Ph.D. supervisors Prof. Siglinda Perathoner for the continuous support of my Ph.D. study and related research, for her patience, motivation, and immense knowledge. Her advice on both the research as well as my career has been priceless. I have been very lucky to have her constant support during my Ph.D. and to share her passion for the research we have done.

I would like to thank Prof. Gabriele Centi for showing interest in my work from the beginning. Prof. Centi's wise insight has leading me to the right direction on the research. And also his continually passion on scientific research after he achieved the worldwide reputation let me know what is a real scientist should be. All of these will be a source of motivation as I continue academic research.

I am thankful to Prof. Dr. Walter Leitner, Markus Hölscher and his research group at the ITMC, RWTH Aachen University. They taught me from the beginning on homogenous catalysis, such as how to prepare, characterize and test in a reaction. They given me countless opportunities to practice and pursue my ideas as well as their enthusiasm for teaching new ideas and immediate problem-solving abilities has always inspired me. In addition to all the members of the Prof. Leitner group, I would especially like to thank members of Lu Lu, Jens Kothe, Dr. Suman Sen, Akash Kaithal, Meria Ronge, Matilde Solmi and Dr. Giancarlo Franciò for the kind help, sharing ideas and guidance during my stay in the ITMC, RWTH Aachen.

I would like to thank all the past and present members of the Prof. Gabriele Centi and Prof. Siglinda Perathoner research group for making the Ph.D. a very enjoyable experience. I would especially like to thank Dr. Claudio Ampelli for not only always sharing his experience on electrochemisty, but also for being a great friend. I have really enjoyed both working and hanging out with everyone in the laboratory of Catalysis for Sustainable Productions and Energy (University of Messina) and would like to thank

Chalachew, Wei, Chiara, Francesco, Paola, Giorgia, Gianfranco, Salvatore, Rosalba, Katia, Leo, Bhanu, and Atif.

In addition to all the wonderful people with whom I was lucky enough to work, I would also like to thank all my friends, specifically those around Messina and Aachen: Chalachew, Roberto Di Chio, Francesco Tavella, Feng Zeng, Xinde Wang, Ruiyan Sun, Lu Lu, Christian Landini, Matilde Solmi, and Dunyong Deng.

I thank the SINCHEM program, the committee, all the Professors and Ph.D. students for their constant support and encouragement. A special thanks go to Prof. Stefania Albonetti (SINCHEM coordinator) for her help and guidance on all the academic and administrative matters. I would also thank to the SINCHEM local coordinators Dr. Francesca Pollicino and Anna Maria Casella (University of Messina) and Dr. Stefanie Mersmann (ITMC, RWTH Aachen University) for their help provided to carry out my Ph.D. thesis based on the cotutelle between University of Messina (Italy) and RWTH Aachen University (Germany).

And special thanks for Prof. Dr. Dangsheng Su, who is my master supervisor. It is he that introduces me to the wonderful “carbon world”, help me install the sense of research, inspired me to study aboard.

Last but not the least, I would like to thank my family: my parents and wife. Their constant love, encouragement, and support have made me believe in myself and there are no words to describe the love and appreciation I feel for them. I thank you very much from the bottom of my heart.

Shiming Chen

2018, Messina, Italy

LIST OF ABBREVIATIONS

AAS - Atomic Absorption Spectroscopy

CNTs - Carbon Nano Tubes

DFT - Density Functional Theory

DI- Deionized

EDX - Energy Dispersive X-ray

EU - European Union

FC - Fuel Cell

FE – Faraday Efficiency

FID - Flame Ionization Detector

GC - Gas Chromatography

GDL- Gas Diffusion Layer

HT - High Temperature

ICP - OES - Inductively Coupled Plasma-Optical Emission Spectroscopy

ISA - Ionic Strength Adjuster

LT- Low Temperature

NMR - Nuclear Magnetic Resonance spectroscopy

PEM - Proton Exchange Membrane

PNPtBu - 2,6-Bis[[bis(1,1 dimethylethyl)phosphino]methyl]pyridine

SEM - Scanning Electron Microscopy

SOEC - Solid oxide electrolysis cell

STEM - Scanning Transmission Electron Microscopy

TCD - Thermal Conductivity Detector x

TEM - Transmission Electron Microscopy

TGA - Thermo gravimetric Analysis

TPD - Temperature Programmed Desorption

TPR - Temperature Programmed Reduction

XPS - X-ray Photoelectron Spectroscopy

XRD - X-ray Diffraction

ABSTRACT (English)

The present Ph.D. thesis was focused on the development of advanced technics for ammonia synthesis with sustainable methods, i.e. electrocatalytic processes using N_2, H_2O and renewable energy as input sources. Implementing this technology will thus result in a breakthrough change towards a sustainable, low-carbon chemical production based on the use of renewable energy sources. There is thus a rising interest in fossil-fuel-free direct ammonia synthesis.

A flow electrochemical cell was developed for ammonia synthesis directly from water and N_2 at room temperature and atmospheric pressure. Iron supported on carbon nanotubes (CNTs) was used as the electrocatalyst in this hemi-cell. An ammonia formation rate of 2.2×10^{-3} $g_{NH3}\cdot m^{-2}\cdot h^{-1}$ was obtained at room temperature and atmospheric pressure in a flow of N_2, under an applied potential of -2.0 V vs. Ag/AgCl. This value is higher than the ammonia formation rate obtained using noble metals (Ru/C) under comparable reaction conditions. Furthermore, hydrogen gas with total Faraday efficiency as high as 95.1% was obtained.

Reaction condition was optimised with Fe_2O_3-CNT used as electrocatalyst. A 30% wt iron-oxide loading was found to be optimal. The performances greatly depend on the cell design, where the possibility of ammonia crossover through the membrane has to be inhibited. The reaction conditions also play a significant role. The effect of electrolyte (type, pH, concentration) was investigated in terms of current density, rate of ammonia formation and Faradaic efficiency in continuous tests up to 24h of time on stream. A complex effect of the applied voltage was observed. An excellent stability was found for an applied voltage of -1.0 V vs. Ag/AgCl. At higher negative applied voltages, the ammonia formation rate and Faradaic selectivity are higher, but with a change of the catalytic performances, although the current densities remain constant for at least 24h. This effect is interpreted in terms of reduction of the iron-oxide species

above a negative voltage threshold, which enhances the side reaction of H^+/e^- recombination to generate H_2 rather than their use to reduce activated N_2 species, possibly located at the interface between iron-oxide and functionalized CNTs.

Active sites for ammonia synthesis was also explored. We show here that, contrary to expectations, iron-oxide (Fe_2O_3) nanoparticles (supported over carbon nanotubes - CNTs) result more active in the direct electrocatalytic synthesis of ammonia from N_2 and H_2O than the corresponding samples after reduction to form Fe or Fe_2N supported nanoparticles. A linear relationship is observed between the ammonia formation rate and the specific XPS (X-ray- photoelectron spectroscopy) oxygen signal related to O^{2-} in Fe_2O_3 species, which is proofed by both chemically and electrochemically reduced samples. HRTEM (high-resolution transmission electron microscopy) data on the changes during the electrocatalytic tests confirmed that in-situ activated sites for ammonia synthesis were formed, due to the reconstruction of iron oxide particles. This opens new possibilities to understand the reaction mechanism under working conditions and design more efficient electrocatalyst for ammonia synthesis.

Homogenous catalysts for ammonia synthesis was also explored. A series of ruthenium complexes were tested using the same conditions. $Ru(PNP)Cl_2$ (PNP: 2,6-Bis[(di-tert-butylphosphanyl)methyl]pyridine) was found to be the best catalyst for ammonia synthesis among the series of analyzed complexes. This complex was also tested using different conditions, and it was found that suitable amounts of acetic acid can increase its catalytic performance. Comparing different compositions of nitrogen and hydrogen loadings, it was found that the ammonia formation rate increases with increasing nitrogen loading, from which we can deduce that activation of hydrogen was not the rate limitation step in these conditions.

Keywords: ammonia · atmospheric pressure · electrochemistry · heterogeneous catalysis · active sites · homogenous catalysis · sustainable

ABSTRACT (Italian)

Il presente lavoro di tesi è stato incentrato sullo sviluppo di tecniche avanzate per la sintesi dell'ammoniaca attraverso processi sostenibili. Per fare ciò è stato realizzato un processo elettrocatalitico che utilizza N_2, H_2O ed energia da fonti rinnovabili. Esiste un crescente interesse per la sintesi dell'ammoniaca diretta senza l'utilizzo di combustibili fossili. L'implementazione di questa tecnologia determinerà un cambiamento radicale verso una produzione chimica sostenibile e a basse emissioni di CO_2, basata sull'utilizzo di fonti energetiche rinnovabili.

Una cella elettrochimica che opera in flusso è stata sviluppata per effettuare la sintesi dell'ammoniaca direttamente dall'acqua e dall' azoto, operante a temperatura ambiente e pressione atmosferica. Il catalizzatore utilizzato è basato su nanoparticelle di Fe supportate su nanotubi di carbonio (CNT). È stata ottenuta una velocità di formazione di ammoniaca di 2,2 × 10-3 $g_{NH3} \cdot m^2 \cdot h^{-1}$ a temperatura ambiente e pressione atmosferica in un flusso di N_2, sotto l'applicazione di un voltaggio costante di -2,0 V vs Ag/AgCl. Questo valore è risultato superiore al tasso di formazione di ammoniaca ottenuto utilizzando metalli nobili (Ru / C) in condizioni di reazione comparabili. Inoltre, è stato ottenuto idrogeno con un'efficienza faraidica del 95,1%.

La condizioni di reazione sono state ottimizzate per il catalizzatore a base di Fe_2O_3-CNT, con un carico di ossido di ferro del 30% in peso. Le prestazioni dipendono fortemente dal design della cella, in cui è necessario limitare al massimo il crossover dell'ammoniaca attraverso la membrana. Anche le condizioni di reazione hanno un ruolo significativo, l'effetto dell'elettrolita (tipo, pH, concentrazione) è stato studiato in termini di densità di corrente, velocità di formazione dell'ammoniaca ed efficienza Faradaica nei test condotti fino a 24 ore. Lo studio sulla tensione applicata è risultato complesso: è stata trovata un'eccellente stabilità per una tensione applicata di -1,0 V vs. Ag / AgCl, a tensioni più negative, la velocità di formazione dell'ammoniaca e

l'efficienza faraidica sono più elevate, ma con un cambiamento delle prestazioni catalitiche, sebbene la densità di corrente rimanga costante per almeno 24 ore. Questo effetto è da attribuire alla riduzione delle specie di ossido di ferro al di sopra di una soglia di tensione negativa, che migliora la reazione collaterale di ricombinazione H^+ / e^- per generare H_2 piuttosto che reagire con le specie N_2 attivate, possibilmente situate all'interfaccia tra ossido di ferro e CNT funzionalizzati.

Lo studio effettuato sui siti attivi mostra che, contrariamente alle aspettative, le nanoparticelle di ossido di ferro (Fe_2O_3) (supportate su nanotubi di carbonio - CNT) risultano più attive nella sintesi elettrocatalitica diretta di ammoniaca da N_2 e H_2O rispetto ai corrispondenti campioni Fe o Fe_2N realizzati attraverso riduzione. Si osserva una relazione lineare tra la velocità di formazione dell'ammoniaca, e il segnale specifico dell'ossigeno all' XPS (spettroscopia a raggi X-fotoelettronica) relativo a O^{2-} nelle specie Fe_2O_3, che è comprovato da campioni sia chimicamente che elettrochimicamente ridotti. I dati HRTEM (microscopia elettronica a trasmissione ad alta risoluzione) sui cambiamenti durante i test elettrocatalitici hanno confermato che i siti attivati per la sintesi dell'ammoniaca vengono formati in situ a causa della ricostruzione di particelle di ossido di ferro. Questo apre nuove possibilità per comprendere il meccanismo di reazione in condizioni di lavoro e progettare elettrocatalizzatori più efficienti per la sintesi dell'ammoniaca.

Utilizzando le stesse condizioni di reazione, sono stati anche esplorati catalizzatori omogenei per la sintesi dell'ammoniaca utilizzando una serie di complessi di Rutenio. Il catalizzatore $Ru(PNT)Cl_2$ (PNP: 2,6-Bis[(di-tert-butylphosphanyl)methyl]pyridine) è risultato essere il miglior catalizzatore per la sintesi dell'ammoniaca in questo screening. Il catalizzatore è stato testato anche in condizioni diverse, è stato osservato che una quantità adeguata di acido acetico aumenta le sue performance catalitiche. Confrontando la diversa composizione di azoto e idrogeno, è stato riscontrato che la

formazione di ammoniaca aumenta con l'aumentare del carico di azoto, dal quale si può dedurre che l'attivazione dell'idrogeno non è il fattore limitante in queste condizioni di reazione.

Parole chiave: ammoniaca · pressione atmosferica · elettrochimica · catalisi eterogenea · siti attivi · catalisi omogenea · sostenibile

ABSTRACT (German)

Die vorliegende Arbeit behandelt die Entwicklung einer fortgeschrittenen Technologie für die Ammoniaksynthese mit nachhaltigen Methoden, z.B. ein elektrokatalytischer Prozess mit N_2, H_2O und erneuerbaren Energiequellen. Die Implementierung dieser Technologie wird somit zu einem Durchbruch in Richtung einer nachhaltigen, kohlenstoffarmen chemischen Produktion führen. Die obengenannte Produktion basiert auf den erneuerbaren Energiequellen. Das Interesse an der fossilkraftstoffreien Ammoniak-Direktsynthese nimmt daher zu.

Die Elektrochemische Durchflusszelle wurde für die direkte Ammoniaksynthese von Wasser und N_2 bei Raum-Temperatur und Luftdruck entwickelt. Eisenoxyd Fe_2O_3, das auf Carbon Nanotubes (CNTs) basiert, wurde als Elektrokatalysator in dieser Hemizelle verwendet. Eine Ammoniakbildungsgeschindigkeit von 2.2×10^{-3} $g_{NH3}\cdot m^{-2}\cdot h^{-1}$ wurde bei Raumtemperatur und Luftdruck in Anwesenheit von Stickstoff unter einem angelegten Potential von -2.0 V vs. Ag/AgCl erhalten. Dieser Wert ist höher als die Ammoniakbildungsgeschwindigkeit, die mit Edelmetallen (Ru/C) unter vergleichbaren Reaktionsbedingungen erreicht wird. Darüber hinaus wurde Wasserstoffgas mit einem Gesamtwirkungsgrad von 95.1% erreicht.

Die Reaktionsbedingungen wurden mit Fe_2O_3-CNT (30 Gew.-%) als Elektrokatalys ator optimiert. Dieser Eisenoxidgehalt erwies sich als optimal. Die Leistungen hängen stark vom Reaktordesign ab, wobei die Möglichkeit eines Ammoniak Durchgangs durch die Membran verhindert werden muss. Die Reaktionsbedingungen spielen auch eine wichtige Rolle. Die Wirkung des Elektrolyten (Typ, pH-Wert, Konzentration), Stromdichte, Ammoniakbildungsgeschwindigkeit und Faraday'scher Wirkungsgrad in kontinuierlichen Tests bis zu 24 Stunden am Tag wurden untersucht. Die Nebenreaktion der H^+/e^- Rekombination zur H_2 Erzeugung ist in Konkurrenz mit der direkten Ammoniaksynthese und bring zur Reduzierung aktivierter N_2-Spezies. Die aktiven

Zentern möglicherweise befindet sich an der Grenzfläche zwischen Eisenoxid und funktionalisierten CNTs.

Die Aktiven Zentern für die Ammoniaksynthese wurden ebenfalls in dieser Arbeit untersucht. Wir zeigen hier, dass entgegen den Erwartungen, Eisenoxid (Fe_2O_3) Nanopartikel auf CNTs als Traeger hohe Umwandlungsgeschwindigkeiten von N_2 mit H_2O fuer die elektrokatalytisch Ammoniaksynthese zeigen. Es wird eine lineare Beziehung zwischen der Ammoniakbildungsgeschwindikeit und dem spezifischen XPS (Röntgen-Photoelektronen Spektroskopie) –Sauerstoffsignal in Bezug auf O^{2-} in Fe_2O_3 Zentern dargestellt. HRTEM (Hochaufgelöste Transmissionselektronenmikroskopie) Daten über die Veränderungen während der elektrokatalytischen Tests bestätigten, dass in-situ aktivierte rekonstruierte Eisenoxidpartikel Zentern für die Ammoniaksynthese gebildet wurden. Das eröffnet neue Möglichkeiten, den Reaktionsmechanismus unter Arbeitsbedingungen zu verstehen um einen effizienten Elektrokatalysator für die Ammoniaksynthese zu entwickeln.

Homogene Katalysatoren für die Ammoniaksynthese wurden ebenso untersucht. Mehrere Ruthenium-Komplexe wurden unter den gleichen Bedingungen getestet. $Ru(PNP)Cl_2$ (PNP: 2,6-Bis[(di-tert-butylphosphanyl)methyl]pyridine) erwies sich als der beste Katalysator für die Ammoniaksynthese. verschiedene Bedingungen wurden untersucht und es wurde festgestellt, dass eine geeignete Menge Essigsäure die katalytische Leistung erhöhen kann. Wenn man verschiedene Zusammensetzungen von Stickstoff- und Wasserstoff vegleicht, wurde festgestellt, dass die Ammoniakbildung mit zunehmender Stickstoffbelastung zunimmt, woraus wir ableiten können, dass die Wasserstoff Aktivierung nicht der geschwindigkeitsbegrenzende Step unter diesen Bedingungen war.

Stichworte: Ammoniak · Atmosphärendruck Elektrochemie · heterogene Katalyse · aktive Zentern · homogene Katalyse · Nachhaltigkeit

Table of Contents

LIST OF FIGURES

LIST OF TABLES

CHAPTER 1

1. General Introduction

1.1 The importance of Nitrogen fixation

Nitrogen element is necessary for all known forms of life on Earth. It is a component of all amino acids, such as it is incorporated into proteins and is present in the bases that make up nucleic acids such as RNA and DNA. Along with the carbon cycle and the water cycle, the nitrogen cycle comprises a sequence of events that are key to make the Earth capable of sustaining life. As shown in ***Figure 1-1***, nitrogen cycle in a Terrestrial Ecosystem[1] and its representation with the chemical formula, the major transformations of nitrogen element are nitrogen fixation, nitrification, denitrification, anammox, and ammonification. The nitrification process is dependent on the activities of a diverse assemblage of microorganisms, such as bacteria, archaea, and fungi. The denitrification process is performed by bacterial species such as Pseudomonas and Clostridium in anaerobic conditions. The nitrate is reacted as electron acceptor in the place of oxygen during respiration. The anammox process makes up a major proportion of nitrogen conversion in the oceans. The nitrogen fixation and ammonification provide all the nitrogen into the nitrogen cycle. The amount of ammonia supplied by the ammonification process was hard to be improved due to the stable triple bond of dinitrogen gas. And atmospheric nitrogen has limited availability for biological use, leading to a scarcity of usable nitrogen in many types of ecosystems. So, the process of ammonification is rate-limiting step of the nitrogen cycle.

The relationship between world population and fertiliser consumption with projections to 2050 was shown in ***Figure.1-2***. [2] The population has increased with the increasing amount of fertiliser used in the past 60 years and predicts that more fertilizer is necessary to maintain the increasing population in future. Now, 50% of nitrogen element in our body came from ammonia synthesis by Haber Bosch process.[3], which

means nitrogen fixed by industrial process sustained half of the population.

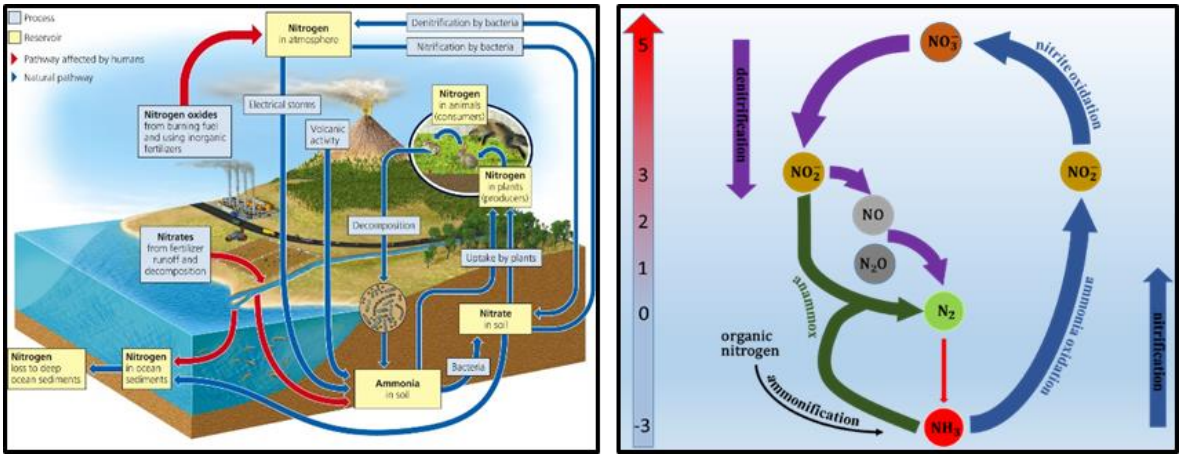

Figure 1-1. *Nitrogen Cycle in a Terrestrial Ecosystem and Its representation with the chemical formula. [8]*

About 80% of the ammonia produced globally is used for nitrogen-based fertilizers. The remaining 20% of the ammonia production is used in explosives, pharmaceuticals, refrigeration, cleaning products and many other industrial processes. Ammonia is also being considered an energy storage media and a source of hydrogen as the hydrogen content in liquid ammonia is 17.6 wt% compared with 12.5 wt% in methanol.[3]

In conclusion, industrial nitrogen fixation not only provides fertilizer to permit half of the population to survive but also provides ammonia used as industrial raw materials and potential energy storage.

1.2 Industrial ammonia production: Haber-Bosch process

The Haber-Bosch process was one of the most successful and well-studied reactions, which named after Fritz Haber (1868–1934) and Carl Bosch (1874–1940). Haber first proposed to use a high-pressure reaction technique. Furthermore, in order to overcome the low conversion-per-pass of ammonia, he introduced an important concept, the reaction rate, which used space-time yield to replace reaction yield. Closed process flow

and loop operation technology were developed according to these concepts. With suitable catalysts, by circulating nitrogen and hydrogen over the catalyst at a pressure of 150-200 atmospheres at a temperature of about 500° C, industrial-scale production could be realized. Haber's unprecedented creations established the basis for not only ammonia synthesis but also the entire chemical engineering science.

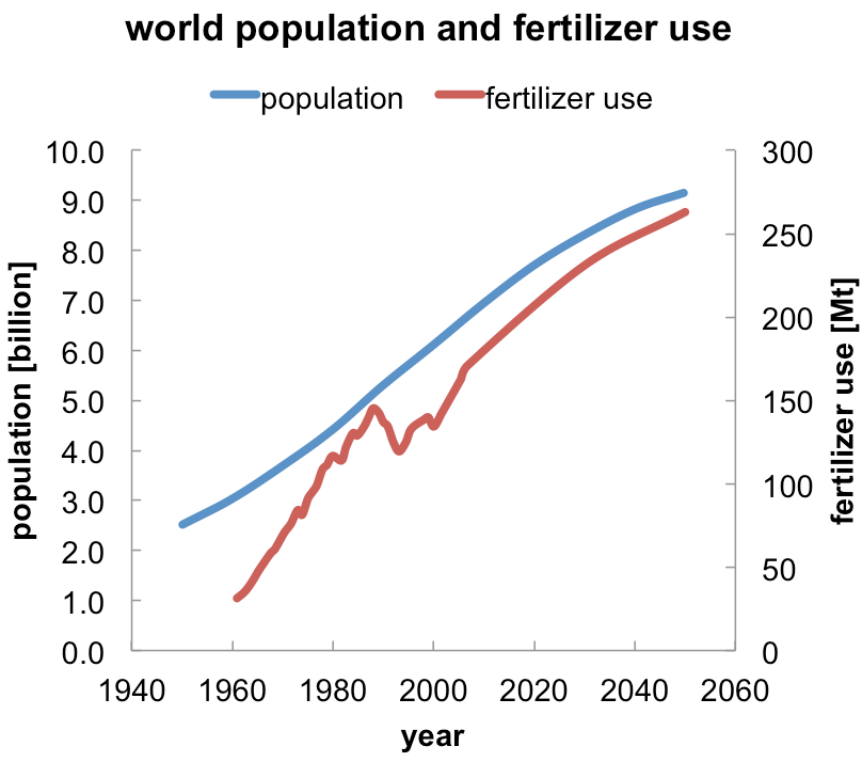

***Figure 1-2**. World population and fertilizer consumption, with projections to 2050. [10]*

From 1909 until 1913, Carl Bosch transformed Fritz Haber's tabletop demonstration of a method to fix nitrogen using high-pressure chemistry into an important industrial process to produce megatons of fertilizer and explosives. His contribution was to make this process working on a large industrial scale. To do this, he constructed a plant and equipment that would function effectively under high gas pressures and high temperatures. There were many more obstacles as well, such as discovering a practical catalyst, designing large compressors and safe high-pressure furnaces. In order to find a stable and efficient catalyst, 2500 of different catalysts were tested for 6500 times. The first full-scale Haber-Bosch plant was erected in Oppau, Germany, now part of

Ludwigshafen. With the process complete, large amounts of ammonia were able to be synthesized, which were available for the industrial and agricultural fields. [4]

Fritz Haber (1868–1934) The Nobel Prize in Chemistry 1918 "for the synthesis of ammonia from its elements"

Carl Bosch (1874–1940) The Nobel Prize in Chemistry 1931 "in recognition of their contributions to the invention and development of chemical high pressure methods"

Gerhard Ertl (1936–) The Nobel Prize in Chemistry 2007 "for his studies of chemical processes on solid surfaces"

The detailed molecular mechanisms of the catalytic synthesis of ammonia over iron (Haber Bosch process) was after studied and determined by Gerhard Ertl. Great success on ammonia industry has changed the history of world's food production. According to the statistics from UN Food and Agriculture Organization (FAO), fertilizer contributes more than 40% to food production. Thus, the catalytic ammonia synthesis technology proposed by Haber and Bosch was one of the most important contributions to human beings. To remember that, Haber, Bosch, and Ertl, who had given the input with the developing of the ammonia synthesis industry, were awarded with the Nobel Prize in Chemistry.

After a century of development, catalytic synthesis of ammonia has made tremendous progress. The production capacity of single set equipment has been improved from the original 5 t of daily ammonia production to the current 2200 t. The reaction pressure has dropped to 10-15 MPa from the original 100 MPa. The energy consumption has decreased to 27.2 GJ from the original 78 GJ, which is close to the theoretical energy

consumption of 20.1 GJ. But as the second largest chemicals, the ammonia production still consumes 2% of total energy supply in the world and releases more than 400 Mt of CO_2, which accounts for 1.6% of total global CO_2 emissions. [3] So more sustainable routes, with which renewable energy could be used and less CO_2 emitted, were necessary to be developed.

1.3 Advantages of electrochemical Nitrogen fixation

The Haber-Bosch process was well developed during the last century; the total energy efficiency was as high as 70%.[5] At the same time, about 2% of the world's total natural gas output was used to produce hydrogen for this process. It was not possible to break through of this highly developed process. From the academic view, routes that can be operated at a lower temperature, lower pressure and with water instead of hydrogen, could be a promising way to produce ammonia. Many routes were studied, such as plasma-induced nitrogen fixation, biological nitrogen fixation, metallo-complexes nitrogen fixation and electrochemical nitrogen fixation. All these routes were at the starting stage. Without a breakthrough of these methods, the Haber Bosch process could not be able to be replaced.

However, electrochemical ammonia production is a promising route for ammonia production, due to the following reason:

- The high pressures and high temperature conditions are not essential;
- H_2O instead of H_2 could be used as hydrogen source;
- Comparing with the heating system in Haber Bosch, which could activate both reactants and products (reverse reactions), the electricity could be more selectable for the reactant with a suitable catalyst.

- Renewable and clean electricity, such as solar and wind energy, could be used for ammonia synthesis minimizing CO_2 emissions;
- Process scaling down without decreasing the energy efficiency can be addressed;
- This solution offers attractive possibilities for a distributed production of fertilizers.

1.4 State of the art on the electrocatalytic synthesis of NH_3

Various approaches have been investigated in the electro-catalytic synthesis of NH_3, as reviewed in some recent papers.[6-10]

The electrochemical cell was divided into three categories, according to the type of electrolyte (liquid electrolyte, molten salt electrolyte, and solid-state electrolyte), as shown in ***Figure 1-3***.

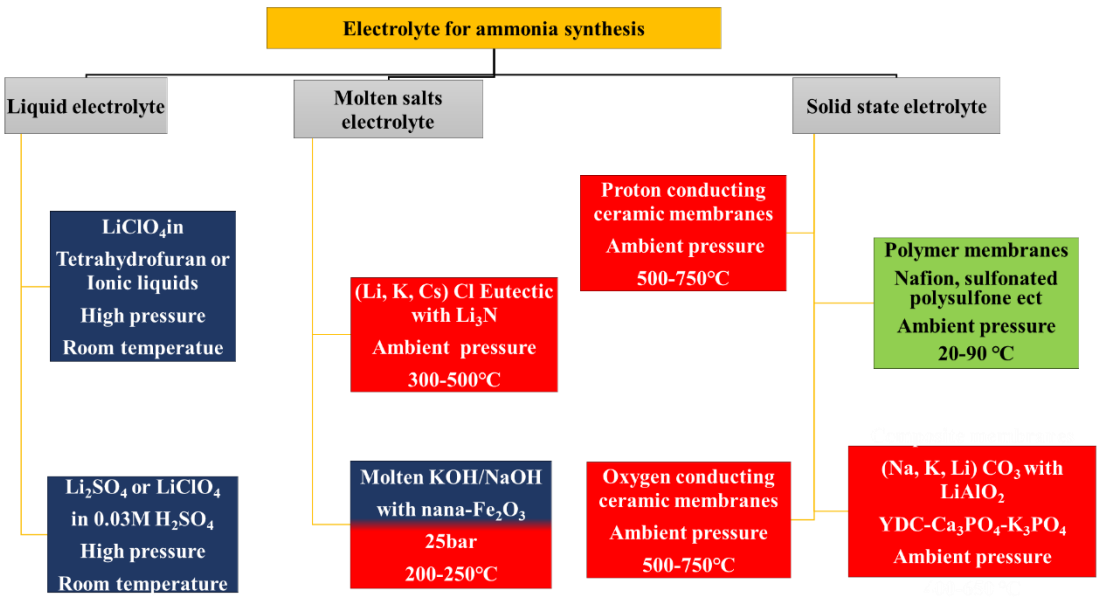

Figure 1-3. *Various electrolytic options under consideration for ammonia synthesis.*

1.4.1. Liquid electrolyte-based systems

There was very limited information available in the literature on the synthesis of ammonia using liquid electrolytes in comparison with solid electrolytes. Nagakazu Furuya and Hiroshi Yoshiba developed an electrochemical cell with a gas diffusion electrode for ammonia synthesis at room temperature and atmospheric pressures in 1989. [11, 12] In their study, N_2 and H_2 were used as reactants. Catalysts, such as Fe fine powder and carbon black, metal oxides, metal sulfides, and ZnSe, TiB, and SiC were studied. Electrolytes under consideration were solutions of KOH, $KHCO_3$, $(COOK)_2$, K_2HPO_4, K_2CO_3, KH_2PO_4, CH_3COOK, and K_3PO_4. This was the first work on electrochemical ammonia synthesis from H_2 and N_2 at room temperature and atmospheric pressure. Unfortunately, all the systems were found to be not active for more than 30 minutes.

In 1994, Tsuneto et al. investigated organic solvent-based electrolytes to synthesize ammonia at near room temperatures and high pressures.[13] In their study, lithium perchlorate ($LiClO_4$ 0.2 M) in tetrahydrofuran was used as the electrolyte, and ethanol (0.18 M) was used as the hydrogen source. A current efficiency of 58% for ammonia production was achieved under the condition that iron was used as catalyst, 50 bar of nitrogen was supplied to the working electrode at 50 ºC.

In 2000, G. Kyriacou et al. reported the possibility of using N_2 and H_2O as reactant for ammonia synthesis instead of N_2 and H_2.[14] This was the first paper, using H_2O without H_2 to synthesize ammonia. In this study, Ru was electrochemically deposited on a carbon felt pressed together with a Nafion membrane used as working electrode and 2M of KOH solution as electrolyte. The ammonia production rates of 2.1×10^{-11} and 2.8×10^{-12} $mol\cdot cm^{-2}\cdot s^{-1}$ were observed at 90 ºC and 20 ºC respectively at atmospheric pressure.

In 2009, Pappenfus et al. used hydrophobic ionic liquids as electrolytes with $LiClO_4$ as

the source of Lithium ions and ethanol as hydrogen source for ammonia synthesis at room temperature. Köleli et al. in 2010 and 2011 published two papers on ammonia synthesis reading a maximum ammonia yield of 3.68×10^{-10} mol·cm^{-2}·s^{-1} at 60 bar.[15, 16]

Limited papers using liquid state electrolytes for ammonia synthesis were found. Hydrogen was used as hydrogen source in most of works. Much lower ammonia formation rates were observed when H_2O was used as hydrogen source. More efforts are necessary on this field.

1.4.2. Molten salt-based electrolyte systems

Only a few of papers could be found on electrochemical ammonia synthesis with molten salts as electrolyte. Yasuhiko Ito et al. used a eutectic of LiCl, KCl, and CsCl as the electrolyte with Li_3N (0.5 mol%) dissolved as the source of nitride ions (N^{3-}). The nitride ions were easier reacted with protons to give ammonia than dinitrogen. But it is hard to transform dinitrogen to the nitride ions to close the catalytic cycle. The best ammonia formation rate of 3.3×10^{-9} mol·cm^{-2}·s^{-1} was observed at high temperatures. In 2014, Licht S. et al. used molten KOH and NaOH mixtures with nano-Fe_2O_3 as electrolyte, and steam as hydrogen source for ammonia synthesis. The ammonia formation rate of 2×10^{-10} mol·cm^{-2}·s^{-1} was regarded as the highest value when H_2O was used as hydrogen source.[17]

Higher ammonia production rates were observed compared with liquid electrolyte systems. However, when molten salts were used as electrolyte, the reaction has to run at high temperature, which means more energy necessary for the process compared with other options working at room temperature.

Table 1. *Ammonia production rates achieved with different systems.*

Ref.	WE	Electrolyte	T (°C)	P (bar)	R_{NH3} ($mol \cdot cm^{-2} \cdot s^{-1}$)	FE (%)	Input
[18]	Pd	SrCe0.95Yb0.05O3-a (SCY)	570	1	4.5×10^{-9}	78	H_2,N_2
[19]	Ag-Pd	$La_{1.9}Ca_{0.1}Zr_2O_{6.95}$ (LCZ)	520	1	1.759×10^{-9}	80	H_2,N_2
[20]	Ag-Pd	$Ba_3(Ca_{1.18}Nb_{1.82})O_{9-a}$ (BCN)	620	1	1.42×10^{-9}	-	H_2,N_2
	Ag-Pd	$Ba_3CaZr_{0.5}Nb_{1.5}O_{9-a}$ (BCZN)	620	1	1.82×10^{-9}	-	H_2,N_2
	Ag-Pd	$Ba_3Ca_{0.9}Nd_{0.28}Nb_{1.8}2O_{9-a}$	620	1	2.16×10^{-9}	-	H_2,N_2
[20]	Ag-Pd	$La_{1.95}Ca_{0.05}Zr_2O_{7-a}$ (LCZ)	520	1	2.0×10^{-9}	-	H_2,N_2
	Ag-Pd	$La_{1.95}Ca_{0.05}Ce_2O_{7-a}$ (LCC)	520	1	1.3×10^{-9}	-	H_2,N_2
[21]	Ag-Pd	CeO_2-$Ca_3(PO_4)_2$-K_3PO_4	650	1	9.5×10^{-9}	40	H_2,N_2
[22]	Ag-Pd	$Ce_{0.8}$ $La_{0.2}O_{2-a}$	650	1	7.2×10^{-9}	-	H_2,N_2
	Ag-Pd	$Ce_{0.8}$ $Y_{0.2}O_{2-a}$	650	1	7.5×10^{-9}	-	H_2,N_2
	Ag-Pd	$Ce_{0.8}$ $Gd_{0.2}O_{2-a}$	650	1	7.7×10^{-9}	-	H_2,N_2
	Ag-Pd	$Ce_{0.8}$ $Sm_{0.2}O_{2-a}$	650	1	8.2×10^{-9}	-	H_2,N_2
[23]	Ag-Pd	$Ce_{0.8}Y_{0.2}O_{1.9}$-$Ca_3(PO_4)_2$-K_3PO_4	650	1	6.95×10^{-9}	-	CH_4,N_2
[24]	Ag-Pd	$BaCe_{0.9}Sm_{0.1}O_{3-a}$ (BCS)	620	1	5.23×10^{-9}	-	H_2,N_2
	Ag-Pd	$BaCe_{0.8}Gd_{0.1}Sm_{0.10}O_{3-a}$	620	1	5.82×10^{-9}	-	H_2,N_2
[25]	Ag-Pd	$La_{0.9}Sr_{0.1}Ga_{0.8}Mg_{0.2}O_{3-a}$	550	1	2.37×10^{-9}	70	H_2,N_2
[26]	Ag-Pd	$La_{0.9}Ba_{0.1}Ga_{1-x}MgxO_{3-a}$	520	1	1.89×10^{-9}	60	H_2,N_2
[27]	Ag-Pd	$BaCe_{1-x}Gd_xO_{3-a}$ (BCG)	480	1	4.63×10^{-9}	70	H_2,N_2
[28]	Ag-Pd	$BaCe_{1-x}Y_xO_{3-a}$ (BCY)	500	1	2.1×10^{-9}	60	H_2,N_2

[29]	Ru	$SrCe_{0.95}Yb_{0.05}O_{3-a}$ (SCY)	650	1	4.9×10^{-13}	-	H_2O,N_2
	Ru	Yttria-stabilized-Zirconia (YSZ)	650	1	1.12×10^{-13}	-	H_2O,N_2
[30]	Ag-Pd	$BaCe_{1-x}Dy_xO_{3-a}$ (BCD)	530	1	3.5×10^{-9}	80	H_2,N_2
[31]	BCYF	$BaCe_{0.85}Y_{0.15}O_{3-a}$ (BCY)	530	1	4.9×10^{-9}	60	H_2,N_2
[32]	Ag-Pd	$BaCe_{1-x}Ca_xO_{3-a}$ (BCC)	480	1	2.69×10^{-9}	50	H_2,N_2
[33]	Ag-Pd	$Ba_xCe_{0.8}Y_{0.2}O_{3-a}$+0.04ZnO	500	1	2.36×10^{-9}	-	H_2,N_2
[34]	Ag-Pd	$BaCe_{0.9x}Zr_xSm_{0.1}O_{3\ a}$ (BCZS)	500	1	2.67×10^{-9}	80	H_2,N_2
[35]	$CoFe_2O_4$	$(Li/Na/K)_2\ CO_3$ – $LiAlO_2$	400	1	2.32×10^{-10}	2.5	H_2,N_2
[36]	LSFCu–SDC	$(Li/Na/K)_2CO_3$-$Ce_{0.8}Sm_{0.2}O_{2-a}$	450	1	5.39×10^{-9}	3.6	H_2,N_2
[37]	Rh	$BaCe_{0.2}Zr_{0.7}Y_{0.1}O_{2.9}$	600	1	1.28×10^{-8} (2.9×10^{-9})*	6.2	H_2,N_2

* purely catalytic rate (without any applied potential)

1.4.3. Solid electrolyte system

Most of the groups that were working on electrochemical ammonia synthesis focused on solid electrolyte system. The first work with solid electrolyte on electrochemical ammonia synthesis was published by M. Stoukides et al. in 1998 on *Science.* [18]

In their study (as shown in ***Figure 1-4***.), a reversed fuel-cell was used as reactor, which means a fixed voltage was applied between the cathode and anode of the fuel cell, at the same time N_2 was introduced into the cathode chamber and H_2 was introduced into the anode chamber. [18] Pd was used both on the cathode and anode as catalyst and electron conductor. A mixed oxide of $SrCe_{0.95}Yb_{0.05}O_{3-\sigma}$(SCY) was used as solid electrolyte located between the electrodes. In these conditions, an ammonia formation

rate of 3.1×10^{-9} mol·cm^{-2}·s^{-1} was observed at 570ºC and atmospheric pressure. This system eliminated the necessity of high pressure during the reaction. Since the paper was published, different kinds of solid electrolytes (mainly perovskites) were investigated in the similar conditions. The related works ordered by date were shown in Table 1. It was found that in most of the cited references in Table 1, a Ag-Pd alloy was used both on the cathode and anode side as catalyst and electron conductor using N_2 and H_2 as reactant working at high temperature (T > 500°C). The results show that the ammonia formation rates were in the same order of magnitudes. In 2009, Skodra and Stoukides tried to replace H_2 with H_2O as hydrogen source, but it was found that the yield of ammonia decreased four orders of magnitude and the current efficiency decreased. The highest ammonia formation rate reported for these conditions was of 1.28×10^{-8} mol·cm^{-2}·s^{-1} for $BaCe_{0.2}Zr_{0.7}Y_{0.1}O_{2.9}$ as electrolyte at 600 ºC.

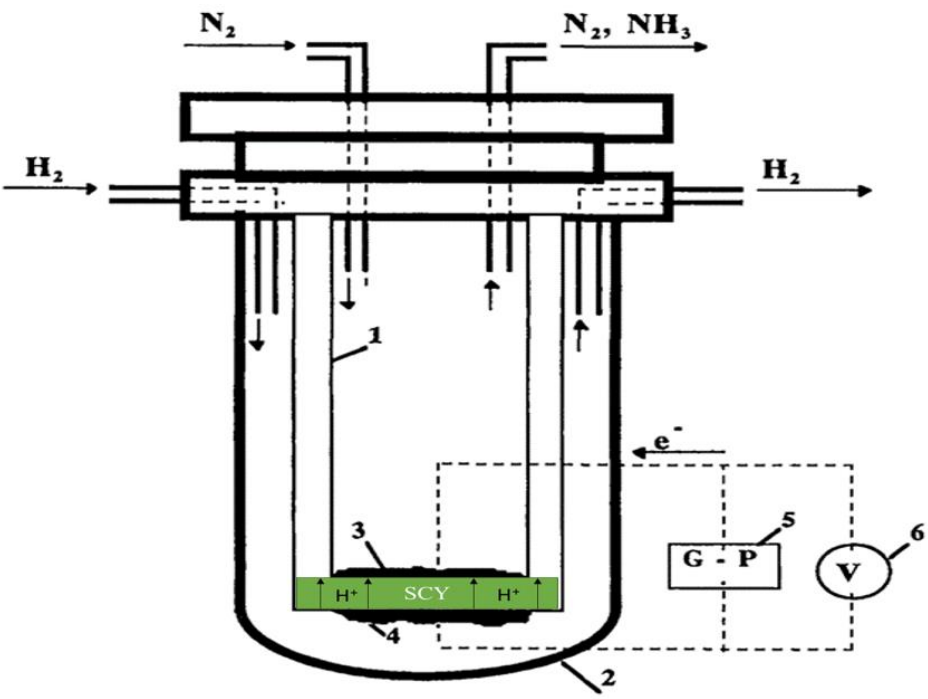

Figure 1-4*.Schematic diagram of cell-reactor: 1, SrCe0.95Yb0.05O3-σ(SCY); 2, quartz tube; 3, cathode(Pd); 4, anode (Pd); 5, galvanostat -potentiostat; 6,voltmeter. [18]*

Since ammonia could decompose at 400 ºC or higher temperature, low reaction temperatures will allow the preferable thermodynamics condition. The low conductivity of solid electrolytes, however, determines the need to operate at higher reaction temperature, above 350-400°C to have enough conductivity. In ***Figure.1-5*** various proton and oxygen ion conductivities of ceramic electrolytes for ammonia synthesis are reported. [38]

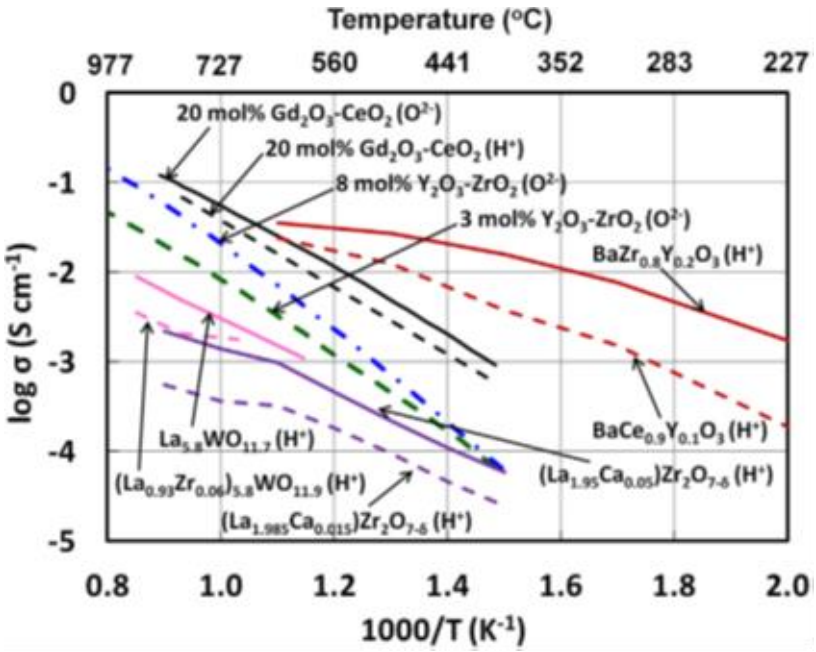

Figure 1-5. *Proton and oxygen ion conductivity of various ceramic electrolytes for ammonia synthesis. 20 mol%Gd_2O_3-CeO_2 (O^{2-}), 8 mol% Y_2O_3-ZrO_2 (O^{2-}), 3 mol% Y_2O_3-ZrO_2 (O^{2-}); 20 mol% Gd_2O_3-CeO_2 (H^+)[22]; $BaZr_{0.8}Y_{0.2}O_3$ (H^+), $BaCe_{0.9}Y_{0.1}O_3$ (H^+) [39]; $(La_{1.95}Ca_{0.05})Zr_2O_7Ld$ (H^+), $(La_{1.985}Ca_{0.015})Zr_2O_7Ld$ (H^+) [40]; $La_{5.8}WO_{11.7}$ (H^+), $(La_{0.93}Zr_{0.06})_{5.8}WO_{11.9}$ (H^+) [41]*

To overcome the drawback for the low conductivity of perovskites kinds of solid electrolytes at low temperature, polymer electrolyte membranes such as Nafion® were recognized as promising materials for the reaction. The conductivity of Nafion is $4.5x10^{-2}$ $S{\cdot}cm^{-1}$ at 80ºC. There are comparatively fewer studies in ammonia electro-synthesis at temperatures below 100°C and even fewer papers for the more challenging synthesis from N_2 and H_2O, i.e. without feeding H_2. On the other hand, this was clearly the necessary approach to investigate the possibility to use ammonia synthesis for the

storage of renewable electrical energy.

The first report on ammonia synthesis from N_2 and H_2 at room temperature and atmospheric pressure was made by Furuya and Yoshiba,[42] but a very fast deactivation (the reaction stops within 30 minutes) was observed. Better results at T < 100°C were observed by using as electrodes mixed oxides such as $SmBaCuNiO_{5+\delta}$ or $Sm_{1.5}Sr_{0.5}NiO_4$ at the cathode and Ni-$Ce_{0.8}Sm_{0.2}O_{2-\delta}$ at the anode (Nafion or other proton-conducting membranes as electrolyte).[43-46] In all cases, H_2 and N_2 were used as the feed , where the behaviour of these systems feeding N_2 and H_2O is up to three orders of magnitude lower regarding the reaction rate of ammonia formation, as shown in the ***Table 1***. [28,34]

Kordali et al. [14] reported the use of H_2O rather than H_2. These authors used cathode based on Ru/C, Nafion as electrolyte and Pt as anode, finding a rate of $1.9x10^{-7}$ $g_{NH3}\cdot h^{-1}\cdot cm^{-2}$ at 20°C (at -1.10 V of potential; the rate of ammonia formation is about four times higher at 90°C) with a Faradaic efficiency of 0.28 % (slightly lower at 90°C). Data on the stability of the performances were not given, neither was exactly indicated the loading of Ru per cm^2 in the electrode. Better rates of ammonia electrosynthesis using H_2O and N_2 as feed was reported recently by Lan and Tao[47] on a Pt/C anode, although NH_4^+ was present in the $Li^+/H^+/NH_4^+$ mixed conducting electrolyte. The authors indicated that these ammonium ions do not contribute to the rate of ammonia formation, even if the reported data do not exclude this possibility. Faradaic efficiency was also low, below 0.1% at room temperature.

Tetra-hexahedral gold Nano rods (THH Au NRs, ***Figiure 1-6***) which have multifaceted surfaces composed of a mixture of various types of high-index sites, have been recently used as NRR electrocatalysts.[48] They were fabricated by a seeded growth method using a binary surfactant mixture and were applied in a three-electrode configuration with an alkaline electrolyte. As the negative potential increases to -0.2 V vs. RHE, the

N_2 reduction reaction rate rises, offering an NH_3 yield of 1.648 $\times 10^{-6}$ g cm^{-2} h^{-1}, higher than that of Au nanoparticles (1.052 $\times 10^{-6}$ g cm^{-2} h^{-1}). Beyond this potential, competitive adsorption of H-adatoms occurs on the electrode surface, resulting in decreased efficiency. A current efficiency of 4% was achieved for the THH Au NRs electrocatalyst at -0.2 V vs. RHE. It was found that N_2H_4 was also produced during the NRR. DFT calculations in Fig. 8d demonstrates that the catalytic process tends to follow an alternating associative mechanism, with the step from Au-NN* to Au-NNH* being the limiting step. The relatively low NH_3 production rate is still a significant problem for the catalyst. It is likely that surfactant molecules used in the synthesis process remained covering the catalyst surface, resulting in blocked active sites. Thus, the surfactant molecules should be removed from the Au NRs surface to improve the active site density. In addition, the production of other nanostructured Au materials such as ultrathin two-dimensional nanosheets and nonporous Au materials might be useful in increasing the active site density.

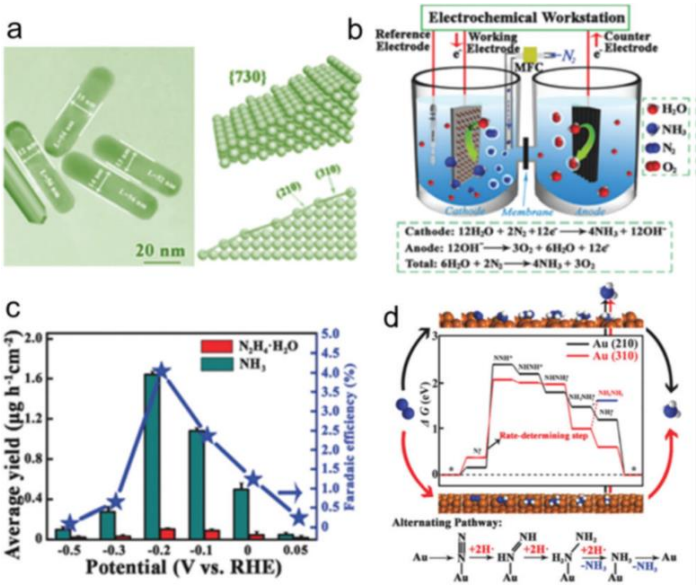

Figure 1-6 (a) Transmission electron microscopy image of Au THH NRs and the geometric model. (b) Setup of the electrolytic cell used for the NRR. (c) NH3 yield and Faradic efficiency at each given potential. (d) Free energy diagram and catalytic pathway of N2 reduction on the Au THH NRs. [48]

1.5 Challenge of electrocatalytic synthesis of NH_3

1.5.1. The competition of hydrogen evolution

The standard electrode potential of two important intermediates during the electrochemical nitrogen reduction, $H_2NNH_3^+$ and $HONH_3^+$ are also known:[49]

$$N_2 + 5H^+ + 4e^- = H_2NNH_3^+ \qquad E^0 = -0.23\,V\ vs.RHE \qquad (1)$$

$$2H_2NNH_3^+ + 3H^+ + 2e^- = 2NH_4^+ \qquad E^0 = +1.27\,V\ vs.RHE \qquad (2)$$

Or

$$N_2 + 2H_2O + 2e^- = 2HONH_3^+ \qquad E^0 = -1.87\,V\ vs.RHE \qquad (3)$$

$$HONH_3^+ + 2H^+ + 2e^- = NH_4^+ + H_2O \qquad E^0 = +1.35\,V\ vs.RHE \qquad (4).$$

There are two possible routes for the electrochemical reduction of nitrogen. Equation (1) and equation (3) should be the rate-limiting steps, due to the much more negative potentials required for the problem obtained following equation (2) and equation (4). However, both of equilibrium potentials are lower than the equilibrium potentials necessary for hydrogen evolution. It means that the hydrogen evolution is unavoidable during the nitrogen reduction. This indicates that we should design an electrochemical cell to reduce hydrogen evolution and find catalysts with higher overpotential for hydrogen evolution and lower potential for nitrogen reduction reaction, in order to achieve higher Faradic efficiency for nitrogen activation, which was one of the challenges.

1.5.2. Using H_2O instead of H_2 as hydrogen source for electrochemical ammonia synthesis at low temperature and ambient pressure

Due to the in-situ hydrogen evolution in the electrochemical cell during nitrogen reduction reaction, it was possible to use H_2O as hydrogen source instead of H_2, which could provide a possibility of breaking the connection between ammonia productions

with fossil fuels (used for hydrogen production). However, the ammonia formation rate using H_2O was 3~4 orders of magnitude lower than the rate using H_2 as hydrogen source. To overcome this gap, a bi-functional catalyst should be devolved (i.e. both active for hydrogen evolution and nitrogen activation).

1.5.3. Thermodynamics or dynamic preferable ways of electrochemical ammonia synthesis

It was found that equilibrium potentials of equation (1) $E^0 = -0.23\ V\ vs. RHE$ was more positive than equilibrium potentials of equation (3) $E^0 = -1.87\ V\ vs. RHE$, which means the route (1)-(2) was preferable from the view point of thermodynamics. From the view point of dynamic, the equation (3) required less electrons, the route (3)-(4) is preferable. Both thermodynamics and dynamic determine the final ammonia formation rate. The main difference of this two routes is that the time of disassociation of the N-N bond, i.e. in the route (1)-(2), where the N-N bond breaks at the last step. If the catalyst could be able to activate or stabilize both N atom in the same time, the ammonia formation will prefer to follow the route of (1)-(2), which could be active at less negative potential. Till now the low ammonia formation rate of electrochemical nitrogen reduction was the main limitation for the industrial ammonia production. And very limited information on the mechanism of this reaction are reliable. Understanding the mechanism could help develop more efficient catalysts.

1.6 The detection methods of electrochemical ammonia synthesis

A crucial point of all data reported in literature for the electrochemical ammonia synthesis is the quantitative detection of the small quantities of formed NH_3. The amounts of ammonia formed is too low to be detected by online gas chromatography or mass spectrometry. To accurately calculate efficiency and production rate, ammonia

(ammonium ion) detection is therefore mainly carried out by colourimetric assays such as Nessler reagent, phenate and indophenol blue tests. However, certain ions dissolved in solution may interfere with these colourimetric tests. Ammonium ion-selective electrodes, ^{15}N isotope testing, and enzymatic testing are alternative detection methods which can avoid possible false-positive results. To obtain accurate data, it is suggested to double check the values with a second ammonia detection method.

Still, it is not possible to observe the ammonia formation rate timely with the existing methods. The lack of timely detection methods for ammonia detection of electrochemical processed was also an obstacle to deep understand the process.

1.7 Carbon-based electrocatalysts for nitrogen activation

Nanocarbon is a term increasingly used to indicate the broad range of carbon materials having a tailored nanoscale dimension and functional properties that significantly depend on their nanoscale features. CNT and graphene belong to this class of materials comprising many more types of carbon materials, such as nanofibers, -coils, -diamonds, -horns, -onions, and fullerene. The alternative definition (also often used) is nanostructured carbon. Both definitions include also ordered mesoporous carbon materials obtained, for example, by a replica method from mesoporous silica or other ordered oxides, which are then removed after the template synthesis of the mesoporous carbon. The nanocarbon class of materials is typically extended to include carbon nanocomposites with metal ions, metal oxide, metals, and quantum dots used in various applications as advanced electrodes for energy conversion and storage, as well as other applications such as catalysis. These carbon/inorganic nanohybrids are at the frontier of research for the development of advanced devices for sustainable energy and development, including artificial leaves. ***Figure 1-7*** provides a schematic illustration of some nanocarbons. [50, 51]

Nanocarbons show interesting characteristics, which differentiate them from the

conventional supports (mainly oxides) used to prepare catalysts. Between them, it may be cited the following aspects:

– the different surface characteristics and interaction with the supported metal particles (and reactants/intermediates/products as well), due to the presence of a graphitic character (tuneable within some extend) and the presence of surface groups, the latter depending on the source of carbon and the process of preparation;

– the high surface area and the possibility of a fine control of the porosity;

– the robustness and chemical inertness, except in the presence of oxygen at high temperature (typically above 400 ºC);

– the high electronic and heat conductivity (although great depending on the preparation);

– the presence of surface groups induced by post- or pretreatment allowing to control the degree of hydrophobicity;

– the low cost of production, between the cheaper of catalytic support materials.

Together with its tunable electronic conductivity, nanocarbons are ideal material for the use in developing electrodes.[51]

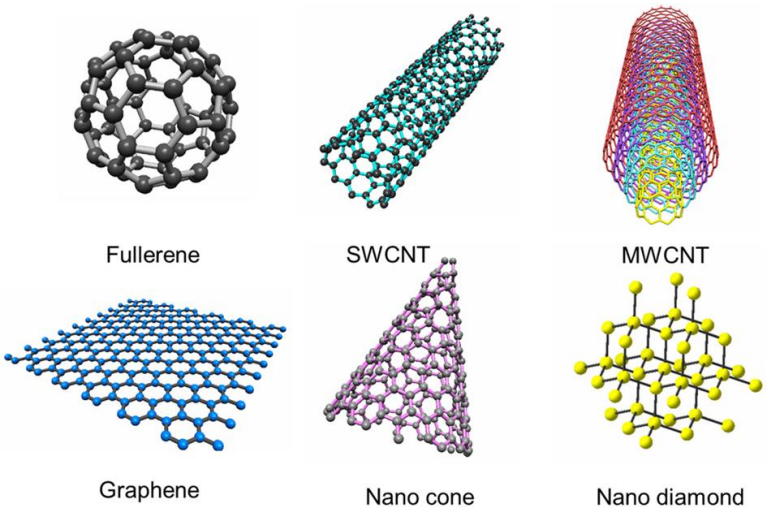

Figure 1-7 *Schematic illustration of some nanocarbon.*

1.8 Thesis aim and scope

Ammonia synthesis, produced on a > 150 Mtons world scale in a multi-step process starting mainly from natural gas, is the largest-scale chemical process and top largest chemical process in terms of energy consumption, with about 2.5 EJ use on a world scale and between 1.8-2.1 ton CO_2 emitted per ton of NH_3 produced, depending on plant efficiency. Therefore, over 300 Mtons CO_2 emissions are associated with ammonia production. This value could be decreased by over 80% in a direct electrocatalytic process using N_2, H_2O and renewable energy as input sources. [52, 53]

The principal goal of this thesis is to develop carbon-based electrocatalyst to synthesis ammonia with water as hydrogen source at room temperature and atomspheric pressure, which is consider to be a sustainable way to produce ammonia.

In chapter 2, we have shown here the possibility to realize the synthesis of ammonia under very mild conditions (room temperature and ambient pressure) starting from H_2O and N_2, and using electrical energy which could be provided from renewable energy sources, fully in line with the requirement to move to a "solar-driven chemistry" not based on the use of fossil fuels, with a consequent decrease of the greenhouse gases emissions. Present data represent a breakthrough on the type of electrocatalysts used, but also contain the elements to indicate an expected further progress. We thus believe that these results could open a new direction in the development of systems for the electrocatalytic synthesis of ammonia from H_2O and N_2.

In Chapter 3, present data evidence that 30% Fe_2O_3-CNT is the best electrocatalyst among iron based catalysts supported on carbon nanotubes. The performances greatly depend on the cell design, where the possibility of ammonia crossover through the membrane has to be inhibited. The reaction conditions also play a significant role. When an acid is used as electrolyte, the current density is determined by proton concentration but if a base is used as electrolyte, the water transport determines the

current density. The electrolyte (type, pH, concentration) plays a critical role on the selectivity of ammonia, but does not influences greatly the ammonia formation rate. A complex effect of the applied voltage was observed. An excellent stability was found for an applied voltage -1.0 V. At higher negative applied voltages, the ammonia formation rate and Faradaic selectivity are higher, but with a change of the catalytic performances, although the current densities remain constant for at least 24h of experiments. This effect is interpreted in terms of reduction of the iron-oxide species above a negative voltage threshold, which enhances the side reaction of H^+/e^- recombination to generate H_2 rather than their use to reduce activated N_2 species, possibly located at the interface between iron-oxide and functionalized CNT.

In chapter 4, The linear relationships between ammonia formation rate and the amount of O1(Fe-O-Fe) species detected by XPS, which are related to O^{2-} in Fe_2O_3 or FeOOH species, was confirmed by both chemical reduced samples (i.e. Fe-CNT, Fe_2N-CNT) and electrochemical activated Fe_2O_3-CNT (i.e. by in-situ activation at -2.0V). This indicated that the O1 (Fe-O-Fe) species are associated with the active site for ammonia electrochemical synthesis. Furthermore, only small iron-oxide particles that strongly interacted with CNT, showed the significant increased ability for ammonia synthesis comparing to the bulk iron oxide. This is due to the small iron oxide partials that are sitting at the defect or functional groups of carbon (i.e. with charge density different from bulk iron oxide). An in-situ activation at -2.0V for Fe_2O_3-CNT, leading to the reconstruction of bulk iron-oxide particles and creating more defect sites on CNT, give enhanced formation of the interface between iron-oxide nanoparticles and (defective) carbon, with a significant increase in the ammonia formation rate. These results thus provide new insights about the nature of the active sites for NH_3 synthesis from N_2 and H_2O at ambient temperature/pressure, which are significantly different from the industrial Haber-Bosch catalysts.

In Chaper 5, we synthsize ammonia with pressured nitrogen and hydrogen in autoclave with homogenous catalysts. This is an attempt to develop new process for ammmonia synthesis. It can also provide the possibility to compare its performace with the electochemical process discribed in the previous chapter.

1.9 References

1. Miller, G. and S. Spoolman, Living in the environment: principles, connections, and solutions. 2011: Nelson Education.
2. Alexandratos, N. and J. Bruinsma, World agriculture towards 2030/2050: the 2012 revision. ESA Work. Pap, 2012. 3.
3. Liu, H., Ammonia synthesis catalyst 100 years: Practice, enlightenment and challenge. Chinese Journal of Catalysis, 2014. 35(10): p. 1619-1640.
4. www.nobelprize.org/nobel_prizes/chemistry/laureates/index.html
5. Rafiqul, I., et al., Energy efficiency improvements in ammonia production—perspectives and uncertainties. Energy, 2005. 30(13): p. 2487-2504.
6. Oshikiri, T., K. Ueno, and H. Misawa, Selective Dinitrogen Conversion to Ammonia Using Water and Visible Light through Plasmon-induced Charge Separation. Angewandte Chemie, 2016. 128(12): p. 4010-4014.
7. Kosaka, F., T. Nakamura, and J. Otomo, Electrochemical Ammonia Synthesis Using Mixed Protonic-Electronic Conducting Cathodes with Exsolved Ru-Nanoparticles in Proton Conducting Electrolysis Cells. Journal of The Electrochemical Society, 2017. 164(13): p. F1323-F1330.
8. Díez-Ramírez, J., et al., Enhancement of Ammonia Synthesis on a Co3Mo3N-Ag Electrocatalyst in a K-βAl2O3 Solid Electrolyte Cell. ACS Sustainable Chemistry & Engineering, 2017. 5(10): p. 8844-8851.
9. Vasileiou, E., et al., Electrochemical enhancement of ammonia synthesis in a BaZr 0.7 Ce 0.2 Y 0.1 O 2.9 solid electrolyte cell. Solid State Ionics, 2016. 288: p. 357-362.
10. Li, F.F. and S. Licht, Advances in understanding the mechanism and improved stability of the synthesis of ammonia from air and water in hydroxide suspensions of nanoscale Fe(2)O(3). Inorg Chem, 2014. 53(19): p. 10042-4.
11. Yoshiba, N.F.a.H., Electroreduction of nitrogen to ammonia on gas-diffusion electrodes modified by Fe-phthalocyanine. J. Electroanal. Chem., 1989.
12. Yoshiba, N.F.a.H., Electroreduction of nitrogen to ammonia on gas-diffusion electrodes loaded with inorganic catalyst. 1990.

13. Akira Tsuneto, A.K.a.T.S., Lithium-mediated electrochemical reduction of high pressure N,to NH 3. 1994.

14. Kordali, V., G. Kyriacou, and C. Lambrou, Electrochemical synthesis of ammonia at atmospheric pressure and low temperature in a solid polymer electrolyte cell. Chemical Communications, 2000(17): p. 1673-1674.

15. Köleli, F. and D.B. Kayan, Low overpotential reduction of dinitrogen to ammonia in aqueous media. Journal of Electroanalytical Chemistry, 2010. 638(1): p. 119-122.

16. Köleli, F., et al., Investigation of N2-fixation on polyaniline electrodes in methanol by electrochemical impedance spectroscopy. Journal of Applied Electrochemistry, 2011. 41(4): p. 405-413.

17. Licht, S., et al., Ammonia synthesis by N2 and steam electrolysis in molten hydroxide suspensions of nanoscale Fe2O3. Science, 2014. 345(6197): p. 637-640.

18. Marnellos, G. and M. Stoukides, Ammonia synthesis at atmospheric pressure. Science, 1998. 282(5386): p. 98-100.

19. Xie, Y., Preparation of La1.9Ca0.1Zr2O6.95 with pyrochlore structure and its application in synthesis of ammonia at atmospheric pressure. Solid State Ionics, 2004. 168(1-2): p. 117-121.

20. Li, Z., et al., A novel method for preparation of doped Ba3(Ca1.18Nb1.82)O9−δ: Application to ammonia synthesis at atmospheric pressure. Solid State Ionics, 2005. 176(11–12): p. 1063-1066.

21. Wang, B., et al., Doped ceria-Ca-3 (PO4) 2-K3PO4 composite electrolyte: Proton conductivity at intermediate temperature and application in atmospheric pressure ammonia synthesis. CHINESE JOURNAL OF INORGANIC CHEMISTRY, 2005. 21(10): p. 1551-1555.

22. Liu, R.-Q., et al., Synthesis of ammonia at atmospheric pressure with Ce 0.8 M 0.2 O 2− δ (M= La, Y, Gd, Sm) and their proton conduction at intermediate temperature. Solid State Ionics, 2006. 177(1): p. 73-76.

23. Wang, B.H., et al., Synthesis of ammonia from natural gas at atmospheric pressure with doped ceria–Ca3 (PO4) 2–K3PO4 composite electrolyte and its proton conductivity at intermediate temperature. Journal of Solid State Electrochemistry, 2006. 11(1): p. 27-31.

24. Li, Z., et al., Preparation of double-doped BaCeO 3 and its application in the synthesis of ammonia at atmospheric pressure. Science and Technology of Advanced Materials, 2007. 8(7): p. 566-570.

25. Zhang, F., et al., Proton conduction in La0.9Sr0.1Ga0.8Mg0.2O3−α ceramic prepared via microemulsion method and its application in ammonia synthesis at atmospheric pressure. Materials Letters, 2007. 61(19–20): p. 4144-4148.

26. Chen, C. and G. Ma, Preparation, proton conduction, and application in ammonia synthesis at atmospheric pressure of La0.9Ba0.1Ga1–x Mg x O3–α. Journal of Materials Science, 2008.

43(15): p. 5109-5114.

27. Chen, C. and G. Ma, Proton conduction in BaCe1−xGdxO3−α at intermediate temperature and its application to synthesis of ammonia at atmospheric pressure. Journal of Alloys and Compounds, 2009. 485(1–2): p. 69-72.

28. Guo, Y., et al., Preparation via microemulsion method and proton conduction at intermediate-temperature of BaCe1−xYxO3−α. Electrochemistry Communications, 2009. 11(1): p. 153-156.

29. Skodra, A. and M. Stoukides, Electrocatalytic synthesis of ammonia from steam and nitrogen at atmospheric pressure. Solid State Ionics, 2009. 180(23-25): p. 1332-1336.

30. Wang, W.B., et al., Microstructures and proton conduction behaviors of Dy-doped BaCeO3 ceramics at intermediate temperature. Solid State Ionics, 2010. 181(15–16): p. 667-671.

31. Wang, W.B., et al., Ammonia synthesis at atmospheric pressure using a reactor with thin solid electrolyte BaCe0.85Y0.15O3−α membrane. Journal of Membrane Science, 2010. 360(1–2): p. 397-403.

32. Liu, J., et al., Proton conduction at intermediate temperature and its application in ammonia synthesis at atmospheric pressure of BaCe1−x Ca x O3−α. Journal of Materials Science, 2010. 45(21): p. 5860-5864.

33. Zhang, M., J. Xu, and G. Ma, Proton conduction in Ba x Ce0.8Y0.2O3−α + 0.04ZnO at intermediate temperatures and its application in ammonia synthesis at atmospheric pressure. Journal of Materials Science, 2011. 46(13): p. 4690-4694.

34. Wang, X.Y., Jinling Xu, Jianhong Wang, Ma, Guilin*, Chemical Stability, Ionic Conductivity of BaCe0.9 xZrxSm0.10O3-a and Its Application to Ammonia Synthesis at Atmospheric Pressure. 2011.

35. Amar, I.A., et al., Electrochemical synthesis of ammonia based on a carbonate-oxide composite electrolyte. Solid State Ionics, 2011. 182(1): p. 133-138.

36. Amar, I.A., et al., Electrochemical synthesis of ammonia based on doped-ceria-carbonate composite electrolyte and perovskite cathode. Solid State Ionics, 2011. 201(1): p. 94-100.

37. Vasileiou, E., et al., Ammonia synthesis at atmospheric pressure in a BaCe0.2Zr0.7Y0.1O2.9 solid electrolyte cell. Solid State Ionics, 2015. 275: p. 110-116.

38. Giddey, S., S.P.S. Badwal, and A. Kulkarni, Review of electrochemical ammonia production technologies and materials. International Journal of Hydrogen Energy, 2013. 38(34): p. 14576-14594.

39. Malavasi, L., C.A. Fisher, and M.S. Islam, Oxide-ion and proton conducting electrolyte materials for clean energy applications: structural and mechanistic features. Chemical Society Reviews, 2010. 39(11): p. 4370-4387.

40. Omata, T. and S. Otsuka-Yao-Matsuo, Electrical properties of proton-conducting Ca2+-doped

La2Zr2 O 7 with a pyrochlore-type structure. Journal of The Electrochemical Society, 2001. 148(6): p. E252-E261.

41. Shimura, T., S. Fujimoto, and H. Iwahara, Proton conduction in non-perovskite-type oxides at elevated temperatures. Solid State Ionics, 2001. 143(1): p. 117-123.

42. Furuya, N. and H. Yoshiba, Electroreduction of nitrogen to ammonia on gas-diffusion electrodes modified by Fe-phthalocyanine. J. Electroanal. Chem., 1989(263): p. 171-174.

43. Lan, R., J.T. Irvine, and S. Tao, Synthesis of ammonia directly from air and water at ambient temperature and pressure. Sci Rep, 2013. 3: p. 1145.

44. Wang, J. and R.-Q. Liu, Property research of SDC and SSC in ammonia synthesis at atmospheric pressure and low temperature. Acta Chim. Sin, 2008. 66: p. 717-721.

45. Liu, R. and G. Xu, Comparison of electrochemical synthesis of ammonia by using sulfonated polysulfone and nafion membrane with Sm1. 5Sr0. 5NiO4. Chinese Journal of Chemistry, 2010. 28(2): p. 139-142.

46. Xu, G., R. Liu, and J. Wang, Electrochemical synthesis of ammonia using a cell with a Nafion membrane and SmFe0.7Cu0.3−x Ni x O3 (x = 0−0.3) cathode at atmospheric pressure and lower temperature. Science in China Series B: Chemistry, 2009. 52(8): p. 1171-1175.

47. Lan, R. and S. Tao, Electrochemical synthesis of ammonia directly from air and water using a Li+/H+/NH4+ mixed conducting electrolyte. RSC Advances, 2013. 3(39): p. 18016.

48. Shi, M.M., et al., Au Sub-Nanoclusters on TiO2 toward Highly Efficient and Selective Electrocatalyst for N2 Conversion to NH3 at Ambient Conditions. Advanced Materials, 2017.

49. Speight, J.G., Lange's handbook of chemistry. Vol. 1. 2005: McGraw-Hill New York.

50. Su, D.S., S. Perathoner, and G. Centi, Nanocarbons for the development of advanced catalysts. Chemical reviews, 2013. 113(8): p. 5782-5816.

51. Centi, G., S. Perathoner, and D.S. Su, Nanocarbons: opening new possibilities for nano-engineered novel catalysts and catalytic electrodes. Catalysis Surveys from Asia, 2014. 18(4): p. 149-163.

52. Centi, G., E.A. Quadrelli, and S. Perathoner, Catalysis for CO2 conversion: a key technology for rapid introduction of renewable energy in the value chain of chemical industries. Energy & Environmental Science, 2013. 6(6): p. 1711.

53. Perathoner, S. and G. Centi, CO2 Recycling: A Key Strategy to Introduce Green Energy in the Chemical Production Chain. Chemsuschem, 2014. 7(5): p. 1274-1282.

54. Cherkasov, N., A.O. Ibhadon, and P. Fitzpatrick, A review of the existing and alternative methods for greener nitrogen fixation. Chemical Engineering and Processing, 2015. 90: p. 24-33.

55. Federation, W.E. and A.P.H. Association, Standard methods for the examination of water and wastewater. American Public Health Association (APHA): Washington, DC, USA, 2005.

CHAPTER 2

2. Verification of the possibility of Electrocatalytic ammonia synthesis at room temperature and atmospheric pressure from water and nitrogen

2.1 Introduction

Ammonia is produced on a large-scale (> 150 Mtons·y^{-1}) via the Haber–Bosch process developed in the early 1900s and still operating at high temperatures and pressures. This is the top largest chemical process in terms of energy consumption (about 2.5 EJ on a world scale) and thus one of top chemical synthesis processes to address to decrease the world total GHG (greenhouse gas) emissions related to chemical and petrochemical processes (about 1.24 $GtCO_2$-eq annually).[1] Although understanding of the ammonia synthesis catalysts is still in progress,[2] improvements in energy efficiency of ammonia synthesis have been minor and incremental over the last five decades with respect to the major improvements in energy use for this process occurred prior to 1930.[1] It is evident that a change in the impact of ammonia synthesis would require a change of technology, which could be fostered from the actual trend in rethinking industrial production to move from centralized large-scale processes to small-medium size distributed processed.[3] Another general driver for a change in technology for ammonia synthesis is the push to move to a "solar-driven chemistry", i.e. the possibility of using renewable energy rather than fossil fuels in chemical production.

There are thus various elements which restarted the interest on the development of alternative processes to the Haber Bosch one for ammonia synthesis. Various alternative approaches for ammonia synthesis have been investigated, including plasma-induced methods, biological methods, metallo-complexes methods, photocatalytic methods, and electrochemical methods. [4, 5] Among these methods, the last one appears as a promising solution particularly for the possibility to drive the process by using electrical

energy produced from renewable sources. In this way, the ammonia electrocatalytic production may be considered a way to store excess of renewable energy.

The state-of-the art on the electrocatalytic synthesis of NH_3 is discussed in some recent papers.[6-12] We should emphasize here only that very few studies have investigated the ammonia electrosynthesis at temperatures below 100°C and even less the highly challenging synthesis from N_2 and H_2O, i.e. without feeding H_2, but generating in-situ by water electrolysis. Kordali et al. [8] Firstly reported the use of H_2O rather than H_2. These authors used Ru/C as cathode, Nafion as electrolyte and Pt as anode, finding a rate of 1.9×10^{-7} $g_{NH3} \cdot h^{-1} \cdot cm^{-2}$ at 20°C (at -1.10 V of potential; the rate of ammonia formation is about four times higher at 90°C) with a Faradaic efficiency of 0.28 % (slightly lower at 90°C). Data on stability of the performances were not given, neither was exactly indicated the loading of Ru per cm^2 in the electrode. Better rates of ammonia electrosynthesis using H_2O and N_2 as feed were reported recently by Lan and Tao[13] on a Pt/C anode, although NH_4^+ was present in the $Li^+/H^+/NH_4^+$ mixed conducting electrolyte. The authors indicated that these ammonium ions do not contribute to the rate of ammonia formation, even if the reported data do not exclude this possibility. Faradaic efficiency was also low, below 0.1% at room temperature. Therefore, there are still quite limited results on the electrosynthesis of ammonia from H_2O and N_2 at room temperature and pressure, and data were only reported for noble metal based electrodes. It is thus still not reported the possibility of using alternative catalysts (not based on noble metals), which may have a different reaction mechanism, and for which an electrocatalytic behaviour is clearly present.

2.2 Scope of this chapter

The objective of this work is thus to analyse this possibility using a different type of electrodes, based on iron metal nanoparticles supported on conductive carbon nanotubes (CNT). This electrocatalyst is then deposited on a carbon paper-type

electrode to form a gas diffusion layer (GDL) type electrode joint to a Nafion membrane to prepare the membrane-electrode assembly. A non-conventional type of electrocatalytic cell was also developed for these tests, where the membrane-electrode assembly separates the two parts of the cell (Fig. 1), the first containing a diluted aqueous solution of $KHCO_3$ for water electrolysis and to generate the protons and electrons used in the other hemi-cell, where N_2 electrocatalytic conversion to NH_3 is realized in a gas-phase type flow electrocatalytic hemi-cell.

2.3 Low level of ammonia detection

Due to low ammonia formation rates around, 0.01-10 $\mu g \cdot h^{-1} \cdot cm^{-2}$, it was necessary to check which analytical detection method was the most suitable one for low ammonia concentrations quantification. The method used for low ammonia concentration detection was adapted from the standard methods for the examination of water and wastewater. [14] Ammonia concentration was detected by spectrophotometry with salicylic acid and/or ion selective electrode analysis (Orion™ High-Performance Ammonia Electrode 9512HPBNWP) methods. Initially, two absorbers (in series) were used to probe the ammonia produced. But it was found that all the ammonia was collected by the first absorber and no ammonia was measured in the second absorber. Therefore, only a single absorber was used in the remaining experiments.

2.3.1. Ammonia-selective electrode method

Apparatus: Electrometer; ammonia ion selective electrode - ISE (Thermo Scientific Orion high performance ammonia ion selective electrode Cat.No.9512HPBNWP); Magnetic stirrer.

Reagents: Ammonia-free water; Standard ammonium chloride solution: 1000 ppm as NH_4^+; Ionic Strength Adjuster (ISA).

Procedures

- Preparation of ammonia standards: a series of standard solutions were prepared with ammonium concentrations of 1 ppm, 0.5 ppm, 0.1 ppm, and 0.05 ppm (as NH_4^+) in 0.001 M H_2SO_4 (absorber).
- Electrometer calibration: First, the electrode was soaked in ammonia electrode storage solution (1 ppm standard with alkaline reagent) for at least 15 min; second, the meter measurement mode was changed to mV mode; third, 50 mL of each standard was introduced to beaker; fourth, 0.5 mL of alkaline solution was added to beaker; fifth, record the reading value until it was stable for 2 minutes; sixth, the standard curve was prepared with reading (mV) as Y axis and the value of lg(ppm) as X axis.
- Electrode slope check: The slope should be between 54 and 60 in a temperature range of 20-25 °C.
- 0.5 mL of alkaline was added 50 mL of sample. Record the value when it was stable for 2 minutes.
- Calculate this value with the calibration curve.

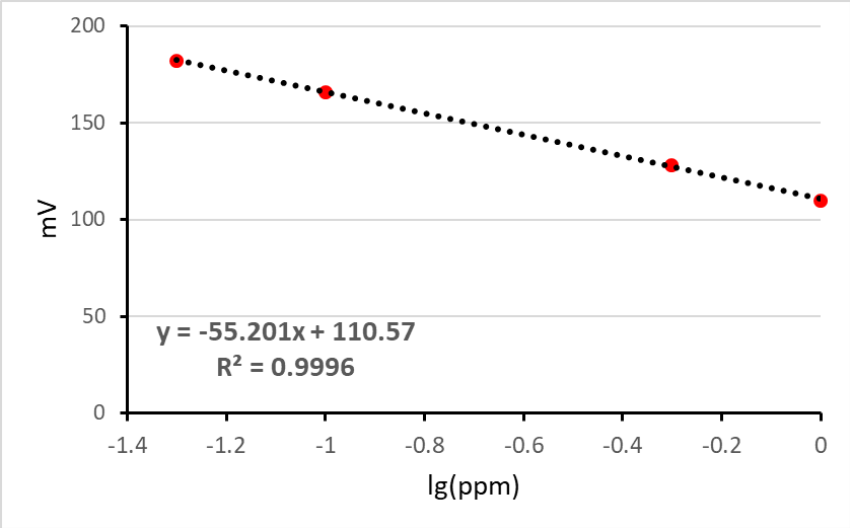

***Figure 2-1**. Calibration of NH_3 in 0.001M H_2SO_4 from 0.05 ppm to 1 ppm.*

2.3.2. Spectrophotometry measurement with salicylic acid

Apparatus: A spectrophotometer (Thermo Fischer Evolution 200) was used at fixed wavelength (λ=690 nm) with a light path of 1 cm.

Regents used: *Coloring solution:* sodium salicylate (0.4 M) and sodium hydroxide (0.32 M); **Oxidation solution**: sodium hypochlorite (ρ_{Cl}=4~4.9) and sodium hydroxide (0.75M); *Catalyst solution:* 0.1 g $Na_2[Fe(CN)_5NO]\bullet 2H_2O$ diluted to 10ml with deionized water. *Standard ammonium solution.*

Procedure:

4 mL of sample was taken. Then 50 µL of oxidizing solution, 500 µL of colouring solution and 50 µL of catalyst solution were added respectively to the sample solution. Absorbance measurements were performed after 1 hr at λ=690 nm. The calibration curve below was used to calculate the ammonia concentration.

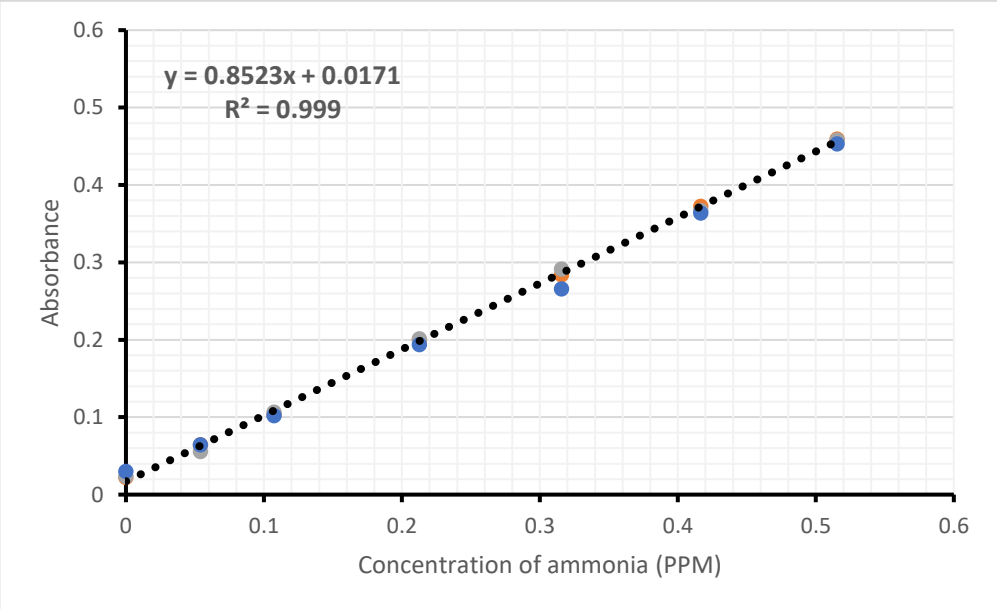

Figure 2-2 *Spectrophotometry with salicylic acid with three repetitions calibrations.*

Wavenumber selectivity: the maximum absorbance is centered at 690 nm. Comparing the curves in the same conditions, these give similar value on different calibration sets.

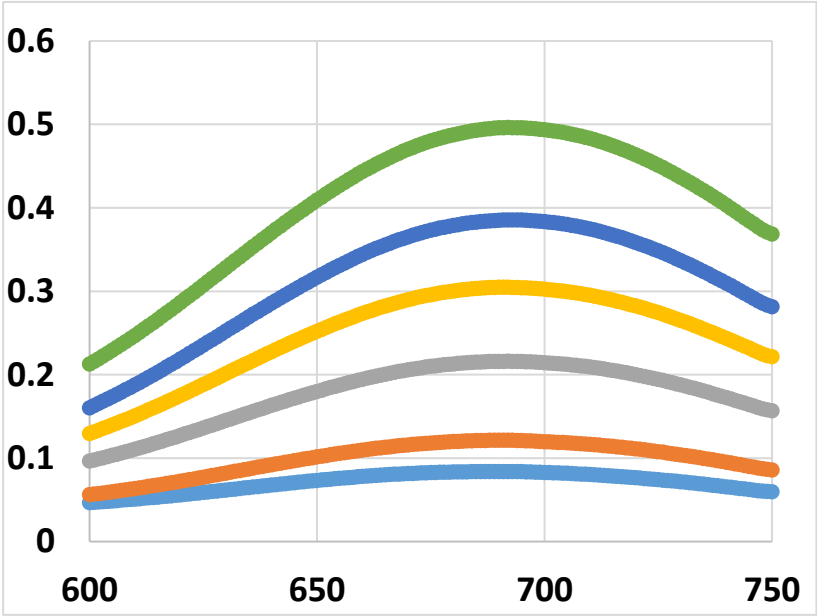

Figure 2-3 *Wave scan of the solution to select the detection wavenumber of the light.*

Both of this methods could be used as for ammonia (0.05 ppm -1 ppm) quantification. The final pH of the detection solution could affect the location of the maximum absorbance wavenumber. So keeping the same pH between samples and standard solution is important to acquire data with minimum errors.

2.4 Design of electrochemical cell for ammonia synthesis

The schematic view of the electrocatalytic flow reactor for ammonia synthesis is shown in ***Figure 2-4***. The cell operates at 20°C and atmospheric pressure. In the cathode hemi-cell where the reduction of N_2 to NH_3 occurs, operates in gas-phase (electrolyte-less conditions); in the anode hemi-cell where the oxidation of H_2O to O_2 occurs, operates in liquid-phase (0.5M $KHCO_3$ used as electrolyte). The hemi-cell where ammonia is synthetized operates with a continuous flow of nitrogen as reactants, after passing through the catalyst layer, the gas mixture (nitrogen and as produced hydrogen and ammonia) was introduced to a dilute sulfuric acid (0.001 mol/L). This design allows an easy recovery of ammonia from the gas stream leaving the cell. After reaction, the

ammonia in the absorber was quantified by Spectrophotometry measurement with salicylic acid. A membrane electrode was used to separate the anode and cathode chamber. The membrane-electrode assembly was used as working electrode in the cathode chamber, while Platinum was used as counter electrode and Ag/AgCl was used as reference in the anode chamber. The membrane-electrode assembly was fabricated by hot pressing a Nafion membrane (pre-purified) and the gas diffusion layer (Sigracet GDL 24BC).

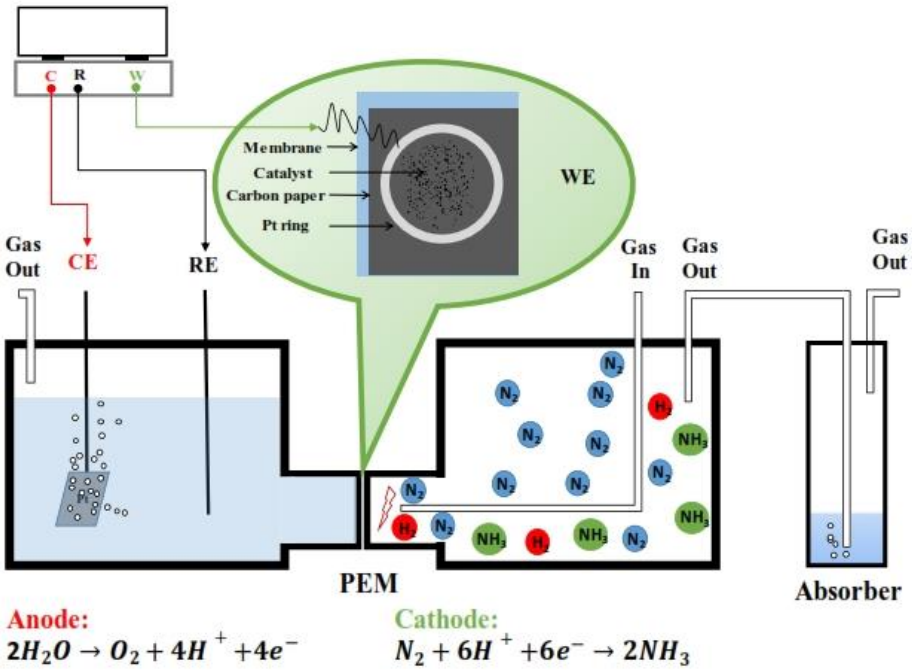

Figure 2-4 *Schematic view of the electrocatalytic flow reactor for ammonia synthesis, with the cathode cell operating under electrolyte-less conditions (gas phase). PEM indicates Proton Exchange Membrane.*

2.5 The affection of reference position

In the three-electrode system, the applied voltage is the potential difference between working electrode (WE) and reference electrode (RE), and the current density correspond to the current flow between working electrode (WE) and counter electrode (CE). The position of reference electrode will affect the current density when the same

voltage is applied. In other words, if a the constant current value was set, the different voltage could be observed by changing the position of reference. To confirm this idea, we modified the design of our cell, in which we are able to change the position of RE. After that a constant current (-8 mA) was applied, and the change in voltage with respect to the distance between RE and WE was detected. The working electrode (WE) was placed at x=0, and the counter electrode was fixed at x= 45 mm. Different distances between RE and WE were used i.e 1 mm, 5 mm, 10 mm, 15 mm, 20 mm, 30 mm, 40 mm 50 mm, and 60 mm. The voltage readings for each distance were therefore recorded after 10 min of stabilitization. The results obtained are summarized in ***Figure 2-5***. A linear correlation (R^2=0.9992) of the potential was obtained by varying the distance between RE and WE. In this work, all the data were acquired at a fixed reference position (15mm away from WE).

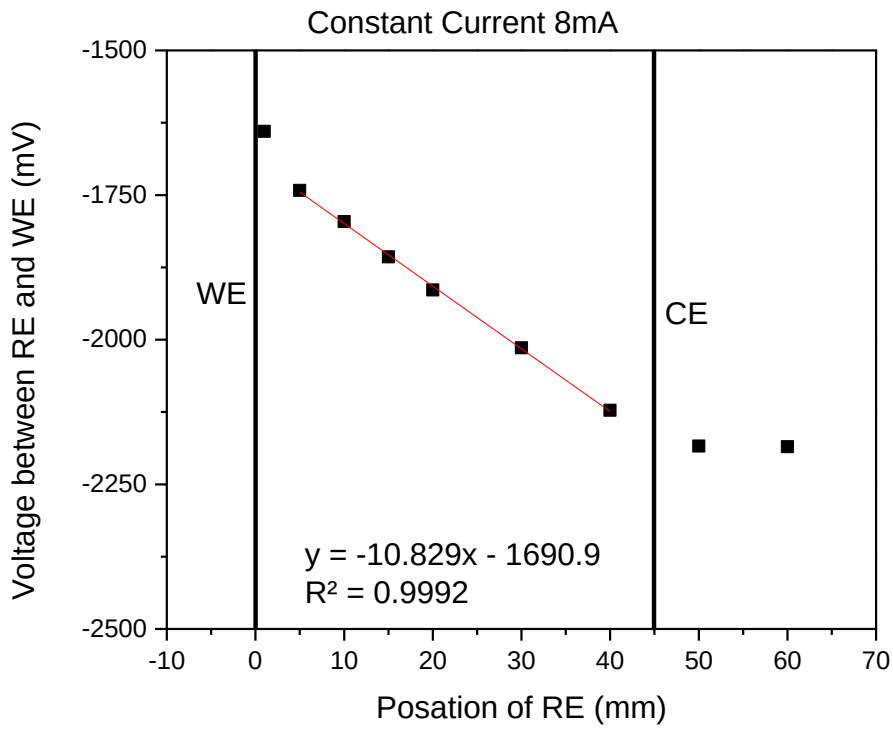

Figure 2-5. *Study the relationship between RE position and Voltage reading at -8 mA current.*

2.6 Preparation of the membrane electrode

2.6.1. Materials and Chemicals

Pyrograph®-III, CNT PR-24XT was used as pristine carbon nanotube (CNT). Commercial gas diffusion layer (SIGRACET GDL 24BC) was supplied by SGL Group. Commercial (Sigma-Aldrich) Fe(III)-oxide nanoparticle dispersion (<30 nm average particle size, 20 wt. % in ethanol), Nafion solution (10 wt.%), Nafion® 115 membrane, and all of other chemicals (no special instructions) were purchased from Sigma-Aldrich Co. LLC.

2.6.2. Electrocatalysts synthesis

o-CNT: 1 g of CNT was suspended in 100 mL concentrated HNO_3 (65 % Sigma Aldrich) and treated in a reflux setup at 100℃ for 3 hours, followed by rinsing until neutral pH and filtered. The sample was then dried at 80℃ overnight and grounded to obtain homogeneous o-CNT.

Fe_2O_3-CNT: 100 mg of the pretreated o-CNT was suspended in 10 mL of 2 mol/L $Fe(NO_3)_3$ solution and 1 mL ethanol was added to the suspension. The solution was ultrasonicated for 10 minutes, then filtered and dried at 80℃ overnight. The dried sample was then calcined for 2 hours at 350 ℃ in the furnace. Finally, the obtained sample was grounded in order to get uniform samples.

Ru/C: 2 cm^2 of carbon paper (GDL) was suspended in 30 mL of 0.05 mol/L $RuCl_3$ solution. The carbon paper was used as cathode and Pt was used as anode. The current density of 25 mA/cm^2 was applied for 1 hour. The carbon paper was washed with water and dried at 80℃ over night.

2.6.3. Preparation of the Gas diffusion layer (GDL)

Catalyst ink: 10 mg of the as prepared catalyst was suspended in 1~2 mL ethanol and 1-2 drops of Nafion solution was added. The solution was sonicated for 90 minutes to

get an uniform solution (catalyst ink).

GDL: The catalyst ink was deposited drop wise to evenly spread on to the Carbon paper that was used as support and then dried at 80℃ overnight.

2.6.4. Membrane electrode assembly

The following steps were used to assemble the final membrane electrode:

Nafion membrane pretreatment: Nafion® 115 membrane was cut in to small pieces and treated with some amount of 3 wt.% H_2O_2 water solution for 1 hour at 80℃. Then stirring in 0.5 mol/L H_2SO_4 solution for 1 hour at at 80℃ with stirring and following by rinsing until neutral pH. Finally, the obtained Nafion was kept in deionized water.

Hot-pressing: the GDL after depositing the catalyst and pretreated Nafion membrane were hot pressed together at 80 atm and 130 ℃ for 90 s. The active catalytic material was located between these two layers.

The membrane electrodes prepared in our study are named as follow:

Fe_2O_3-CNT: the membrane electrode with 10 mg of Fe_2O_3-CNT deposited on GDL and hot pressed with the Nafion membrane;

Ru: the membrane electrode with Ru electrodeposited on GDL and hot pressed with the Nafion membrane;

nano-Fe_2O_3: the membrane electrode with 10 mg iron-oxide on GDL and hot pressed with the Nafion membrane;

o-CNT: the membrane electrode with 10 mg o-CNT deposited on the GDL and hot pressed with the Nafion membrane;

blank: the membrane electrode without catalyst deposited on GDL and hot pressed with the Nafion membrane;

2.7 Reaction conditions and calculations

2.7.1. Reaction conditions

All the electrochemical measurements were carried out on AMEL 2551 potentiometer at 20℃. A Pt wire was used as the counter electrode. All the potentials were measured against Ag/AgCl reference electrode (3.0 M KCl). A catalyst deposited on a membrane-electrode assembly with 2 cm^{-2} active area was used as working electrode that separated the cathode and anode part of the cell. 10 mL/min of N_2 (purity, 99.9999%) was introduced to the cathode part of the system from 30 min before till the end of the reaction.

2.7.2. Calculations

- **Ammonia formation rates** were calculated using the following equation:

$$R_{NH_3}(mol \cdot cm^{-2} \cdot s^{-1}) = \frac{x(ppm) \times 10^{-3}(g/mg) \times V(L)}{Mr_{NH_4^+}\ (g/mol) \times t(s) \times S(cm^{-2})}$$

Where:

$R_{NH_3}(mol \cdot cm^{-2} \cdot s^{-1})$: is ammonia formation rate in $mol * cm^{-2}s^{-1}$.

X (ppm): is ammonia concentration in the detection solution in ppm (mg/L)

V (L): is volume of solution in liter.

$Mr_{NH_4^+} = 18\ (g/mol)$.

t (s): is the reaction time in seconds.

S: is active area of the membrane electrode in cm^2.

- **Faraday efficiency** of ammonia and hydrogen were calculated using the following equations:

$$FE_{NH_3}(\%) = \frac{3 \times R_{NH_3}(mol \cdot cm^{-2} \cdot s^{-1}) \times t(s) \times S(cm^{-2}) \times F}{I(A) \times t(s)} \times 100\%$$

$$FE_{H_2}(\%) = \frac{2 \times P_{H_2}(\%) \times F_{N_2}(mL/min) \times t(s) \div 60(s/min) \times F}{I(A) \times t(s) \times V_m(L/mol) \times 10^3(mL/L)} \times 100\%$$

Where:

F: Faraday constant,

I(A): the average of current during the reaction,

$P_{H_2}(\%)$: is the percentage of H_2 in the total gas flow.

$F_{N_2}(mL/min)$: the flow rate of N_2, 10 mL/min was used in the study.

V_m: the molar volume in standard condition (V_m = 22.4 L/mol).

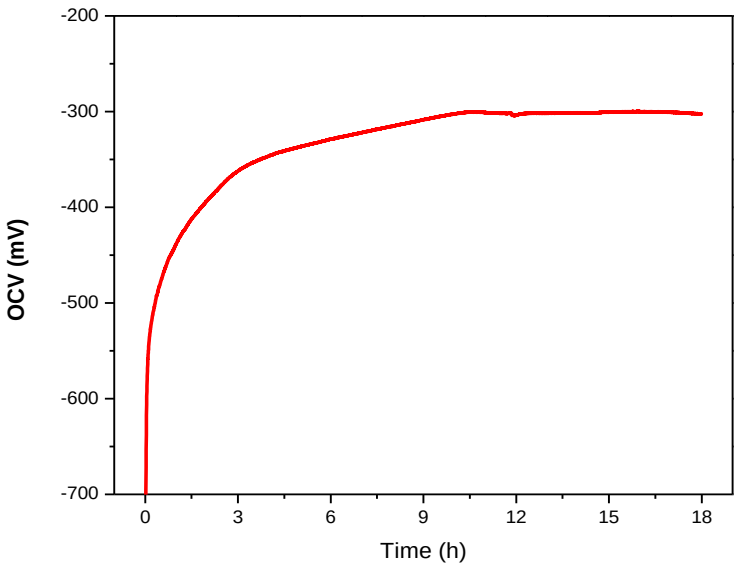

Figure 2-6 *The open circuit voltage (OCV) record when N_2 and H_2 (v:v=2:1) were introduced to cathode the chamber together.*

2.8 Results and discussion

The reaction was studied under both open and closed circuit conditions. In the case of open circuit condition (i.e. without application of a potential; this open circuit condition corresponds to the base catalytic activity of the electrode), the catalyst was first pre-activated by applying -2.0 V vs. Ag/AgCl voltage for 6 hours under N_2 flow, in order to have a preconditioning similar to that present during closed circuit operations. Then, N_2 and H_2 (v:v=2:1) were introduced together to the cathode chamber and the absorber, and the open circuit potential (OCV) value was recorded at the same time, ***see Figure 2-6***. The change in OCV is related to the partial reduction of the iron-oxide particles by H_2, as shown by electrocatalyst characterization. This reduction is a slow process and about 9h are necessary to arrive to a steady-state OCV value. In these tests, the presence of H_2 in the feed is necessary, because H_2 is produced on-site by water electrolysis in closed circuit operations. For this reason, H_2 is absent in the N_2 feed during closed circuit operations.

In the case of closed-circuit condition, the catalyst was first pre-activated using the same procedure applied for the OCV measurement. Then a N_2 flux was sent to the cathode chamber and to the absorber, and the following voltages (-2 V, -1.5 V, and -1.0 V vs. Ag/AgCl) were applied in this sequential order to the working electrode. The ammonia formation was monitored by measuring its concentration in the absorber and normalizing the data to the time of reaction and electrode area. NH_3 concentration measured by spectrophotometry method and ion selective electrode analysis . Figure 2-7(a) shows the current density profiles under the different applied voltages. Average current density of -3.88 $mA \cdot cm^{-2}$, -1.85 $mA \cdot cm^{-2}$ and -0.0955 $mA \cdot cm^{-2}$ were obtained when voltages of -2.0 V, -1.5 V and -1.0 V vs. Ag/AgCl were applied, respectively. It may be noted that the current density rapidly reaches a constant behaviour, differently from OCV tests, because further reduction of iron does not occur.

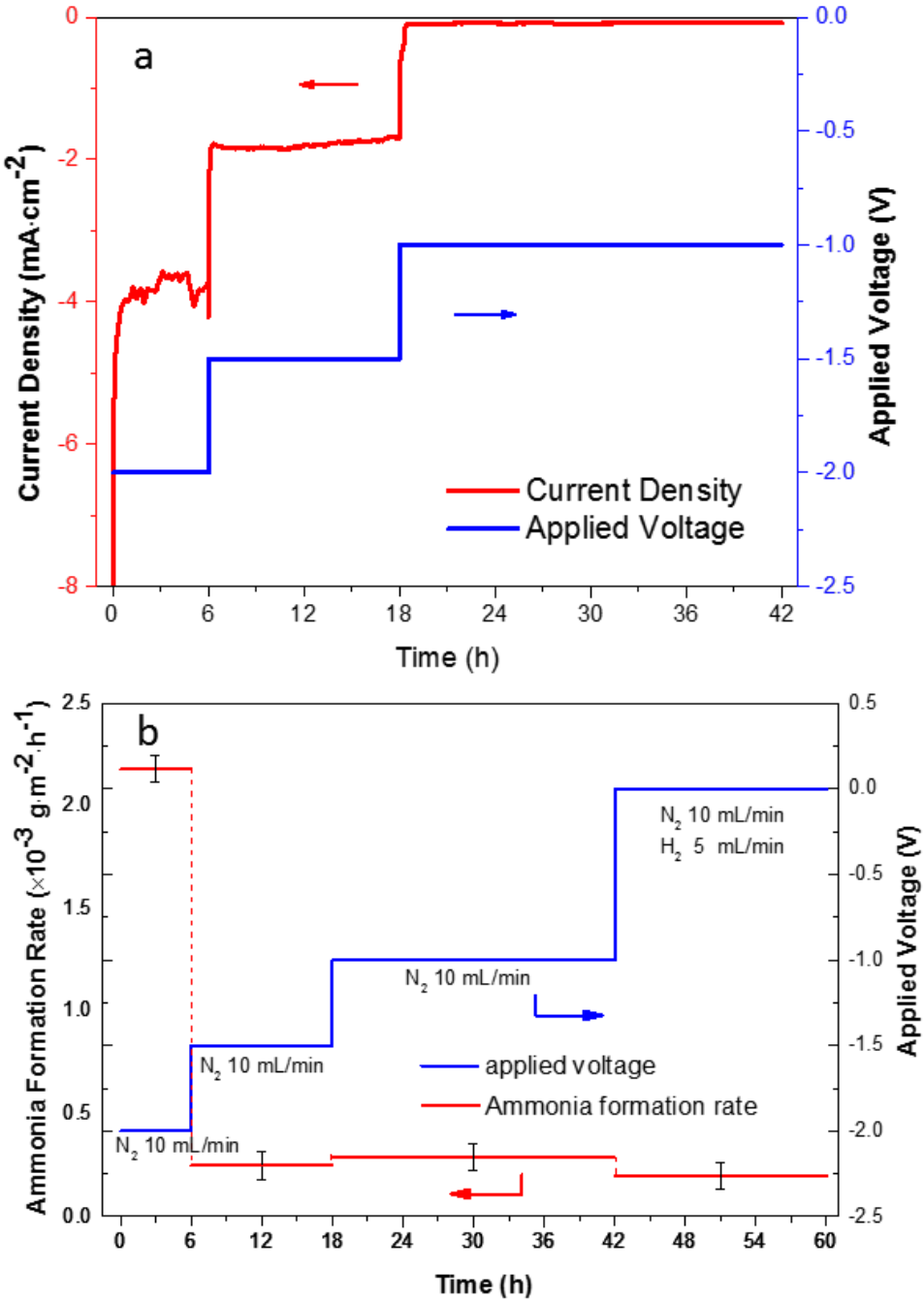

Figure 2-7 *Current density profiles under different applied voltages when the cathode was supplied with 10 ml/min of N_2. (b) Ammonia formation rates under different applied voltages when the cathode was feed with 10 mL/min of N_2. (0 V refers to the OCV test with N_2 and H_2 input).*

The ammonia formation rates under different applied voltages and OCV tests are shown in ***Figure 2-7b.*** Ammonia formation rates of 2.18×10^{-3}, 0.25×10^{-3}, 0.29×10^{-3} $g_{NH3}\cdot m^{-2}\cdot h^{-1}$ were observed with applied voltages of -2.0 V, -1.5 V and -1.0 V vs. Ag/AgCl, respectively. The ammonia formation rates were almost the same of the OCV test when a voltage ≥ -1.5 V vs. Ag/AgCl was applied, while the rate of ammonia formation is about one order of magnitude higher when the potential is - 2.0 V. Liner sweep voltammetry was performed to study the onset potential, as shown in ***Figure 2-8.*** Thus a threshold potential (< - 1.5 V) is necessary in order to have the electrocatalytic synthesis of ammonia from N_2 and H_2O. These rates at each applied voltage could be reproduced, when the voltage is further changed from -1.0 V to -2.0 V, showing the reversibility of the effect.

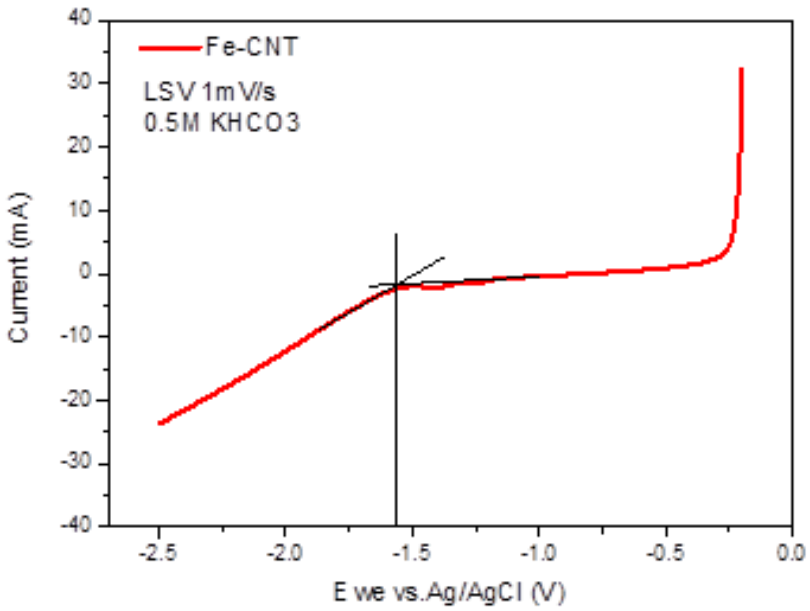

Figure 2-8. *On set potential of Fe_2O_3-CNT in this cell. (conditions: 0.5M $KHCO_3$ as electrolyte, 10mL/min N_2 and scan speed was 1 mV/s from -200 mV to -2500 mV. Accord to the profile, the onset potential of Fe_2O_3-CNT for N_2 reduction is lower than -1.5V vs. Ag/AgCl in our cell.)*

The Faraday efficiency of the reactions is reported in ***Figure 2-9***. For potentials ≥ - 1.5 V, the current densities are quite low and thus significantly affected from the experimental error. The Faraday efficiency in ammonia formation is low, but comparable with that reported earlier under similar reaction conditions.[8,10-12] The low Faradaic efficiency is related to the side reaction of hydrogen evolution, with thus formation of a mixture of NH_3 and H_2 in the N_2 stream leaving the electrochemical cell. Recirculation of this stream improves the overall performances and Faraday efficiency, although this side reaction of H_2 generation should be avoided to improve the behaviour.

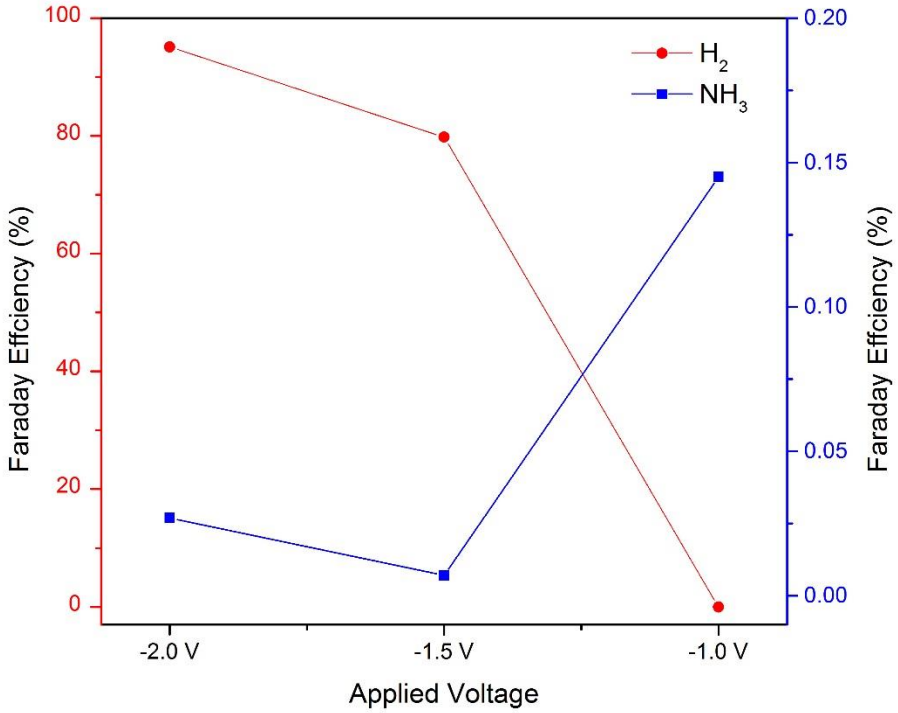

Figure 2-9 *Faraday efficiency values of ammonia formation and H_2 evolution under different applied voltages.*

The total Faraday efficiency obtained when the voltage of -2.0 V vs. Ag/AgCl was applied (95.1%) is higher than the value reported by Licht et al. on *Science* paper in 2014 (65% total Faraday efficiency using a molten salt system at 250°C and 25 bar).[17]

The observed reaction rates of ammonia formation could be further improved in the view of the low Faraday efficiency, which limits the amount of hydrogen available for

the synthesis of ammonia. As a matter of fact, by recirculation of the outlet stream of the electrochemical cell after ammonia absorption (thus a flux of N_2 with some H_2), the rate of ammonia formation is significantly enhanced (not shown here), although as demonstrated the rate of "catalytic" synthesis of NH_3 from N_2 and H_2 is negligible under our experimental conditions. There is thus a synergic effect between presence of H_2 in the feed and the applied voltage, which is under investigation. This is confirmed by literature results[10-12] showing, in general, a higher formation rate of ammonia by feeding H_2 together with N_2, rather than when H_2 is produced on-site by water or steam electrolysis. As shown in ***Figure 2-7***, this effect cannot be attributed to a simple contribution of a catalytic ("thermal") contribution to the reaction rate of ammonia formation, at least in our case.

The role of the electrocatalyst was also investigated to investigate whether there is a specific role of the electrocatalyst used (Fe_2O_3-CNT). For this reason, the behaviour of the electrode-membrane assembly without loading the electrocatalyst (indicated as blank) was investigated, as well the behaviour of the electrode-membrane assembly on which activated carbon nanotube without depositing the iron nanoparticles were deposited (indicated as o-CNT) or on which Fe_2O_3 nanoparticles (< 30 nm on the average) were directly deposited (i.e. without depositing prior on activated CNT). The latter sample is indicated as nano-Fe_2O_3. And in order to directly compare with the work by Kordali et al, electrode-membrane with Ru eletrodeposied on was prepare in the same method. [8] Therefore, being the iron-oxide loading in the latter sample about 14% wt., the total amount of iron-oxide in the nano-Fe_2O_3 sample is about seven times higher. This would compensate the fact that in this nano-Fe_2O_3 sample the average particle size is higher than in Fe_2O_3-CNT sample (5-10 nm). The electrocatalytic surface area results thus comparable in the two samples.

The Fe_2O_3-CNT catalyst used in this study was synthesized starting from commercial

carbon nanotubes, first functionalized by using concentrated HNO_3 to form CNT with various oxygen functional sites, following standard activation procedures for CNTs.[16] This sample is indicated as o-CNT hereinafter. The iron-oxide is then deposited by wet impregnation of the o-CNT. The as prepared Fe_2O_3-CNT or o-CNT were spread out evenly on the GDL and hot pressed with Nafion membrane to form the electrode-membrane assembly used then in the electrocatalytic reactor ((***Figure 2-1***).). The same procedure was used to prepare the samples indicated as nano-Fe_2O_3, o-CNT and blank, with the changes indicated above. The loading of the electrocatalyst on the electrode was about 10 mg in all cases. The GDL deposited with Ru and hot pressed with Nafion membrane indicated as Ru (***Figure 2-10***). The iron-oxide reduces during the activation stage of the electrocatalytic tests, as commented before. Therefore, the indication of iron-oxide here refers to only the starting situation before the electrocatalytic tests.

The behaviour of these electrode-membrane assemblies is reported in ***Figure 2-10***. The experimental conditions are those giving the best results for Fe_2O_3-CNT sample. Current density profiles at applied voltage of -2.0 V vs. Ag/AgCl with Fe_2O_3-CNT, nano-Fe_2O_3, o-CNT, Ru and blank samples are shown in ***Figure 2-10a***, while the ammonia and H_2 formation rates are summarized in ***Figure 2-10b.***

For the blank membrane-electrode assembly, current density of 0.05 $mA \cdot cm^{-2}$ and an ammonia formation rate of 0.46×10^{-3} $g_{NH3} \cdot m^{-2} \cdot h^{-1}$ were obtained when the voltage of -2.0 V vs. Ag/AgCl was applied. This rate of ammonia formation and the current density are similar to those obtained by Fe_2O_3-CNT membrane-electrode assembly, when the potential is ≥ -1.5V, but largely lower to that observed when the applied potential is -2.0 V. (nano-Fe_2O_3 and Ru also in this level)

The o-CNT (or nano-Fe_3O_4 in this version not included) samples show a slightly increase of the rate of ammonia formation (***Figure 2-10b***), but the values still remain about three-four times lower with respect to the case when the Fe_2O_3-CNT electro-

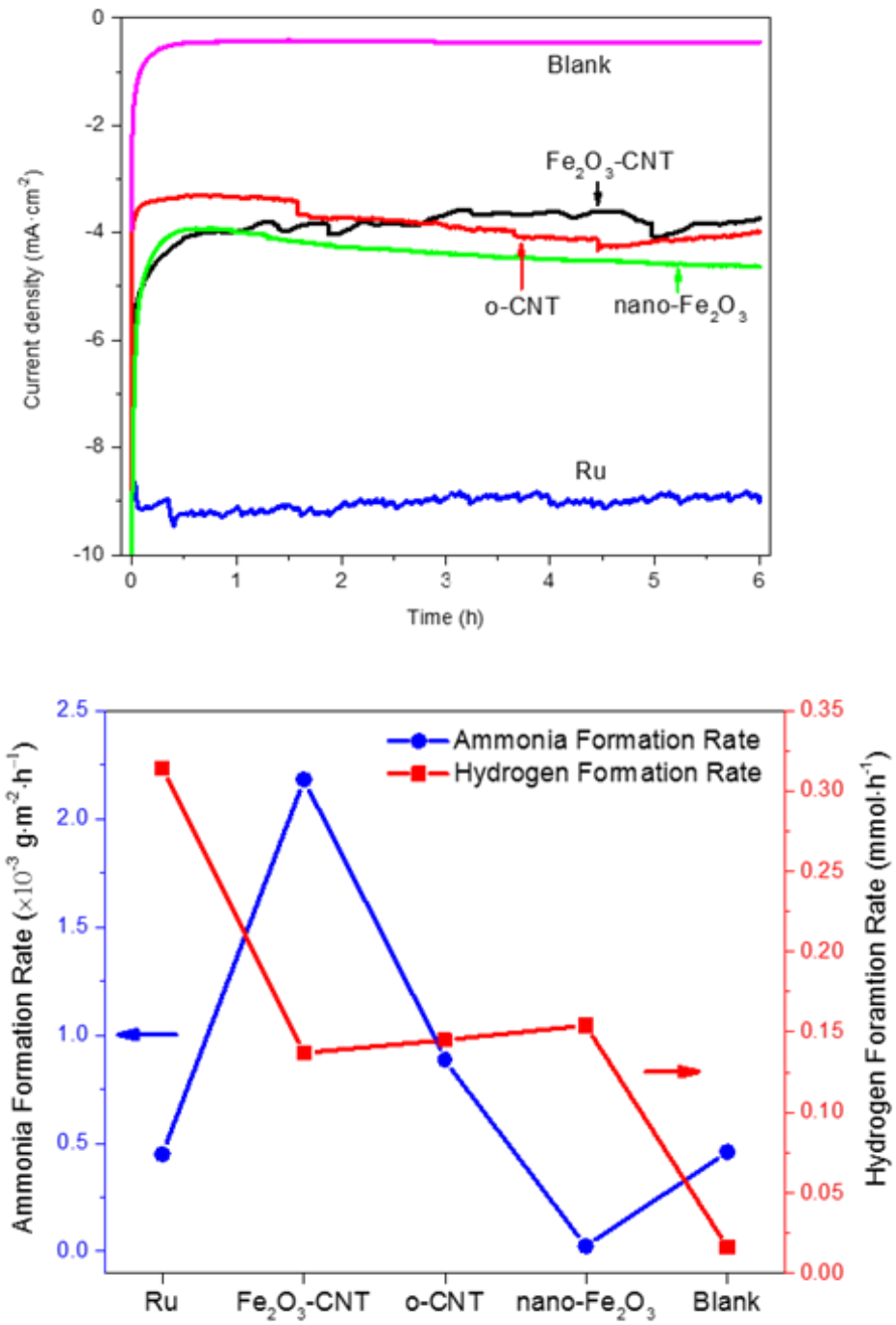

Figure 2-10 *(a) Current density profiles under applied voltage of -2.0 V vs. Ag/AgCl with Ru, Fe_2O_3-CNT, o-CNT, nano-Fe_2O_3 and blank membrane electrodes; (b) Ammonia formation rates and hydrogen percentages in the gas flow with Ru, Fe_2O_3-CNT, o-CNT, nano-Fe2O3 and blank membrane electrodes.*

catalyst is used (for a potential of – 2.0 V). It may be noted that for nano-Fe_2O_3 and o-CNT electrocatalysts, the hydrogen formation rate is higher than in the case of Fe_2O_3-CNT electrocatalyst (***Figure 2-10b***) (Ru curve is an evidence for this comment). This evidences that the rate of NH_3 formation is not depending on the amount of H_2 generated in situ and it is related to the presence of specific sites able to activate N_2 and then hydrogenate it. Due to the synergic effect between iron nanoparticles and CNT, we may advance the hypothesis that these sites are generated at the interface between iron nanoparticles and CNT. Special morphology of iron oxide was induced in the absence of CNT.

It is worth to note that the trend of current density curves vs. time on stream (***Figure 2-10a***) shows a relatively stable behaviour after the initial activation stage (about 1h). Even more extended tests evidenced stable catalytic performances and current densities in the investigated reaction conditions. This indicates the absence of deactivation of the electrocatalytic performances, at least within about 60h of continuous experimentation. It may be also noted in ***Figure 2-10a*** that the transient in current density curves for blank, Ru and o-CNT sample is significantly shorter than for the samples containing iron, in agreement with the previous indication that iron-oxide initially reduces. We may also see that the time to reach a constant current density is longer for nano-Fe_2O_3 sample with respect to Fe_2O_3-CNT, but this could be explained from the average slightly higher size of the iron-oxide nanoparticles in the former sample.

In summary, ammonia was successfully synthesized by electrocatalytic reduction of N_2 using water as hydrogen source at room temperature and atmospheric pressure. Fe_2O_3-CNT was used as electrocatalyst and the performances are higher than those earlier reported using noble metals (Ru/C) as electrocatalyst. Being Ru significantly more active than iron in the catalytic activation of N_2 to ammonia, we believe that the difference of the behaviour is related to specific carbon sites formed likely at the

interface between iron particles and CNT and able to activate N_2, making it more reactive towards hydrogenation. Studies are in progress to demonstrate this suggestion, but the comparison of the performances of different electrocatalysts (***Figure 2-10***) support this indication.

Total Faraday efficiency as high as 95.1% was obtained, even if the Faradaic efficiency to ammonia must be improved. While the overall Faradaic efficiency is an important target, the production of H_2 is less critical, because it may be recirculated and this helps in increasing the rate of ammonia formation, as commented before. Therefore, there are indications both from the design of the electrocatalysts and from the reactor operations that the performances in the electrocatalytic synthesis of ammonia at room temperature and pressure could be further increased. These results, however, proof-the-concept that this reaction could be realized with low-cost type of electrodes which do not contain noble metals and that could be easy fabricated.

2.9 Conclusion

we have shown here the possibility to realize the synthesis of ammonia under very mild conditions (room temperature and ambient pressure) starting from H_2O and N_2, and using electrical energy which could be provided from renewable energy sources, fully in line with the requirement to move to a "solar-driven chemistry" not based on the use of fossil fuels, with consequent decrease of the greenhouse gases emissions. Present data represent a breakthrough on the type of electrocatalysts used, but also contain the elements to indicate an expected further progress. We thus believe that these results could open a new direction in the development of systems for the electrocatalytic synthesis of ammonia from H_2O and N_2.

2.10 References

1. Centi, G., Quadrelli, E. A., & Perathoner, S. (2013). Catalysis for CO 2 conversion: a key technology for rapid introduction of renewable energy in the value chain of chemical

industries. *Energy & Environmental Science*, *6*(6), 1711-1731.

2. Kandemir, T., Schuster, M. E., Senyshyn, A., Behrens, M., & Schlögl, R. (2013). The Haber–Bosch process revisited: on the real structure and stability of "ammonia iron" under working conditions. *Angewandte Chemie International Edition*, *52*(48), 12723-12726.
3. Cavani, F., Centi, G., Perathoner, S., & Trifirò, F. (Eds.). (2009). *Sustainable Industrial Chemistry: Principles, Tools and Industrial Examples*. John Wiley & Sons.
4. Schlögl, R. (2003). Catalytic Synthesis of Ammonia—A "Never-Ending Story"?. *Angewandte Chemie International Edition*, *42*(18), 2004-2008.
5. Broda, H., & Tuczek, F. (2014). Catalytic Ammonia Synthesis in Homogeneous Solution—Biomimetic at Last?. *Angewandte Chemie International Edition*, *53*(3), 632-634.
6. Oshikiri, T., Ueno, K., & Misawa, H. (2016). Selective Dinitrogen Conversion to Ammonia Using Water and Visible Light through Plasmon-induced Charge Separation. *Angewandte Chemie*, *128*(12), 4010-4014.
7. Giddey, S., Badwal, S. P. S., & Kulkarni, A. (2013). Review of electrochemical ammonia production technologies and materials. *International Journal of Hydrogen Energy*, *38*(34), 14576-14594.
8. Kordali, V., Kyriacou, G., & Lambrou, C. (2000). Electrochemical synthesis of ammonia at atmospheric pressure and low temperature in a solid polymer electrolyte cell. *Chemical Communications*, (17), 1673-1674.
9. Cherkasov, N., Ibhadon, A. O., & Fitzpatrick, P. (2015). A review of the existing and alternative methods for greener nitrogen fixation. *Chemical Engineering and Processing: Process Intensification*, *90*, 24-33.
10. Shipman, M. A., & Symes, M. D. (2017). Recent progress towards the electrosynthesis of ammonia from sustainable resources. *Catalysis Today*, *286*, 57-68.
11. Kim, K., Yoo, C. Y., Kim, J. N., Yoon, H. C., & Han, J. I. (2016). Electrochemical synthesis of ammonia from water and nitrogen in ethylenediamine under ambient temperature and pressure. *Journal of The Electrochemical Society*, *163*(14), F1523-F1526.
12. Garagounis, I., Kyriakou, V., Skodra, A., Vasileiou, E., & Stoukides, M. (2014). Electrochemical synthesis of ammonia in solid electrolyte cells. *Frontiers in Energy Research*, *2*, 1.
13. Lan, R., & Tao, S. (2013). Electrochemical synthesis of ammonia directly from air and water using a Li+/H+/NH 4+ mixed conducting electrolyte. *RSC Advances*, *3*(39), 18016-18021.
14. Perathoner, Siglinda, Gabriele Centi, and Dangsheng Su. "Turning perspective in photoelectrocatalytic cells for solar fuels." *ChemSusChem* 9.4 (2016): 345-357.
15. Licht, Stuart, et al. "Ammonia synthesis by N2 and steam electrolysis in molten hydroxide suspensions of nanoscale Fe2O3." *Science* 345.6197 (2014): 637-640.
16. Su, D. S., Perathoner, S., & Centi, G. (2013). Nanocarbons for the development of advanced

catalysts. *Chemical reviews*, *113*(8), 5782-5816.

CHAPTER 3

3. Optimized conditions for Room Temperature Electrocatalytic Synthesis of NH_3 from H_2O and N_2 in a Gas-Liquid-Solid Three-phase Reactor

3.1 Introduction

A major challenge facing chemistry to move to a sustainable, low-carbon future is to avoid the need of using fossil fuels to supply the energy to drive the processes, which accounts for the largest part of carbon oxides emissions. A major current effort is thus to develop novel synthetic paths using directly renewable energy (RE) sources to drive industrial processes.[1] Being ammonia the largest-scale chemical (> 150 Mtons·y^{-1}) with the top largest chemical process in terms of energy consumption (about 2.5 EJ on a world scale), it is not surprising the fast emerging interest to develop new solutions to synthetize NH_3 from N_2 using RE as energy source for the process. Between the various solutions under development, the electrocatalytic conversion of N_2 is one of the most attracting and one of the challenging directions is the possibility of N_2 and H_2O co-electrolysis in very mild conditions, around room temperature and atmospheric pressure. [2-7] This solution offers also attractive possibilities for a distributed production of fertilizers.[2]

While initial studies on the ammonia electrosynthesis from N_2 at temperatures below 100°C with in-situ generation of the H_2 (or H^+/e^- equivalents) from H_2O were based on the use of noble-metal supported catalysts,[8,9] we reported recently that iron nanoparticles supported on carbon nanotubes (Fe/CNT) are effective and stable electrocatalysts in this process. [10] The use of electrocatalysts not containing noble metals is a relevant target to avoid the use of critical raw materials and thus further enhance the sustainability of the novel process.

A general issue present in literature on the ammonia electrosynthesis from N_2 in mild

reaction conditions is that the efficiency of the process greatly depend on the type and configuration of the electrocatalytic reactor and reaction conditions, besides that from the electrocatalyst, although there are often not clear indications on these aspects. The objective of this work is thus to analyse both the optimization of the Fe/CNT electrocatalyst and of the reactor/reaction conditions, in particular the pH and nature of the electrolyte, the iron loading and type of iron species supported on CNTs, and membrane-assembly in the electrocatalytic reactor. A relevant aspect to remark, in fact, is that to improve the scalability and applicability of the results, it is necessary to utilize an electrocatalytic reactor design different from the conventional electrocatalytic cells and closer to the design in proton exchange membrane (PEM)-type fuel cells, where gas-diffusion electrodes on both sides of the proton-conductive membrane are used. This compact design allows a faster scale-up and additional advantages, as remarked for photo-electro catalytic (PEC) cells. [11] However, this design influences also the performances and characteristics of the electrodes to develop. Specifically, we will discuss here how to optimize both the electrocatalysts and reactor/reaction conditions used in the early report, [10] where a non-conventional electrocatalytic cell was used. This cell is characterized by a membrane-electrode assembly separating the two parts of the cell, the first containing a diluted aqueous solution for water electrolysis to generate the protons and electrons used in the other hemi-cell, where N_2 electrocatalytic conversion to NH_3 is realized in a gas-phase type flow electrocatalytic hemi-cell. This configuration allows an easy recovery of ammonia from the flow cell.

3.2 Material and methods

Materials and Chemicals. Pyrograph®-III, CNT PR-24XT were used as carbon nanotubes (CNTs). A commercial gas diffusion layer (SIGRACET GDL 29BC) supplied by SGL Group and Nafion®115 membrane (Sigma Aldrich) were used to prepare the electrode. Nafion solution (10 wt%) was used to prepare the catalyst ink.

Iron (III) nitrate nonahydrate (Sigma Aldrich, 99.9% purity) was used as precursor during the Fe_2O_3-CNT synthesis. Commercial Fe(III)oxide nanoparticle (<30 nm average particle size) was also used as electrocatalyst for comparison.

Preparation of Electrodes. The preparation of electrodes can be summarized in the following steps.

Step I: synthesis of electrocatalysts

Synthesis of the electrocatalysts starts with pretreatment of the commercial CNTs in order to purify and create surface oxygen functionalities (o-CNT). Briefly, 1 g of CNTs was suspended in 100 mL concentrated HNO_3 (Sigma Aldrich, 65%) and treated at 120℃ for 2 h in a reflux setup. The suspension was filtered and washed with DI water until neutral pH. The sample was then dried at 80℃ overnight and grounded to obtain homogeneous o-CNT.

Table 2. *Precursors amount of different iron loading amount sample*

	Theoretical iron loading, %	Iron loading by AAS, %
5% Fe_2O_3-CNT	6.65	6.16
20% Fe_2O_3-CNT	20.22	18.50
30% Fe_2O_3-CNT	29.55	28.68
45% Fe_2O_3-CNT	46.10	45.25

Weight percentage with the respect to the weight of iron oxide (Fe_2O_3).

Fe_2O_3-CNT synthesis: 0.5 g of pretreated o-CNT and $Fe(NO_3)_3 \cdot 9H_2O$ (amount was taken with respect to loading %) were dissolved in 25 mL of DI water with 1 mL ethanol glycol. The mixture was then sonicated for 30 minutes and pH was adjusted to 8 with a 5% ammonia solution. After adjusting the pH, the solvent is eliminated

and the sample then dried at 120°C. The dried sample was then calcined for 2 hours at 400℃ in a tubular furnace under He flow. Finally, the obtained sample was grounded to get a homogeneous catalyst. Different samples with iron loading in the 6-46% wt. range were prepared as reported in Table 2.

Step II: deposition of the elecatrocatalyst on gas diffusion layer (GDL)

10 mg of the as prepared electrocatalyst was suspended in a 5 mL ethanol and 50 µL Nafion solution. The solution was sonicated for 90 minutes to get homogeneous mixture. Finally, the solution was load by spray drying uniformly on the gas diffusion layer (GDL) heated on a hot plate at 100℃. The GDL with electrocatalyst was stored in an oven at 80℃ overnight.

Step III: assembling the electrode

The GDL after depositing the catalyst and a pretreated Nafion membrane were hot pressed together at 80 atm and 130℃ for 30 s. The active composite material was located between these two layers. The membrane electrodes are defined as follow:

Fe_2O_3-CNT: Membrane Electrode Assemblies (MEA) with 10 mg of Fe_2O_3-CNT deposited on GDL and hot pressed with the Nafion membrane;

nano-Fe_2O_3: MEA with 10 mg iron-oxide (deposited using commercial Fe(III) oxide nanoparticle dispersion) on GDL and hot pressed with the Nafion membrane;

o-CNT: MEA with 10 mg o-CNT deposited on the GDL and hot pressed with the Nafion membrane;

blank: MEA without catalyst deposited on GDL and hot pressed with the Nafion membrane.

For the improved cell configuration, additional GDL without electrocatalyst was inserted between the catalyst layer and Nafion membrane.

Catalyst Characterization. Atomic absorption spectroscopy (AAS) was used to analyze the iron loading of the as prepared materials. Catalysts were characterized also by various methods (not reported here), including transmission electron microscopy (TEM) and high-angle annular dark field scanning TEM (HAADF-STEM), X-ray diffraction (XRD), X-ray photoelectron spectroscopy (XPS) and temperature programmed reduction (TPR) to verify their characteristics and reproducibility.

Testing conditions. All the electrochemical measurements were carried out at 20°C using a potentiostat /galvanostat AMEL 2551. A Pt wire was used as the counter electrode. All the potentials were measured against Ag/AgCl reference electrode (3 M KCl). A non-conventional type of electrocatalytic cell (operating at atmospheric pressure and room temperature) was developed for these tests, where the solid membrane-electrode assembly separates gas and liquid zones (**Figure 3-1**).

The liquid chamber contains a liquid electrolyte for water electrolysis to generate the protons and electrons. The protons and electrons were used in the solid membrane (gas-diffusion) electrode, where the electrocatalytic conversion of N_2 to NH_3 took place. The solid zone consists of a Nafion membrane, catalyst layer and gas diffusion layer. The reactant N_2 (acting both as reactant and transport gas for generated ammonia) was continuously fed (20 mL/min of N_2 with purity, 99.9999%), and the flow coming out from the electrocatalytic reactor outlet (containing a mixture of N_2 and ammonia) is sent to a liquid absorber containing a 0.001 M H_2SO_4 solution. The amount of ammonia formed is monitored by a spectrophotometry method. The N_2 may be eventually recycled. The N_2 flow is introduced to the cathode part of the cell 30 min before the starting the reaction and then continuously fed till the end of the test. Further details were described in our previous work. [10]

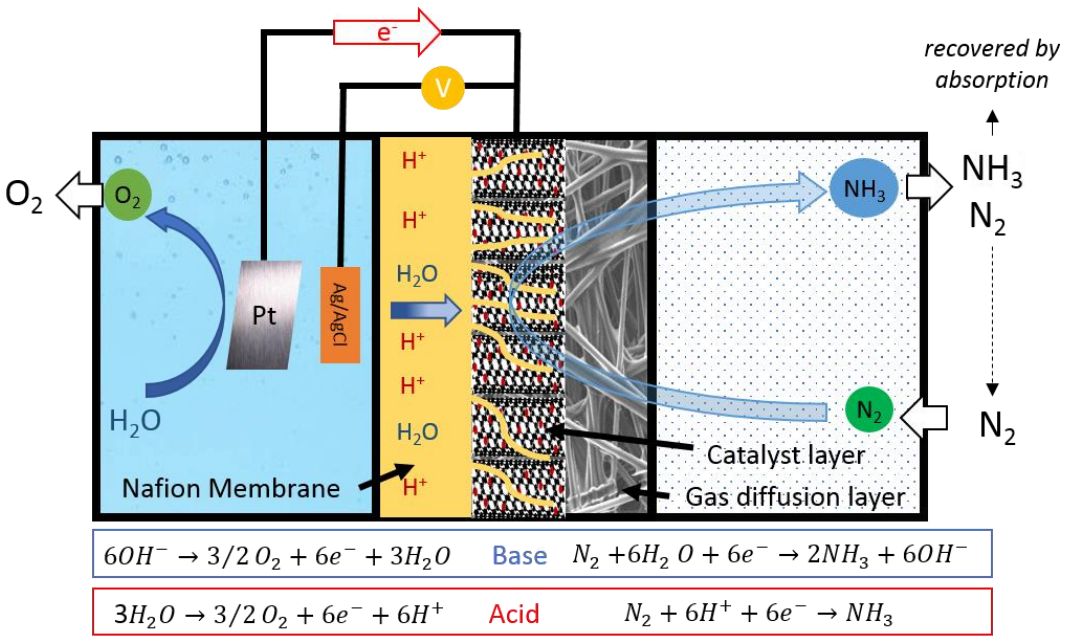

Figure 3-1 *Schematic view of the three-phase reactor for electrochemical ammonia synthesis*

3.3 Results and discussion

3.3.1. The effect of iron content

The effect of iron oxide loading in Fe_2O_3/CNT electrocatalysts on the performances in NH_3 formation by N_2 and H_2O co-electrolysis at room temperature and atmospheric pressure is summarized in ***Figure 3-2***. The following membrane-electrode assemblies were tested: without the catalyst (blank) and with 2.5 mg/cm^2 of o-CNT, 5% Fe_2O_3-CNT, 10% Fe_2O_3-CNT, 30% Fe_2O_3-CNT, 45% Fe_2O_3-CNT and nano-Fe_2O_3 as the electrocatalyst. All the tests were made using 0.5 M KOH as an electrolyte, voltage of -2.0 V vs. Ag/AgCl and a constant flow of 20 mL/min N_2. ***Figure 3-2a*** reports the measured current densities as a function of the time on stream, while Figure 2b summarizes the ammonia formation rate for the various membrane-electrode assemblies.

Since the working electrode is used as cathode, the values of current and applied voltage are negative according to the direction of current. In the following discussions, indications to higher or lower values refer thus to the absolute value. The lowest current density (-0.452 mA/cm^2) was shown by the blank sample, while the highest current density (-7.1 mA/cm^2) was shown by nano-Fe_2O_3. Note, however, that this sample, being composed of only iron-oxide rather than iron-oxide loaded on CNTs contains a higher iron amount. The current density of x-Fe_2O_3-CNT (x= 0, 5%, 20%, 30% and 45%) increased with increasing iron loading. It is worth to point out that the current density shown by the sample 45% Fe_2O_3-CNT is almost the same of that shown by nano-Fe_2O_3, which indicates that the current density would not further increase when the iron loading amount upraises values higher than 45%. Note that in all cases the current density is stable with time and thus there are no indications of deactivation or changes in the membrane-electrode assembly. The tests in ***Figure 3-2a*** are related for reaction times of 4 h, but tests for longer times, up to 50 h of time on stream, showed a similar stable behavior in terms of current density.

The average ammonia formation rates were also measured and reported in Figure 2b. The lowest average ammonia formation rate of 0.75×10^{-12} mol·cm^{-2}·s^{-1} was obtained by the blank sample (carbon paper and Nafion membrane used as working electrode without catalyst). The average of ammonia formation rate shown by o-CNT and nano-Fe_2O_3 was 3.44×10^{-12} mol·cm^{-2}·s^{-1} and 1.49×10^{-12} mol·cm^{-2}·s^{-1}, respectively. These values are lower than the rates obtained by all the other x-Fe_2O_3-CNT(x= 0, 5%, 20%, 30% and 45%) samples. Maximum of ammonia formation rate of 6.74×10^{-12} mol·cm^{-2}·s^{-1} was observed by 30% Fe_2O_3-CNT among all the samples tested.

Only NH_3 and H_2 were detected during all the tests. The total Faradic efficiencies were higher than 90% among all the electrocatalysts. The Faradaic selectivity to ammonia is 0.028% for 30% Fe_2O_3-CNT sample showing the best ammonia formation rate

(6.74×10^{-12} mol·cm^{-2}·s^{-1}). However, the further experimentation reported below evidences how this value, which is in line with literature data under comparable reaction conditions,[3-5] can be largely improved by optimization of cell design and reaction conditions.

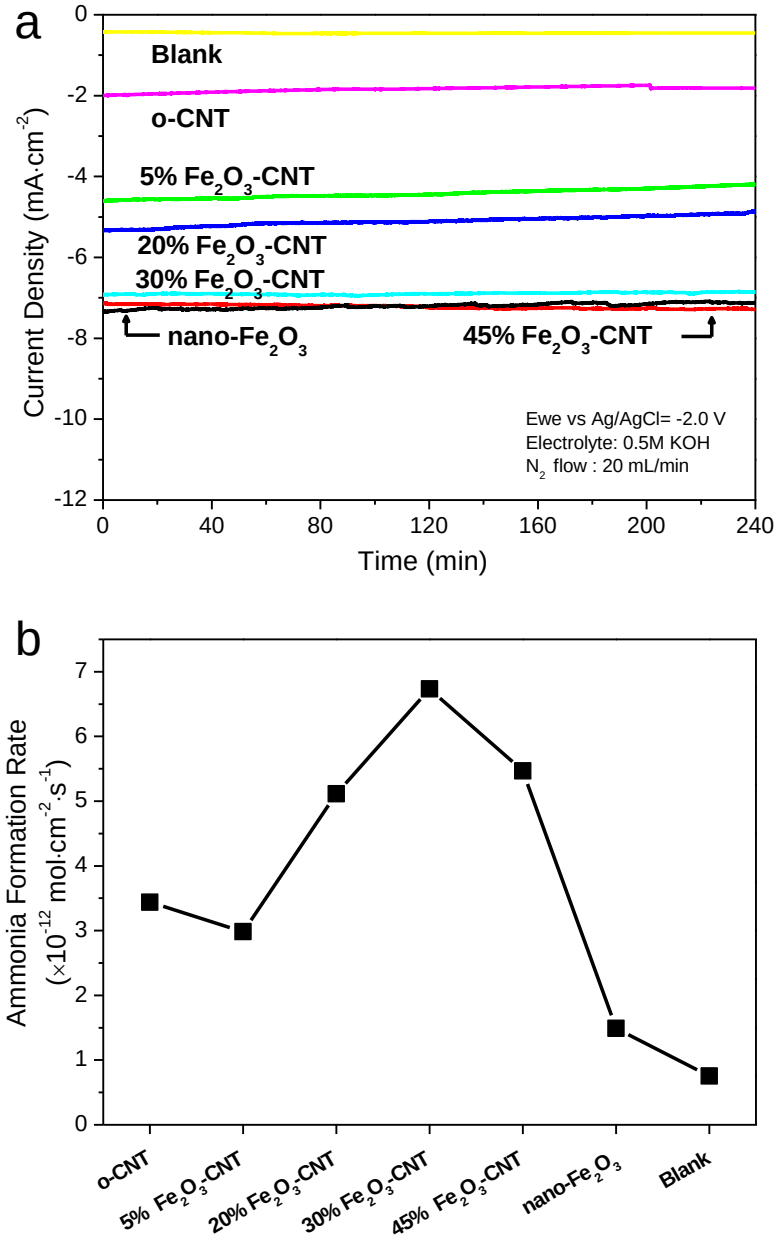

Figure 3-2. *Effect of iron content on: a) current density profile of electrocatalyst; b) average ammonia formation rate.*

3.3.2. Improved cell design.

A key question in cell design as outlined in ***Figure 3-1*** is the possible presence of ammonia (or ammonium ion) crossover through the Nafion membrane. Lan et al.[12] observed, in fact, that in a cell using a Nafion membrane as solid electrolyte, ammonia was detected in both cathode and the anode chambers where oxidation reaction occurred. We have thus analyzed the presence of ammonia in the liquid phase chamber of the cell shown in ***Figure 3-1***. The concentration of ammonia in the liquid phase (anode chamber) reaches the highest value after one hour and then decreases. The explanation of this behavior is that the ammonia formed in the cathodic part, passes in part through the membrane (likely in ammonium ion form) and then reacts in the anode chamber according to the following equations:

$$2NH_3 \rightarrow N_2 + 6H^+ + 6e^- \text{ or } 2NH_3 + 6OH^- \rightarrow N_2 + 3H_2O + 6e^- \quad (1)$$

Part of the ammonia formed results thus consumed according to this mechanism, with a consequent decrease in the efficiency of the process and the rate of ammonia formation. In order to avoid this negative effect, an additional GDL layer was inserted between the electrocatalyst layer and the Nafion membrane, as shown in ***Figure 3-3***. There are two advantages in the design of this cell: i) the ammonia crossover is strongly depressed and ii) the transport distance of water and protons can confine the hydrogen evolution reaction. Due to these advantages, a better ammonia formation rate and Faradaic efficiency are observed. An ammonia formation rate of 1.06×10^{-11} mol·cm^{-2}·s^{-1} with NH_3 Faradaic selectivity of 0.164% was obtained in the modified configuration for the 30% Fe_2O_3-CNT electrocatalyst under the same conditions of previous tests. The ammonia formation rate and NH_3 Faradaic selectivity are therefore 158% and 571% higher than the values acquired with the old configuration (***Figure 3-1***). Moreover, no ammonia was detected in the anode part of the new configuration. Different parameters were also optimized using the modified cell configuration reported in ***Figure 3-3***.

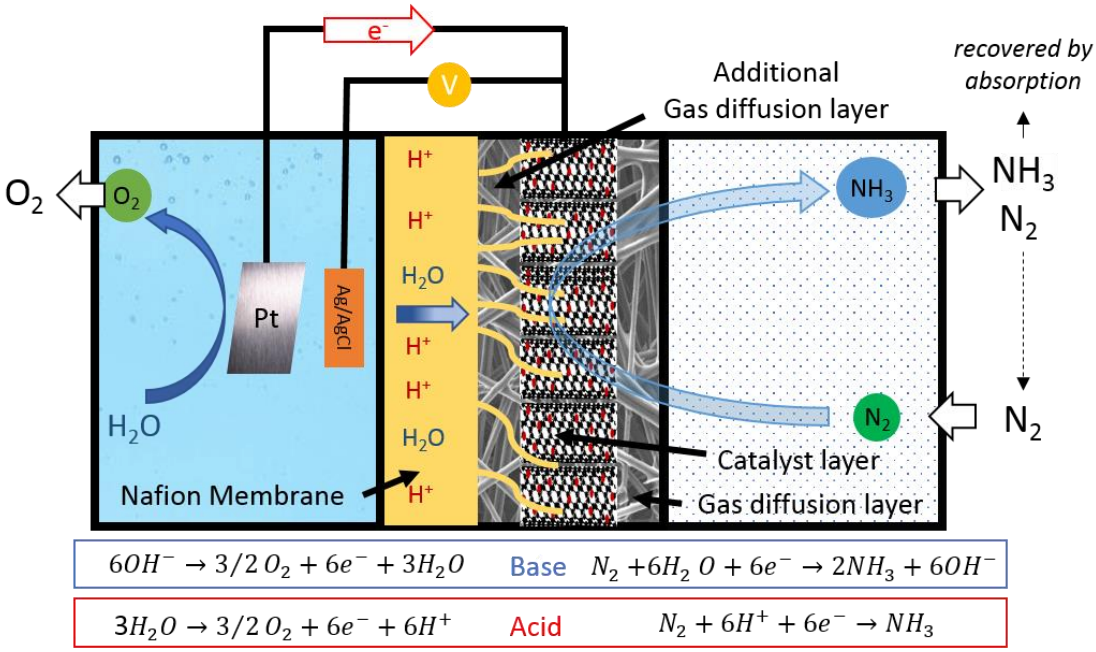

Figure 3-3. *Schematic view of the improved design in the three-phase reactor for electrochemical ammonia synthesis.*

3.3.3. Effect of the electrolyte.

The performances of the 30% Fe_2O_3-CNT electrocatalyst were tested in different electrolytes having different pH values, but maintaining the applied voltage constant at -2.0 V vs. Ag/AgCl. In order to maintain the same conductivity, the electrolytes for these tests were used with different concentrations. Specifically, the following values were utilized:

- 0.5 M KOH (pH=13.7),
- 0.5 M $KHCO_3$ (pH=9.4),
- 0.25 M K_2SO_4 (pH=7),
- 0.25 M $KHSO_4$ (pH=0.6).

As shown in ***Figure 3-4a***, highest current density of -2.75 mA·cm^{-2} was observed for the strong acid 0.25 M $KHSO_4$ (pH=0.6) electrolyte, while the lowest current density

of -1.89 mA·cm^{-2} was observed for the basic 0.5 M $KHCO_3$ (pH = 9.4) electrolyte. The neutral electrolyte (0.25 M K_2SO_4; pH = 7) shows an intermediate current density of -2.29 mA·cm^{-2}. However, the strongest basic electrolyte (0.5 M KOH, pH = 13.7) shows a current density in between those for pH = 7 and pH = 9.4 electrolytes. For a pH above 10, there is thus a deviation in the behavior with respect to the trend expected. This could be explained by considering that both water and proton transport as well as consumption affect the current density. When an acid is used as electrolyte, the current density is determined by the proton concentration. When a base is used as electrolyte, the water transport directly influences the current density due to the low concentration of protons (< 10^{-7} mol/L). The current density thus decrease from -2.09 mA·cm^{-2} for 0.5 M KOH (pH = 13.7) to -1.89 mA·cm^{-2} for 0.5 M $KHCO_3$ (pH = 9.4) becoming dominant the water transportation. In 0.5 M $KHCO_3$ (pH = 9.4), the CO_2 in equilibrium with the bicarbonate hinders the water transportation through the Nafion membrane. It is worth to note also that a higher level of noise is observed in the plots reported for 0.25 M $KHSO_4$ which is probably due to the fact that at the lower pH, the formation of hydrogen gas is enhanced. The hydrogen bubbles stick in part to the electrolytes, giving rise to the observed noise of the current density profile. For all electrolytes, stable current densities are observed.

Figure 3-4b reports a comparison of the ammonia formation rates for the 30% Fe_2O_3-CNT electrocatalyst in the different electrolytes used. The highest ammonia formation rate of 1.06×10^{-11} mol·cm^{-2}·s^{-1} was obtained for the 0.5 M KOH electrolyte, while the lowest rate of 7.87×10^{-12} mol·cm^{-2}·s^{-1} for 0.25 M $KHSO_4$. The total Faradaic efficiency was similar in different electrolytes. However, a significant difference was observed for the Faradaic selectivity to NH_3. The NH_3 Faradaic selectivity of 0.164% obtained by 0.5 M KOH is 225% higher than the value observed by 0.25 M $KHSO_4$. The choice of the electrolyte (type, pH, concentration) thus plays a critical role on the selectivity of NH_3, but has instead a minor effect on the ammonia formation rate.

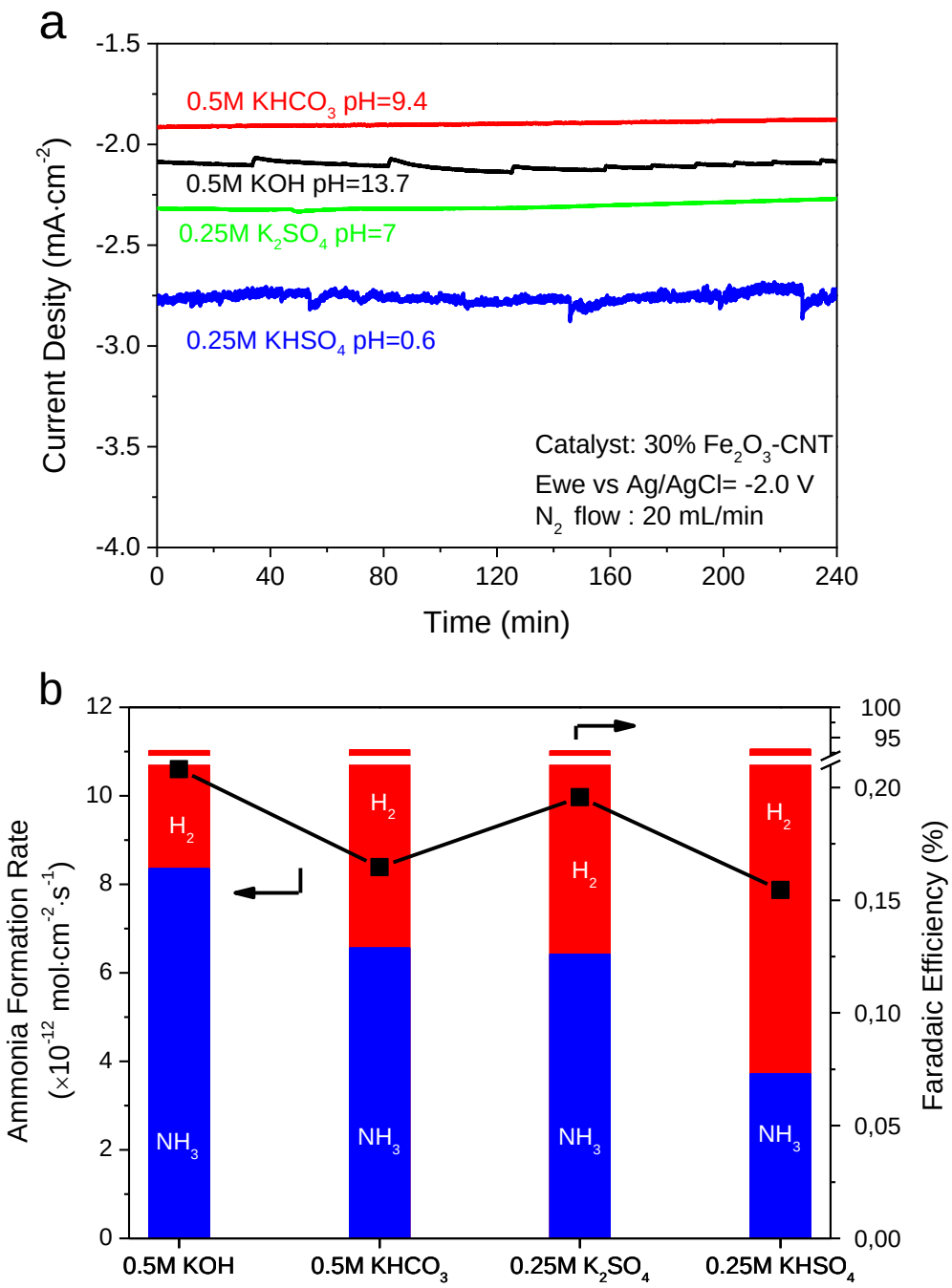

Figure 3-4 *a) Current density profile of electrocatalyst with different electrolyte; b) Average ammonia formation rate and Faradaic efficiency of electrocatalyst with different electrolyte.*

3.3.4. The effect of applied voltage.

The effect of applied voltage was studied using 2.5 mg/cm^2 of 30% Fe_2O_3-CNT as catalyst, and 0.5 M KOH as electrolyte. ***Figure 3-5a*** reports the current density as a function of time on stream for extended reaction tests (24 h). A quite stable behavior can be observed. Current densities of -0.089 mA·cm^{-2}, -0.19 mA·cm^{-2} and -2.03 mA·cm^{-2} were obtained for the applied voltages of -1.0 V, -1.5 V vs. Ag/AgCl and -2.0 V vs. Ag/AgCl respectively. It is worth to point out that current density (as an absolute value) for an applied voltage of -1.5 V vs. Ag/AgCl is about 2 times higher than the value for an applied voltage of -1.0 V, while the current density registered for an applied voltage of -2.0 V vs. Ag/AgCl is about 20 times higher than that for an applied voltage of -1.0 V. An exponential increase of the current density by applying higher voltages is thus present. The same tendency was observed on cumulative (total) amount of ammonia formed (***Figure 3-5b***). The final value after 24 h is 5.28 µg, 9.53 µg, and 11.31 µg of ammonia for an applied voltage of -1.0 V, -1.5 V and -2.0 V vs. Ag/AgCl respectively. It may be noted that for the lowest applied voltage (-1.0 V) the rate of ammonia formation (the tangent of the curves reported in ***Figure 3-5b***) remains constant, whereas the ammonia formation rate decreases with time for the applied voltage of -1.5 V vs. Ag/AgCl. For the -2.0 V vs. Ag/AgCl applied voltage, the rate of ammonia formation passes instead through a maximum.

In order to analyze better these aspects, **Figure 3-6** reports the ammonia formation rate (histogram) and NH_3 Faradaic selectivity (average in 60 min time slots) determined for extended-time experiments. As shown in Figure 6a, the highest ammonia formation rate of 1.89×10^{-11} mol·cm^{-2}·s^{-1} was observed after four hours in the experiment applying -2.0 V vs. Ag/AgCl. The average ammonia formation rate (in 24 h) is about 3×10^{-12} mol·cm^{-2}·s^{-1}, which is 1.5 times higher than the value when the voltage of -1.0 V vs. Ag/AgCl is applied.

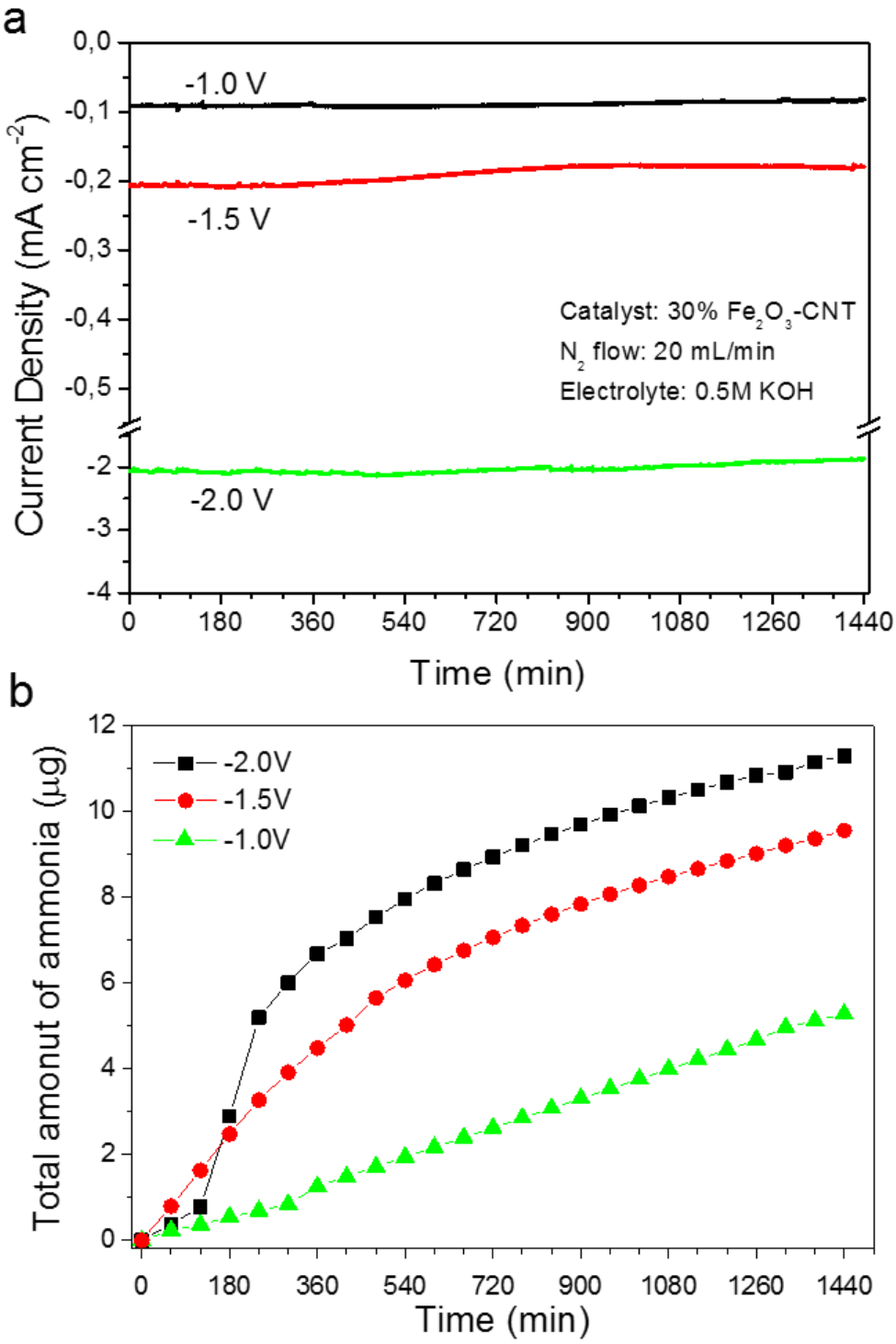

Figure 3-5. *The effect of applied voltage on a) current density and b) total ammonia formation.*

As shown in ***Figure 3-6b***, relative to an applied voltage of -1.5 V, the best NH_3 Faradaic selectivity of 1.04% was observed in the first 3-4 hours. Note that this NH_3 Faradaic selectivity is significantly better than that reported earlier for comparable reaction conditions, for example by Kordali et al.[8] (a Faradaic efficiency of 0.28 %) or Lan and Tao [9] (below 0.1%). The ammonia formation rate maintains over a value of 3×10^{-12} mol·cm^{-2}·s^{-1} for about 780 min at -1.5 V, while for only 600 min at -2.0 V. At -1.0 V, on the contrary, a lower ammonia formation rate is observed (1.86×10^{-12} mol·cm^{-2}·s^{-1}), but which remain constant in 24 h of experiments. The NH_3 Faradaic selectivity remains also constant (0.59%).

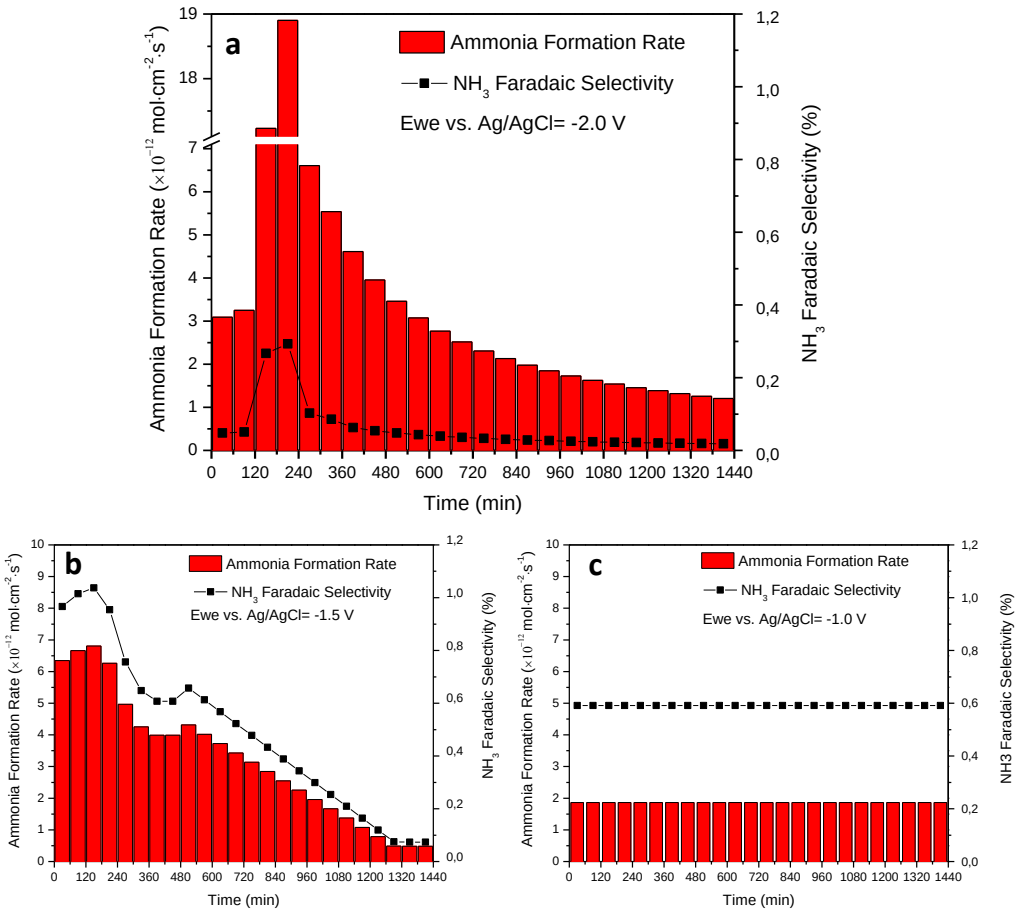

Figure 3-6. *Ammonia formation rate and NH_3 Faradic selectivity for an applied voltage of a) -2.0 V vs. Ag/AgCl; b) -1.5 V vs. Ag/AgCl and c) -1.0 V vs. Ag/AgCl.*

When the voltage of -2.0 V vs. Ag/AgCl is applied, the best ammonia formation rate is observed, but with the rate passing through a maximum and showing a relatively fast decrease. When the voltage of -1.5 V vs. Ag/AgCl is applied, the best current efficiency is observed, with the rate of ammonia formation also decreasing, but with a lower slope. When a voltage of -1.0 V vs. Ag/AgCl is applied, the best stability was observed. Note that instead the current densities (***Figure 3-6a***) remain constant during the same period. Therefore, it is not a leaching (no Fe is detected in the electrolyte) or a major change in the electrode, but likely a change in the nature of the iron sites, with a modification from sites active for ammonia synthesis to sites active in H_2 generation, reducing thus the availability of the H^+/e^- for the reduction of N_2. This explains why the current densities remain stable, while a major change in the rate of ammonia formation and Faradaic selectivity is observed. The change in the surface characteristics of iron nanoparticles induced by the applied voltage explains also why the time on stream behavior depends on the applied voltage.

Further studies are in progress to clarify this question, but we can anticipate that preliminary results indicate that the iron particles supported on CNTs should be in an oxidized form, and the formation of metallic Fe leads to a lowering of the Faradaic selectivity due to enhanced rate of H_2 formation. Operando XAFS (X-ray adsorption fine structure) studies in an electrochemical cell adapted to synchrotron light source oxidized form, and the formation of metallic Fe leads to a lowering of the Faradaic indicate that in similar Fe_2O_3/carbon electrodes a ferrihydrate (FeOOH) structure is present at low negative applied voltages, but increasing the negative voltage above about -1.3 V ~ -1.4 V, the formation of an intermediate hydride species appears which discharges as H_2, leaving Fe^0 behind. On increasing the negative applied voltage and time of reaction, the surface of iron-oxide/hydroxide species start to be reduced and this effect leads to enhanced formation of H_2 detrimental for the NH_3 formation.[13] On the other hand, by application of a higher negative voltage, the driving force for the electron

transfer increases and thus the reaction rate. In order to develop improved Fe/CNT electrocatalysts it is thus necessary to improve the stability of the iron-oxide particles against the in-situ reduction at negative voltages above -1.0 V. At this value, on the contrary, a rather stable activity in ammonia formation is present (**Figure 3-6c**), but the rate and Faradaic efficiencies are low.

3.4 Conclusions

In conclusions, present data evidence that 30% Fe_2O_3-CNT is the best electrocatalyst among iron based catalysts supported on carbon nanotubes. The performances greatly depend on the cell design, where the possibility of ammonia crossover through the membrane has to be inhibited. The reaction conditions also play a significant role. When an acid is used as electrolyte, the current density is determined by proton concentration but if a base is used as electrolyte, the water transport determines the current density. The electrolyte (type, pH, concentration) plays a critical role on the selectivity of ammonia, but does not influences greatly the ammonia formation rate. A complex effect of the applied voltage was observed. An excellent stability was found for an applied voltage -1.0 V. At higher negative applied voltages, the ammonia formation rate and Faradaic selectivity are higher, but with a change of the catalytic performances, although the current densities remain constant for at least 24h of experiments. This effect is interpreted in terms of reduction of the iron-oxide species above a negative voltage threshold, which enhances the side reaction of H^+/e^- recombination to generate H_2 rather than their use to reduce activated N_2 species, possibly located at the interface between iron-oxide and functionalized CNT.

3.5 Reference

1. Perathoner, S.; Centi, G. CO2 recycling: A key strategy to introduce green energy in the chemical production chain. ChemSusChem 2014, 7 (5), 1274-1282.
2. Jewess, M.; Crabtree, R. H. Electrocatalytic Nitrogen Fixation for Distributed Fertilizer Production? ACS Sustainable Chem. & Eng. 2016, 4 (11), 5855-5858.
3. Kyriakou, V.; Garagounis, I.; Vasileiou, E.; Vourros, A.; Stoukides, M. Progress in the Electrochemical Synthesis of Ammonia. Catal. Today 2017, 286, 2-13.
4. Shipman, M. A.; Symes, M. D. Recent progress towards the electrosynthesis of ammonia from sustainable resources. Catal. Today 2017, 286, 57-68.
5. Renner, J. N.; Greenlee, L. F.; Herring, A. M.; Ayers, K. E. Electrochemical synthesis of ammonia: a low pressure, low temperature approach. Electrochem. Soc. Interface 2015, 24, 51-57.
6. Bao, D.; Zhang, Q.; Meng, F.; Zhong, H.; Shi, M.; Zhang, Y.; Yan, J.; Jiang, Q.; Zhang, X. Electrochemical Reduction of N2 under Ambient Conditions for Artificial N2 Fixation and Renewable Energy Storage Using N2/NH3 Cycle. Adv. Mater. 2017, 29, 1604799/1-5.
7. Shi, M.; Bao, D.; Wulan, B.; Li, Y.; Zhang, Y.; Yan, J.; Jiang, Q. Au Sub-Nanoclusters on TiO2 toward Highly Efficient and Selective Electrocatalyst for N2 Conversion to NH3 at Ambient Conditions. Adv. Mater. 2017, 29, 1606550/1-6.
8. Kordali, V.; Kyriacou, G.; Lambrou, Ch. Electrochemical synthesis of ammonia at atmospheric pressure and low temperature in a solid polymer electrolyte cell. Chem. Comm. 2000, (17), 1673-1674.
9. Lan, R.; Tao, S. Electrochemical synthesis of ammonia directly from air and water using a Li+/H+/NH4+ mixed conducting electrolyte. RSC Adv. 2013, 3, 18016-18021.
10. Chen, S.; Perathoner, S.; Ampelli, C.; Mebrahtu, C.; Su, D.; Centi, G. Electrocatalytic Synthesis of Ammonia at Room Temperature and Atmospheric Pressure from Water and Nitrogen on a Carbon-Nanotube-Based Electrocatalyst. Angew. Chemie, Int. Ed. 2017, 56 (10), 2699-2703.
11. Perathoner, S.; Centi, G.; Su, D. Turning Perspective in Photoelectrocatalytic Cells for Solar Fuels. ChemSusChem 2016, 9 (4), 345-357.
12. Lan, R.; Irvine, J. T. S.; Tao, S. Synthesis of ammonia directly from air and water at ambient temperature and pressure. Scientific Reports 2013, DOI:10.1038/srep01145
13. Chiara, C.; Schuster M.; Gibson E.; Gianolio D.; Cibin G.; Wells P.; Garai D.; Solokha V.; Calderon S.; Ampelli, C.; Perathoner, S.; Centi, G.; Arrigo R. Insights by operando XAFS into the high Faraday efficiency and seectivity to acetic acid in the electro-catalytic reduction of CO2 over FeOOH on N-doped carbon. Angew. Chemie, Int. Ed. 2017, submitted.

CHAPTER 4

4. Active species and their dynamic during the electrocatalytic ambient temperature/pressure direct synthesis of ammonia from N_2 and H_2O over iron nanoparticles on CNTs

4.1 Introduction

Ammonia synthesis is the largest-scale chemical process with the higher impact on greenhouse gas emissions, about 350 Mt CO_2 emissions worldwide. This value could be decreased by over 90% in a direct electrocatalytic process using N_2, H_2O and renewable energy as input sources. In fact, CO_2 emissions are 1.83 t_{CO2}/t_{NH3} in the actual ammonia production scheme (via natural gas steam reforming followed by NH_3 synthesis), while the total footprint of the direct electrocatalytic route could be estimated in 0.12 t_{CO2eq}/t_{NH3}. [1] Implementing this technology will thus result in a breakthrough change towards a sustainable, low-carbon chemical production based on the use of renewable energy sources. [2] There is thus a rising interest in fossil-fuel-free direct ammonia synthesis. [3-10]

We reported recently that electrocatalysts based on iron nanoparticles supported on carbon nanotubes (Fe/CNT) are effective and stable electrocatalysts in this process. [11, 12] Iron, on the other hand, is the catalyst for high-temperature and pressure industrial synthesis of ammonia (about 400-450°C and 10-30 MPa). Even if the starting catalyst is iron-oxide, the catalyst operates in the metallic form. There is still debate about the reaction mechanism and modalities of N_2 activation, but it is well established that the first step in high temperature/pressure catalytic hydrogenation of N_2 is the dinitrogen dissociative chemisorption.[13-15] While it is suggested an analogy in the reaction mechanisms between catalysis and electrocatalysis, the N_2 dissociative chemistry at low temperature/pressure is inhibited from the strong chemisorption of these species which blocks the surface reactivity leading eventually to the formation of Fe-N type

species. Abghoui and Skúlason [16, 17] indicated instead by quantum mechanical calculations that transition metal nitride electrocatalysts, particularly NbN· are the most promising. A recent study [18] indicates, on the other hand, that nitride species formation may occur only at much higher pressures. Bao et al. [6] proposed by theoretical studies a reductive adsorption of N_2 to form NNH· species as rate determining step in the electrocatalytic reduction of N_2 to NH_3 at room temperature on gold nanorods. Norskov et al. [7] pointed out that the stability of $*N_2H$ adsorbate is a key for the low-temperature electrocatalytic production of NH_3 from N_2. Both these studies proposed that the rate determining step is the hydrogen addition to dissociated chemisorbed N_2 molecule (similar to what present in *Nitrogenase* enzyme [19, 20]), but there are no experimental proofs about these indications and in general whether the electrocatalytic path is closer to that present at high temperature/pressure on commercial iron catalysts, or rather close to what occurs in nature, where the active centre is also containing iron atoms.

We show here that, contrary to expectations, iron-oxide (Fe_2O_3) nanoparticles (supported over carbon nanotubes - CNTs) are more active in the direct electrocatalytic synthesis of ammonia from N_2 and H_2O than the corresponding samples after reduction to form Fe or Fe_2N supported nanoparticles, i.e. those iron forms which are the indicated active phases in high temperature/pressure catalytic reduction of N_2 to NH_3. Characterization of these electrocatalysts provides indications on the relationship between rate of ammonia in the direct electrocatalytic synthesis and iron species present under working conditions. These results will clarify the difference in the nature of active sites and the reaction mechanism between the catalytic (high temperature/pressure) conventional ammonia synthesis (from N_2 and H_2) and the electrocatalytic (low temperature/pressure) path.

4.2 The scope of this chapter

The induce-activation process was showed during the electrocatalytic ammonia synthesis when iron-oxide supported by CNTs were used as a catalyst at the applied voltage of -2.0V vs. Ag/AgCl. It indicated that new active sites for ammonia direct electrocatalytic synthesis were in-situ created. Due to the negative applied voltage, both ammonia and hydrogen formed on the electrocatalyst. It may be thus expected that some reduced iron species would be the active sites for ammonia synthesis. In order to find and investigate on the active sites, both chemically and electrochemically reduced samples were tested.

4.3 Prepare and performance of chemically reduced Fe_2O_3-CNT

The starting carbon nanotubes (CNTs) were first functionalized by oxidative treatment (o-CNT) to obtain a high stable dispersion of iron oxide nanoparticles located mainly on the external surface of the CNTs, as shown by transmission electron microscopy (TEM).

4.3.1. Characterization of initial iron(III) oxide supported on carbon nanotubes

The iron spices on initial catalyst were confirmed to be alpha type of iron (III) oxide by XRD measurement (***Figure 4-4***). The morphology and microstructure of catalyst 30% Fe_2O_3-CNT were examined by HRTEM, as shown in ***Figure 4-1***. There were large particles whose dimension was about 20×30 nm. The resolution is high enough to measure the lattice spacing of nanoparticle. The interplanar crystal spacing measured by TEM is 2.50 Å, which match with the crystal face [311] of iron (III) oxide, as shown in figure 6a. In addition, numerous particles with the diameter of about 1 nm were observed by TEM and STEM. Furthermore, even larger number of nano-size particles observed by Energy dispersive X-ray spectroscopy (EDX) elemental maps (***Figure 4-1***). Fe and O well distributed all over the carbon nanotubes.

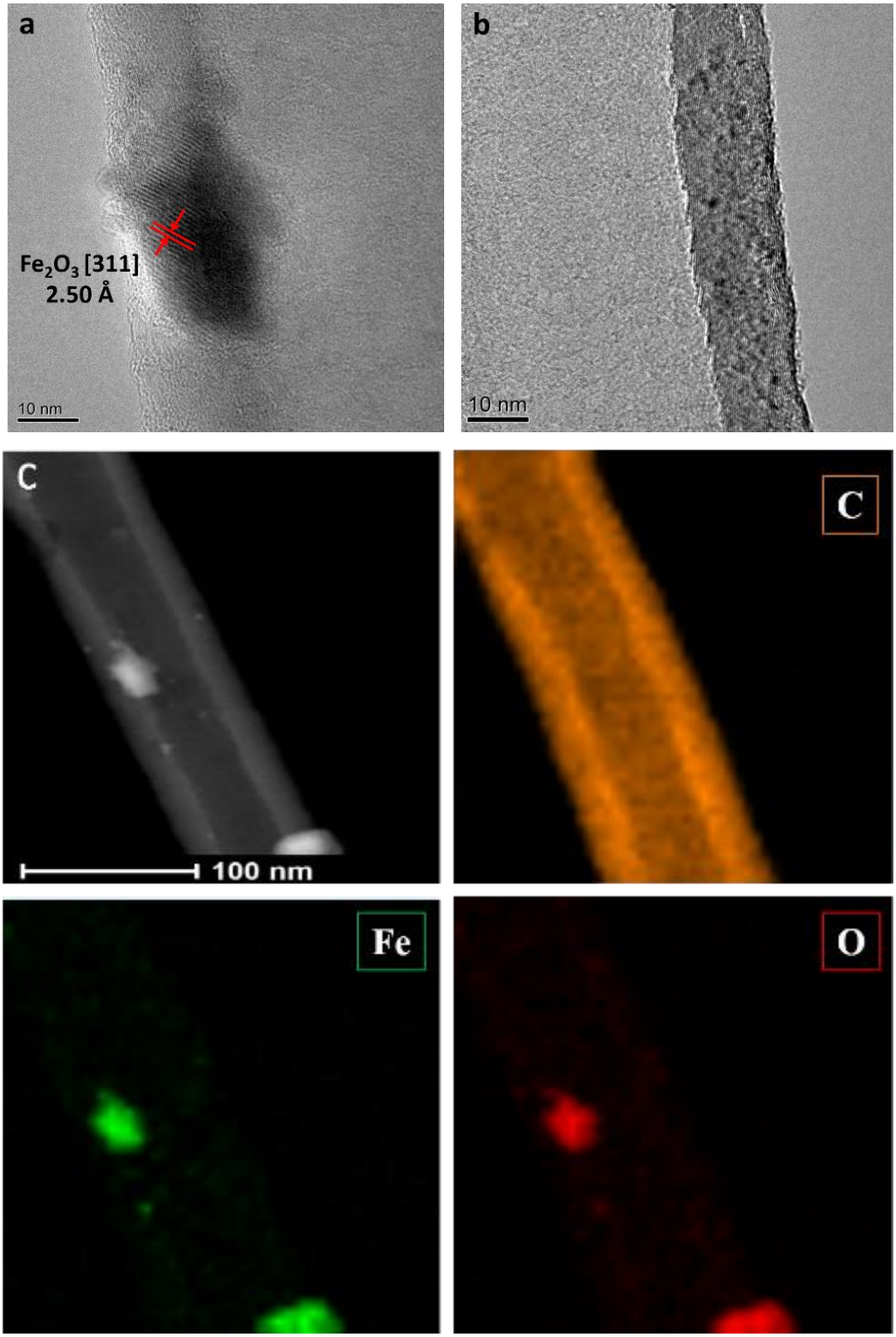

Figure 4-1. *a) and b) HRTEM image of 30% Fe_2O_3-CNT; c) EDX elemental maps of Fe_2O_3-CNT.*

4.3.2. The preparation of chemically reduced iron species supported on carbon nanotubes

In order to study the behavior of Fe_2O_3-CNT during the reduction, TPR (Temperature programmed reduction) was performed in both H_2 and NH_3. The TPR instrument is coupled with mass spectrometry detector.

H_2-TPR: In these temperature programmed reduction experiments using H_2 as reducing agent, an on-line mass quadrupole was utilized to monitor the simultaneous evolution of gas species. Specifically, mass channel of 2, 16, 18, 28 and 44 were monitored, as shown in ***Figure 4-2***. Two negative peaks were observed at 300ºC and 500ºC on mass 2, which indicate that H_2 was consumed. According to Arrigo et al.1, carboxyl functional group on carbon nanotubes (CNT) decomposes into CO_2 and water with formation of defects on the surface of CNT at 300ºC. Therefore, the consumption of H_2 at 300ºC can be attributed to the reduction of these functional groups present on CNT due to the initial oxidative pretreatment. The latter is necessary to allow a stable dispersion of iron species. The parallel change in the masses 16 (CH_4), 18 (H_2O) and 44 (CO_2) confirm this attribution.

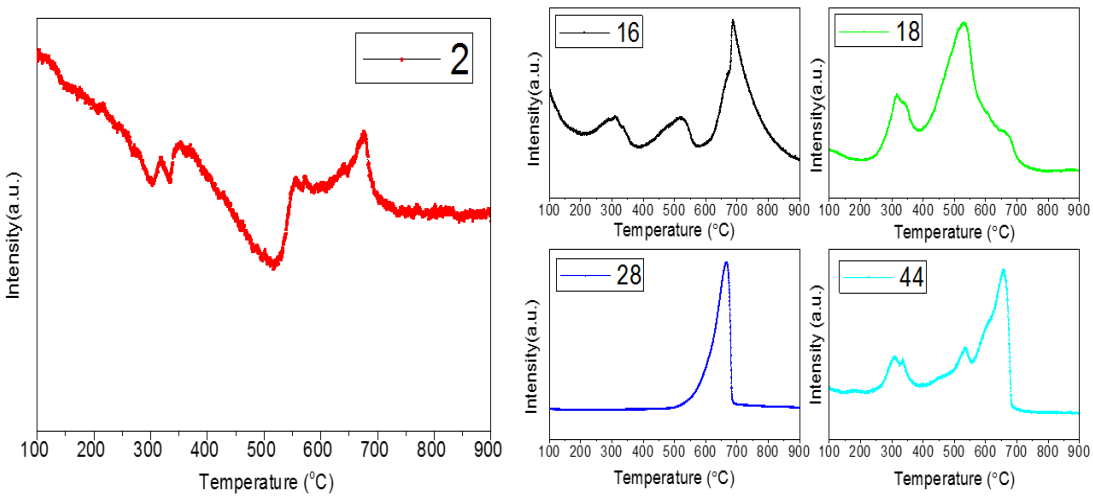

Figure 4-2. *H_2 temperature programmed reduction profile of Fe_2O_3-CNT.*

The strong peak of H_2 consumption at 500ºC is related to the reduction of the iron oxide and the carbonate between iron oxide and carbon nanotube (identified by XPS analysis). This can be further confirmed by the presence of weak peak on masses 16 (CH_4) and 44 (CO_2), as well as intense peak on mass 18 (H_2O) at 500ºC. In addition, intense peaks on masses 16 (CH_4), 28 (CO), and 44 (CO_2) at 650ºC are observed, which are attributed to decomposition of the hydroxyl or ether functional groups on CNTs (also due to the initial oxidative pretreatment of CNT). An intense peak on mass 16 (CH_4) at 700ºC can be resulted from the reaction between hydrogen and carbon nanotubes. In summary, during the H_2-TPR of Fe_2O_3-CNT, carboxyl functional group decomposes at 300ºC, iron oxide reduces at 500ºC, and hydroxyl or ether functional groups decomposes at 650ºC. Hence the reduction temperature of 500ºC was selected to prepare metallic iron on CNT.

NH_3-TPR: In these temperature programmed reduction experiments using H_2 as reducing agent, an on-line mass quadrupole was utilized to monitor the simultaneous evolution of gas species. Mass channel of 2, 13, 14, 15, 17, 18, 28 and 44 were monitored, as shown in ***Figure 4-3.*** Ammonia decomposition starts at 450°C forming N_2 and H_2, and decomposes completely at temperatures higher than 600°C. Peaks on mass 44 (CO_2) were observed at 350°C, 500°C and 550°C. Compared to the reduction by H_2, a shift to higher temperatures (300°C to 350°C) was observed for the decomposition of the carboxyl group due to the formation of an ammonium salt, which is thermally stable. On the contrary, the higher temperature peak shifts from 650°C to 550°C. This decrease in the reduction temperature derives from the coordination of NH_3 to the oxygen of the hydroxyl or ether functional groups present on CNT. This can weaken the bond between C and O, so that the decomposition of hydroxyl or ether functional groups shifts to lower temperature (from 650°C, during reduction in H_2 flow, to 550°C, during reduction in NH_3 flow). For temperatures above 650°C, complete decomposition of ammonia was observed and profiles were similar as for reduction

under a H_2 flow).

Based on the results from NH_3-TPR analysis, a reduction temperature of 500°C was selected to prepare iron nitride on CNTs from the Fe_2O_3-CNT. Formation of Fe_2N after reduction for 4 h under NH_3 flow was confirmed by the XRD analysis

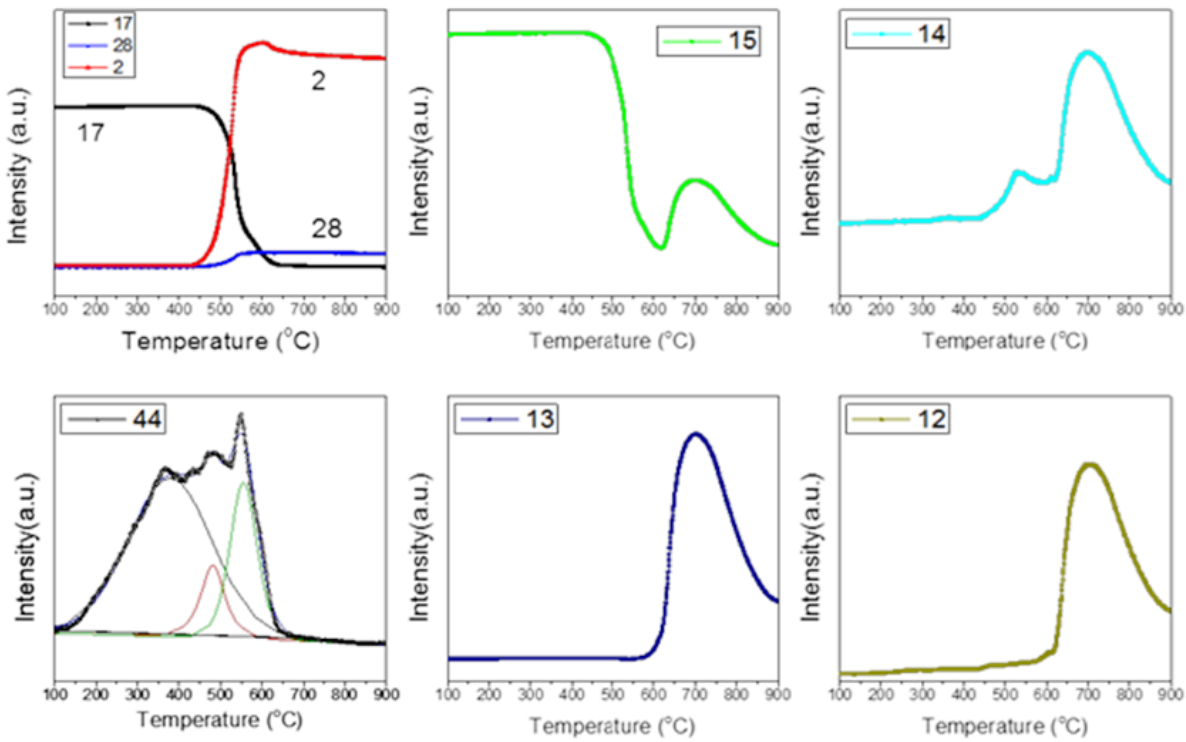

Figure 4-3. *NH_3 temperature programmed reduction profile of 30%-Fe_2O_3-CNT.*

4.3.3. The characterization of chemically reduced iron species supported on carbon nanotubes

For chemical reduced samples, the as prepared Fe_2O_3-CNT were treated by H_2 or NH_3 at a temperature (500°C, 4h) identified in H_2-TPR and NH_3-TPR (TPR – temperature programmed reduction) experiments to obtain the transformation of Fe_2O_3 supported nanoparticles to Fe or Fe_2N nanoparticles, respectively.

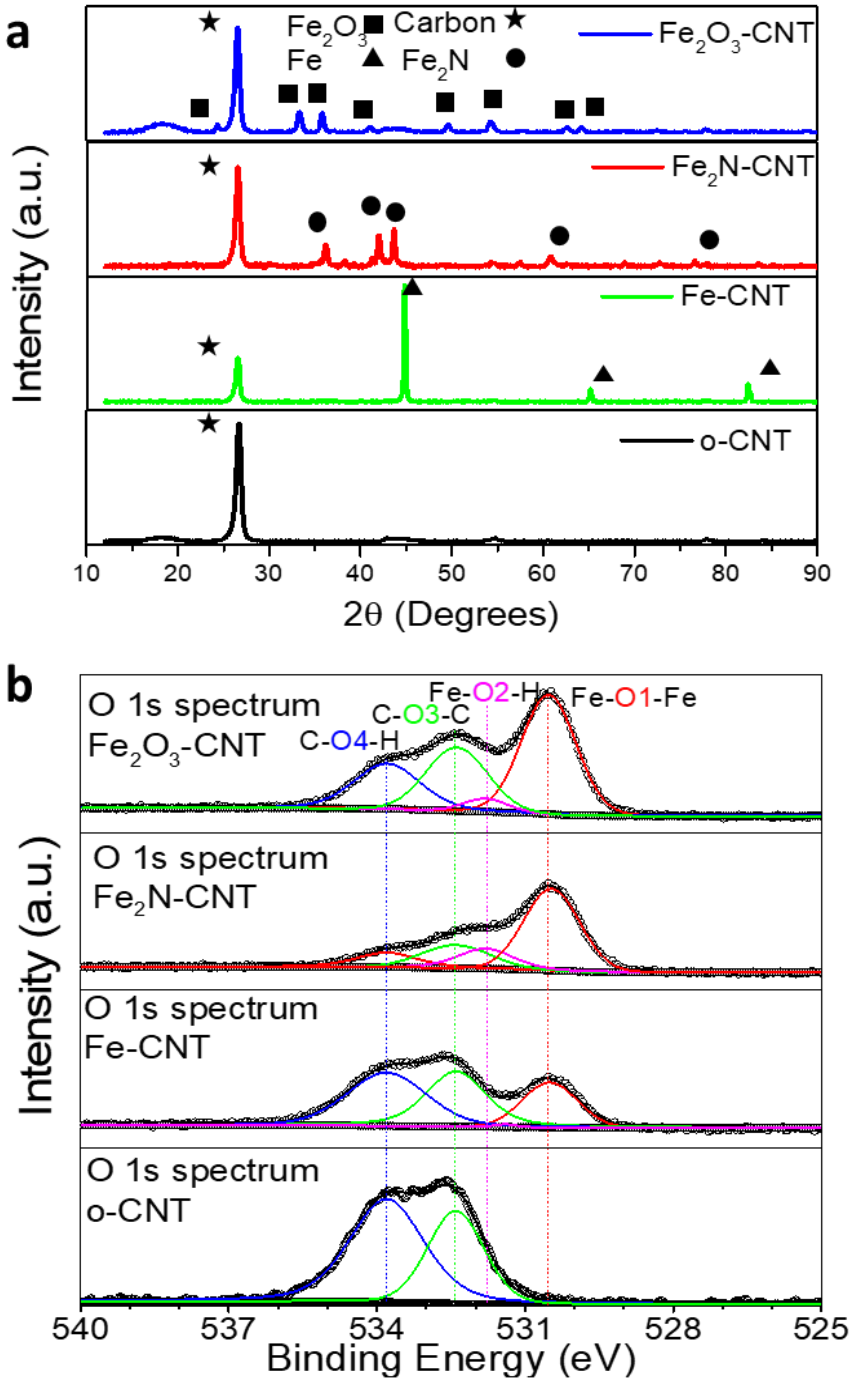

Figure 4-4 *a) XRD pattern of o-CNT and o-CNT supported iron-based catalysts; b) XPS O1s spectra of o-CNT and o-CNT supported iron-based catalysts.*

XRD (X-ray diffraction) measurements (**Figure 4-4a**) evidence that the initial α-Fe_2O_3 nanoparticles are fully transformed to Fe or Fe_2N after this treatment. These samples are indicated as Fe_2O_3-CNT, Fe-CNT, and Fe_2N-CNT, respectively.

XPS (X-ray photoelectron spectroscopy) characterization data of these samples (**Figure 4-4b**) show in all cases the presence of an O1s signal which can be deconvoluted in four components: [21-23]

- **O1** (Fe-O-Fe, 530.5±0.1 eV), related to O^{2-} in Fe_2O_3 or Fe**O**OH species;
- **O2** (Fe-O-H, 531.8±0.1 eV), related to FeO**O**H species;
- **O3** (C-O-C, 532.4±0.1 eV), related to ether functional groups of the carbons substrate;
- **O4** (C-O-H, 533.8±0.1 eV), related to OH and COOH functional groups of the carbon's substrate

After 4h of reduction at 500°C in H_2 or NH_3 flow, an O1s XPS signal related to oxidized iron-oxide species is still observed (**Figure 4-4b**), even if Fe_2O_3 nanoparticles are apparently fully converted to Fe or Fe_2N nanoparticles according to XRD patterns (**Figure 4-4a**). This fact could be explained by the still presence of small, not reduced Fe_2O_3 particles/patches which are below the detection limit of the XRD. HRTEM (high-resolution transmission electron microscopy) and STEM (scanning transmission electron microscopy (**Figure 4-1**) measurements confirm this indication.

Integrated peak areas of the O1s spectra were also compared. After the reduction of Fe_2O_3-CNTs in H_2 flow, the integrated peak areas of all the O1s species were found to be decreased. But, compared to the three types of oxygen, the O3 (Fe-O-Fe) was significantly decreased. This is due to the reduction of Fe_2O_3 to metallic Fe. Additionally, after the treatment with NH_3 flow, the integrated peak area of O1s was also decreased. Among the oxygen species, both O1 (C-O-C) and O2 (C-O-Fe) were decreased significantly which is due to the removal of ether and hydroxyl functional groups at relatively lower temperature during the treatment with NH_3 (as described in the NH_3-TPR section). The O3 (Fe-O-Fe) spectra was also decreased which is due to

the formation of Fe_2N (confirmed by XRD). Furthermore, a new oxygen species was observed after the treatment with NH_3 due to the partial replacement of oxygen by N on the Fe-O-Fe structure for the formation of Fe-O-Fe-N. This O species is corresponds to O4 (Fe-O-Fe-N) (531.8 eV).Moreover, the formation of Fe_2N was also confirmed by the presence of N1s sharp peak at 398.1 eV, as shown in **Figure 4-13**.In the XPS spectra large amount of oxygen (O3) from Fe_2O_3 which was not detected by the XRD analyses was also observed even after the reduction pretreatments by H_2 and NH_3. This can be explained as some of the smaller particles (confirmed by TEM analysis) might not be reduced completely.

4.3.4. The catalytic performance of chemically reduced Fe_2O_3-CNT in Gas-Liquid-Solid Three-phase Reactor

Fe_2O_3-CNT, Fe-CNT, Fe_2N-CNT and o-CNT were tested in Gas-Liquid-Solid Three-phase Reactor for the direct synthesis of NH_3 from N_2 and H_2O at ambient pressure/temperature under an applied voltage of -1.0, -1.5 and -2.0 V vs. Ag/AgCl.

As shown in **Figure 4-5a,** compare with o-CNT, higher current density was observed on the iron doped catalysts (Fe_2O_3-CNT, Fe-CNT, Fe_2N-CNT). Although no significant difference of the current density was recorded among Fe_2O_3-CNT, Fe-CNT, Fe_2N-CNT, lowest current density was obtained by the Fe_2O_3-CNT sample whereas higher current density recorded by the Fe-CNT catalyst, due to the difference of their conductivity.

No relevant differences in the current density among the different electrocatalysts were observed at -1.0 V vs. Ag/AgCl. A stable current density and ammonia production was noted during the entire experiments of 24h (**Figure 4-5a**). The highest ammonia formation rate (1.86×10^{-12} $mol\cdot cm^{-2}\cdot s^{-1}$) at an applied voltage of -1.0 V vs. Ag/AgCl. (**Figure 4-6b**) was shown by the Fe_2O_3-CNT. The catalytic performance of Fe_2N-CNT was similar to that of o-CNT, indicating that Fe_2N was essentially inactive for ammonia

synthesis with the applied voltage of -1.0 V vs. Ag/AgCl.

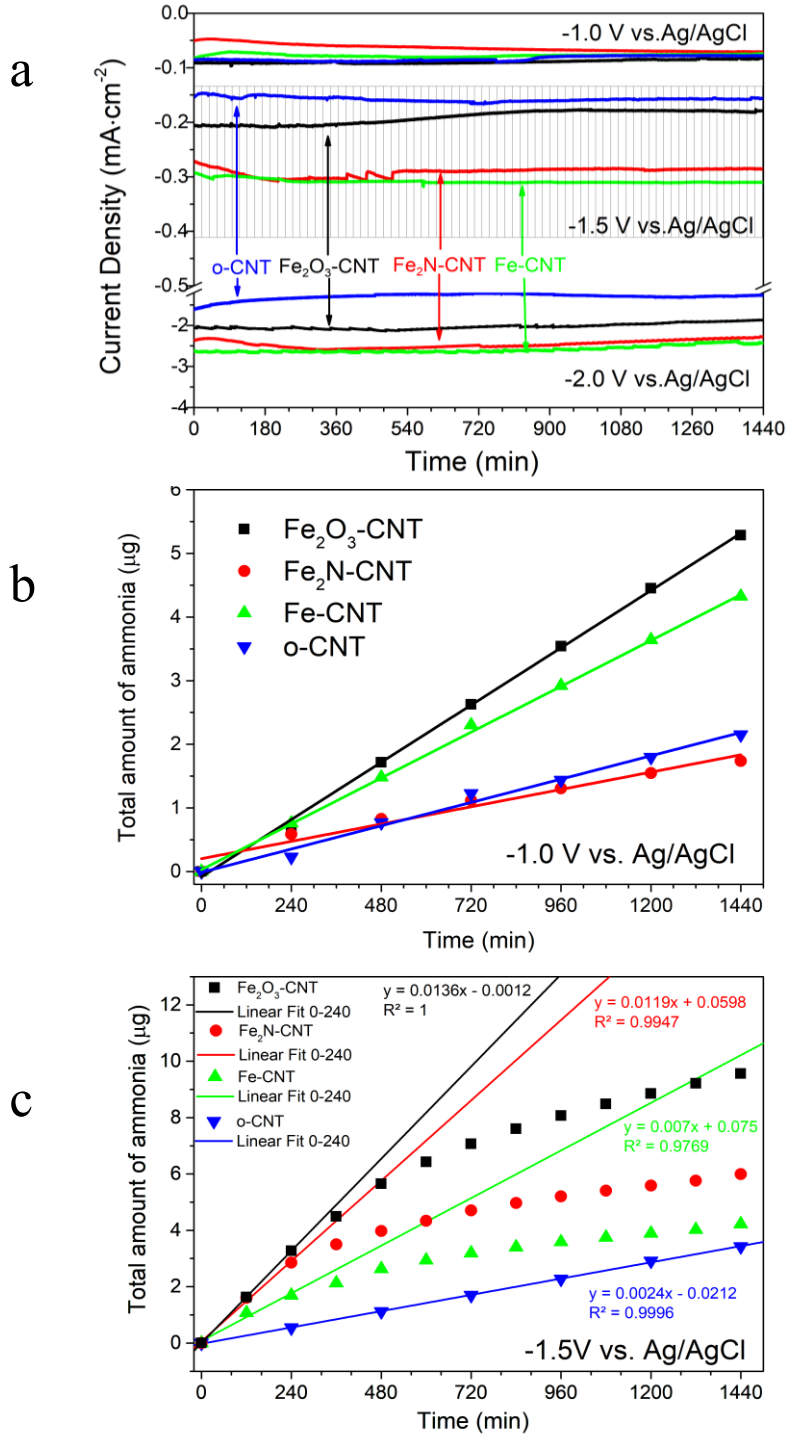

Figure 4-5. *Electrocatalytic performances of Fe_2O_3-CNT, Fe-CNT, Fe_2N-CNT, and o-CNT. a) current density; b) total amount of ammonia produced at -1.0 V vs. Ag/AgCl; c) total amount of ammonia produced at -1.5 V vs. Ag/AgCl;*

When the voltage of -1.5 V vs. Ag/AgCl was applied, the current densities were about two times higher than those at -1.0 V vs. Ag/AgCl. The highest current density was observed for Fe-CNT, while the lowest current density by o-CNT, i.e. the support used for preparing the electrocatalysts. 9.56, 5.99, 4.22 and 3.42 µg of ammonia were produced respectively by Fe_2O_3-CNT, Fe_2N-CNT, Fe-CNT, and o-CNT during 24 hours. The ammonia formation rate was stable during the testing period (24h) only for the o-CNT electrocatalyst. Whereas for iron-based electrocatalysts decreases as a function of the time of reaction. However, the ammonia formation rate was nearly constant in the first 3-4 hours, allowing to estimate the initial rates of reaction (**Figure 4-5c**): 0.816, 0.714, 0.42 and 0.144 µg/h for Fe_2O_3-CNT, Fe_2N-CNT, Fe-CNT, and o-CNT, respectively, at the applied voltage of -1.5V vs. Ag/AgCl.

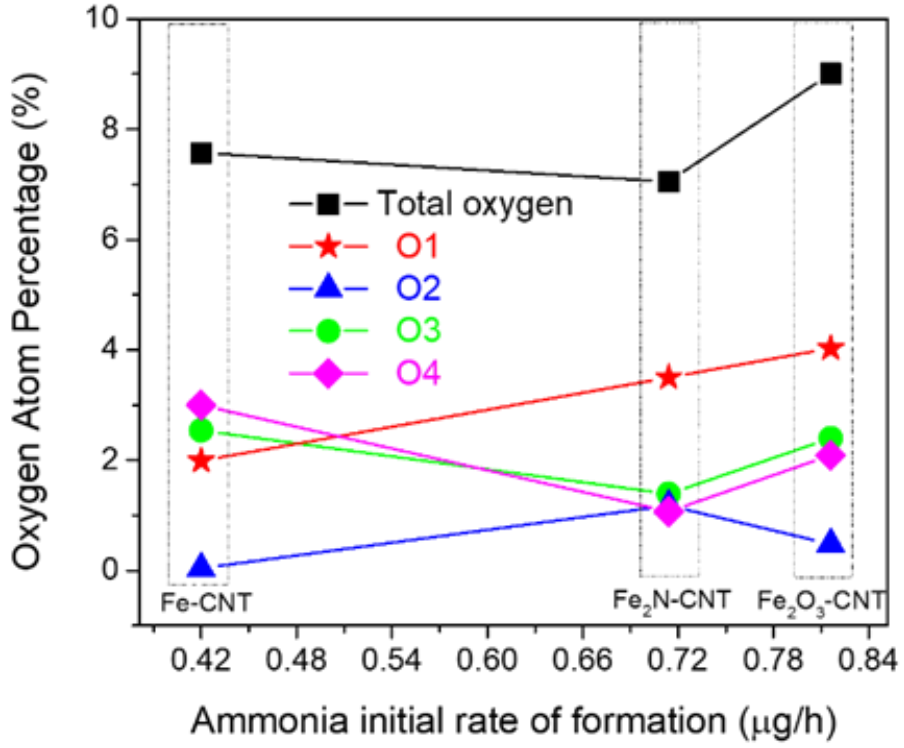

Figure 4-6. *The relationship observed between the different O1s species and total oxygen amount detected by XPS and the initial ammonia formation rates for different iron-containing CNT samples at an applied voltage of -1.5 V vs. Ag/AgCl.*

To correlate these initial rates of ammonia formation with the surface characteristics of the catalysts, the amount of the different oxygen species were quantified by deconvolution of the XPS O1s spectra. The results are reported in **Figure 4-6** as a function of the initial ammonia formation rate (at -1.5V vs. Ag/AgCl) of the iron-based electrocatalysts. The activity of the electrocatalysts towards ammonia synthesis depends linearly on the O1 (Fe-O-Fe) type of oxygen, differently from the other oxygen signals (O2-O4) or the total amount of oxygen. Therefore, O1 (Fe-O-Fe) species are directly relate to ammonia formation rate when CNT supported iron based catalysts was used.

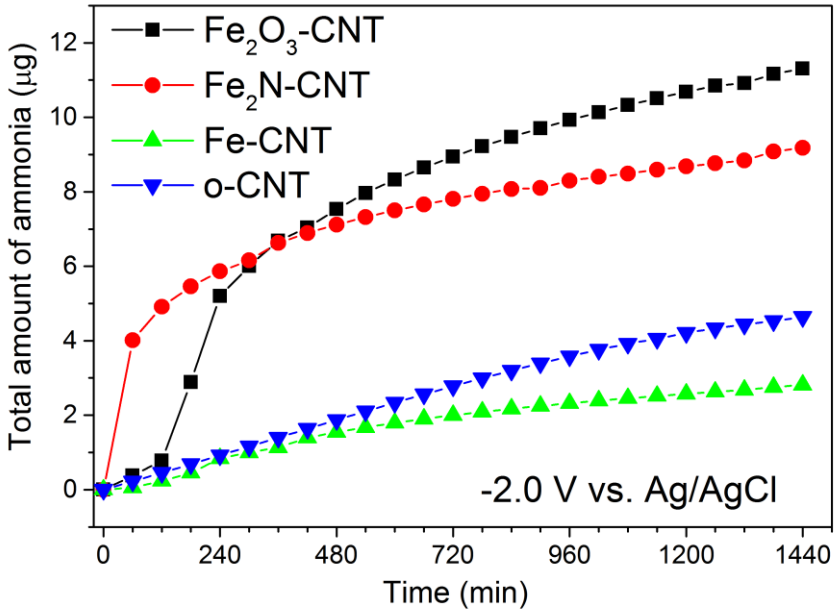

Figure 4-7. *Electrocatalytic performances of Fe_2O_3-CNT, Fe-CNT, Fe_2N-CNT, and o-CNT. Total amount of ammonia produced at -2.0 V vs. Ag/AgCl;*

For the applied voltage of -2.0 V vs. Ag/AgCl, the data was shown in **Figure4-7.** It is obvious that the current density of -2.0V vs. Ag/AgCl was significantly higher than that observed at -1.5 V vs. Ag/AgCl (**Figure 4-5a**). At the end of tests (-2.0 V vs. Ag/AgCl), all the samples showed similar ammonia formation rate compared to o-CNT (**Figure 4-7**). This could be in good agreement with the fact that all the active iron species were

consumed during the reaction. It can be deduced that the total ammonia production amount should positive correlation related to active iron species. The total ammonia production after 24h at -2.0V vs. Ag/AgCl is the following: Fe_2O_3-CNT: 11.31 μg; Fe_2N-CNT: 9.18 μg and Fe-CNT: 2.81 μg. This amount linearly correlates with the intensity of the XPS O1 (Fe-O-Fe) signal (***Figure 4-8***), further remarking the role of this species in the electrochemical ammonia synthesis. Both of the linear relationships between ammonia synthesis performance and with the intensity of the XPS O1 (Fe-O-Fe) signal suggested that iron oxide supported by CNTs should concede to be active sites for ammonia synthesis.

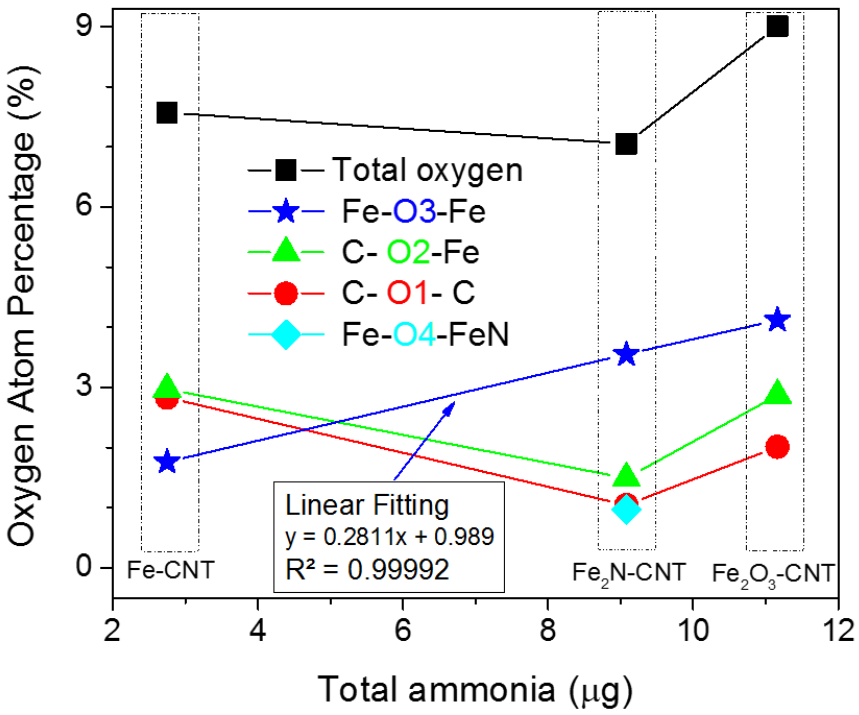

Figure 4-8. *Linear relationship observed between total ammonia amount with respect to different O1s spices of different iron-containing CNT samples at an applied voltage of -2.0 V vs. Ag/AgCl.*

Furthermore, a clear induction time in Fe_2O_3-CNT is present (***Figure 4-7***). The slope of the curve of the total amount of ammonia formed vs. time of reaction is the ammonia formation rate, which reaches the highest value of 1.275×10^{-11} mol·cm^{-2}·s^{-1} after about 3h. The rate of ammonia formation passes through a maximum in Fe_2O_3-CNT sample after 3h of reaction at -2.0V, differently from what was observed for the same sample, at less negative applied potential values (***Figure 4-5b and c***). The presence of a maximum in rate of ammonia formation for Fe_2O_3-CNT sample at -2.0V vs. Ag/AgCl clearly indicates that new active sites for ammonia synthesis are generated during the electrocatalytic reaction, when an enough negative potential is applied. Therefore, studying the in-situ electro-chemically reduced samples was a more convinced methods to study the active sites for ammonia synthesis.

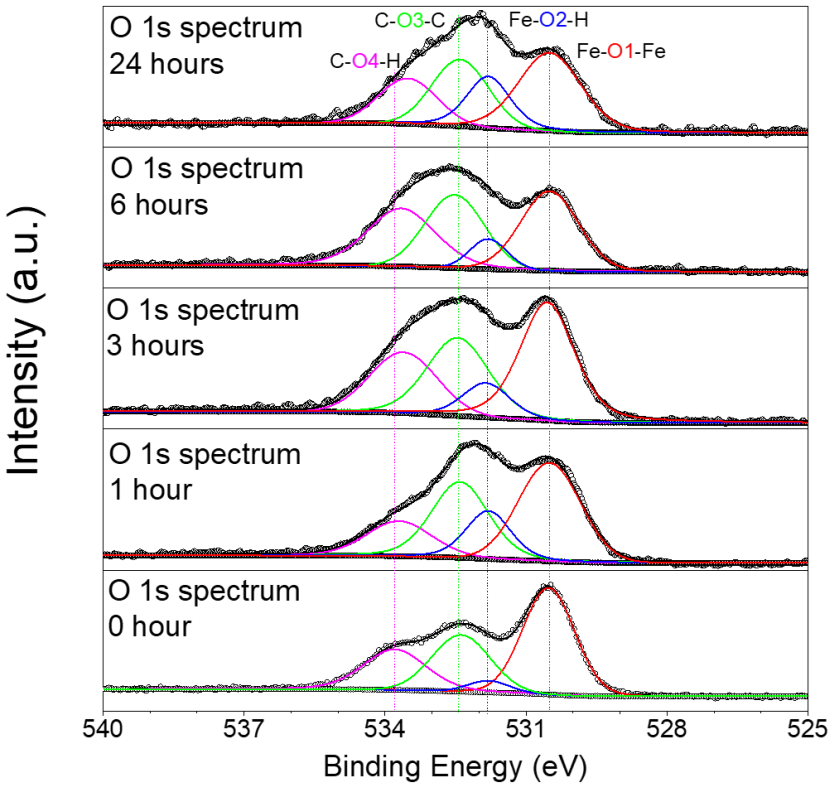

Figure 4-9. *O1s XPS spectra of Fe_2O_3-CNT samples after different times (0h, 1h, 3h, 6h, and 24h) of operations at a constant voltage of -2.0 V vs. Ag/AgCl.*

4.4 Prepare and performance of electro-chemically reduced Fe2O3-CNT

4.4.1. The preparation of electro-chemically reduced iron species supported on carbon nanotubes

During the test that a negative voltage was applied, ammonia and hydrogen gas were produced on catalyst. Accordingly, reduced iron species would be formed inevitable. In order to study the activity of different iron species supported on carbon nanotube, the electrochemical reduced iron species were prepared.

Table 3. *Rate of ammonia formation and O1s XPS signals (ex-situ measurements) as a function of the time on stream for Fe_2O_3-CNT at an applied voltage of -2.0 V vs. Ag/AgCl.*

Time on stream (h)	Rate of ammonia formation ($x10^{-12}$ mol·cm^{-2}·s^{-1})	Total O1s (%)	O1 (Fe-O-Fe) (%)	O2 (Fe-O-H), (%)
0	3.09	9.01	4.03	0.35
1	10.24	5.12	1.96	0.80
3	12.75	5.53	2.23	0.54
6	4.28	4.52	1.47	0.35
24	1.23	3.33	1.23	0.61

In order to find these active sites, the Fe_2O_3-CNT samples were activated for a different time in same conditions for NH_3 synthesis at -2.0V vs. Ag/AgCl, and the activated samples were ex-situ characterized by XPS and HRTEM. ***Figure 4-9***.reports the XPS O1s profiles of the fresh Fe_2O_3-CNT sample and after 1h, 3h, 6h, and 24h of activation. The O1s XPS spectra were deconvoluted in four components using the same parameters described above. The total Oxygen amount decreases sharply in the first hour and

decreases with a lower rate in the following 23 hours. (***Table 3***) This is due to the reconstruction of bulk iron oxide particles in the first hour, as shown later by HRTEM images (***Figure 4-11***). It is necessary to note that the bulk iron oxide particles that were reconstructed at electrochemical reduction condition, were also easily reduced by NH_3 and H_2 as discussed in the previous text.

The amount of O3 and O4 species (related to oxygen functional groups on CNT) remains nearly constant with time on stream. The percentage of O2 species (related to FeO**OH**) in the total O1s, increases from 3.8% (0 hour) to 18% (24 hours). This was consistent with operando XAFS (X-ray absorption fine structure) studies in an electrochemical cell adapted to synchrotron light source on a similar Fe_2O_3/carbon electrode, although for a different reaction (CO_2 reduction).[8] These experiments showed the ferrihydrate (FeOOH) structure reduced at an applied voltage lower than -1.5 V vs. Ag/AgCl, with a parallel increase in the side reaction rate of H^+/e^- recombination to H_2. These results suggest that at a potential below -1.5 V vs. Ag/AgCl, the iron-oxide nanoparticles were reduced leading to an enhanced side reaction of H_2 evolution, with a decreased availability of converting activated N_2 to NH_3. This transformation explained the progressive decrease in the rate of ammonia formation with time on stream.

We have analyzed how the ammonia formation rate and the intensity of the XPS signal of O1 species change during the 24h of experiments at -2.0V for the Fe_2O_3-CNT sample. (***Figure 4-10***). The same linear relationship (observed in ***Figure 4-6*** and ***Figure 4-8***) between corresponding ammonia formation rate with O1 (Fe-O-Fe) species by ex-situ XPS was observed. This was a stronger proof that O1 (Fe-O-Fe) species should be considered as the active sites for ammonia synthesis, which also agreed with

a

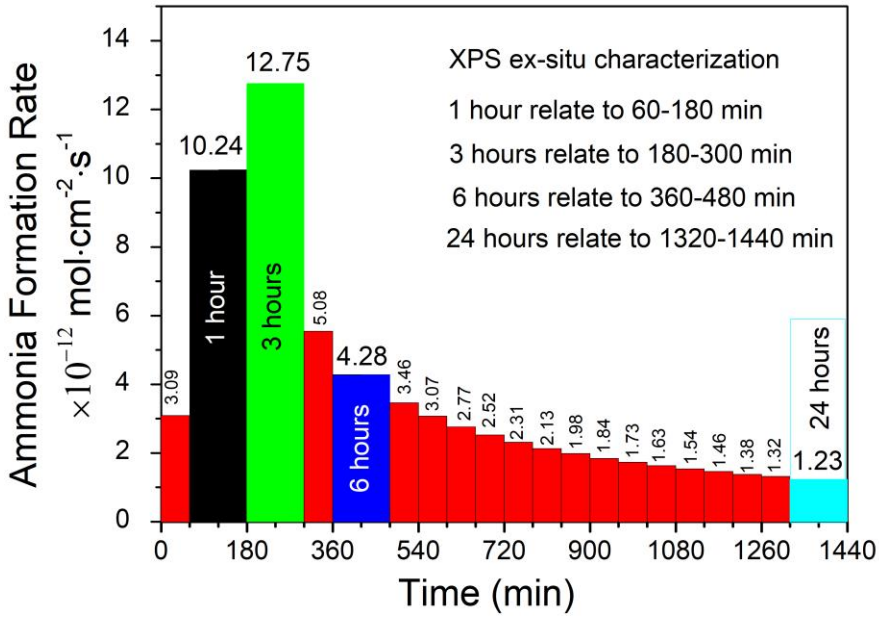

b

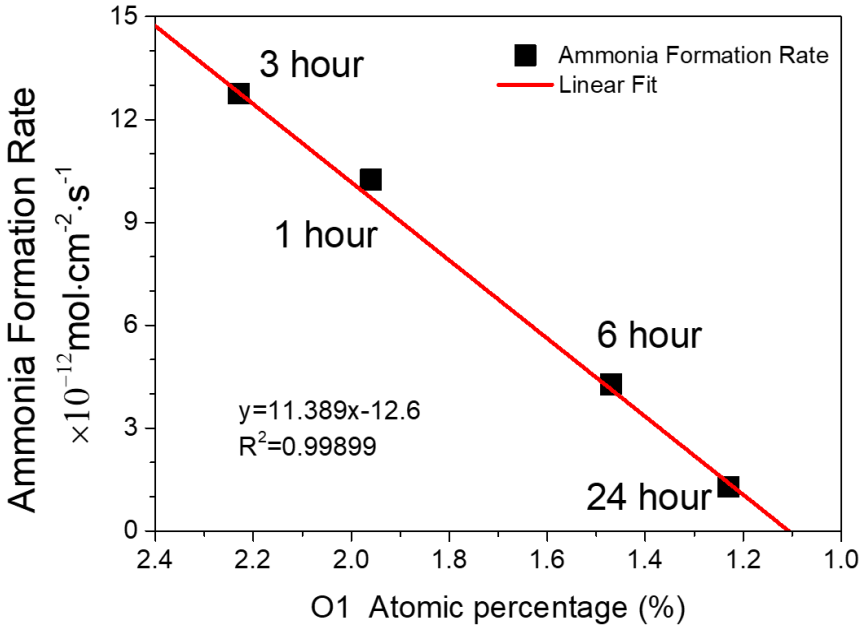

Figure 4-10. *a) The time on stream of ammonia formation rate; b) Relationship observed between amount of O1 species of used samples (1h, 3h, 6h and 24h) under -2.0 V vs. Ag/AgCl and the ammonia formation rate of the concerned time.*

the conclusion from samples that were chemically treated with H_2 and NH_3. However, it was worth to note that the fresh Fe_2O_3-CNT (0h) could not be included in the linear relationship showed in ***Figure 4-10b***. Fe_2O_3-CNT after 1h activation at -2.0V, the intensity of O1 species strongly decreases (***Figure 4-9***), while the rate of ammonia formation significantly increases from 3.09 to 12.75×10^{-12} $mol\cdot cm^{-2}\cdot s^{-1}$ (***Table 3***). Both the phenomena suggested that not all of the O1 species detected by XPS were active for ammonia synthesis. The bulk iron oxide, which was easy to be chemically and electrochemically reduced, was not active for ammonia synthesis. The true active sites located likely at the interface between carbon and this O1 species. Strained C-C bonds or defect sites of CNT strongly interact with small iron oxide particles (O1 species) at the interface, which could activate selectively N_2 to NH_3.

To proof the concept, the ex-situ samples were analyzed by TEM (***Figure 4-11***). The fresh Fe_2O_3-CNT shows iron oxide particles located mainly on the external surface of CNTs. Particle size in the 3-20 nm range (***Figure 4-11a***) and smaller particles (***Figure 4-1***) were observed. They were well distributed along the CNT axis. The bigger particles were well crystalline (***Figure 4-1***), which could be detected by XRD. After in-situ activation of 1 hour at -2.0 V vs. Ag/AgCl, no XRD signal of iron oxide was observed, this corresponded to the reconstruction of bulk iron-oxide particles as shown in ***Figure 4-11b***. At the same time, the ammonia formation rate increased about 3 times. For the longer time of activation at -2.0V vs. Ag/AgCl (3 hours), the as-produced small iron-oxide particles were better distributed along the CNT, which gave rise of another 20% increase of ammonia formation rate (***Figure 4-11c***). The in-situ produced small iron-oxide particles were sitting at the defect site or ending segment of the CNT, which could stabilize and activate the small iron-oxide particles (***Figure 4-11c***). Comparing to fresh sample, the total iron oxide amount of activated samples were decreased (***Table 3***), but the ammonia formation rate increased 3~4 times. These results thus confirm the indication that the active sites for ammonia synthesis were located at the interface

between small iron-oxide particles and CNT, which explain the good correlation with O1 (Fe-O-Fe) species obtained by XPS.

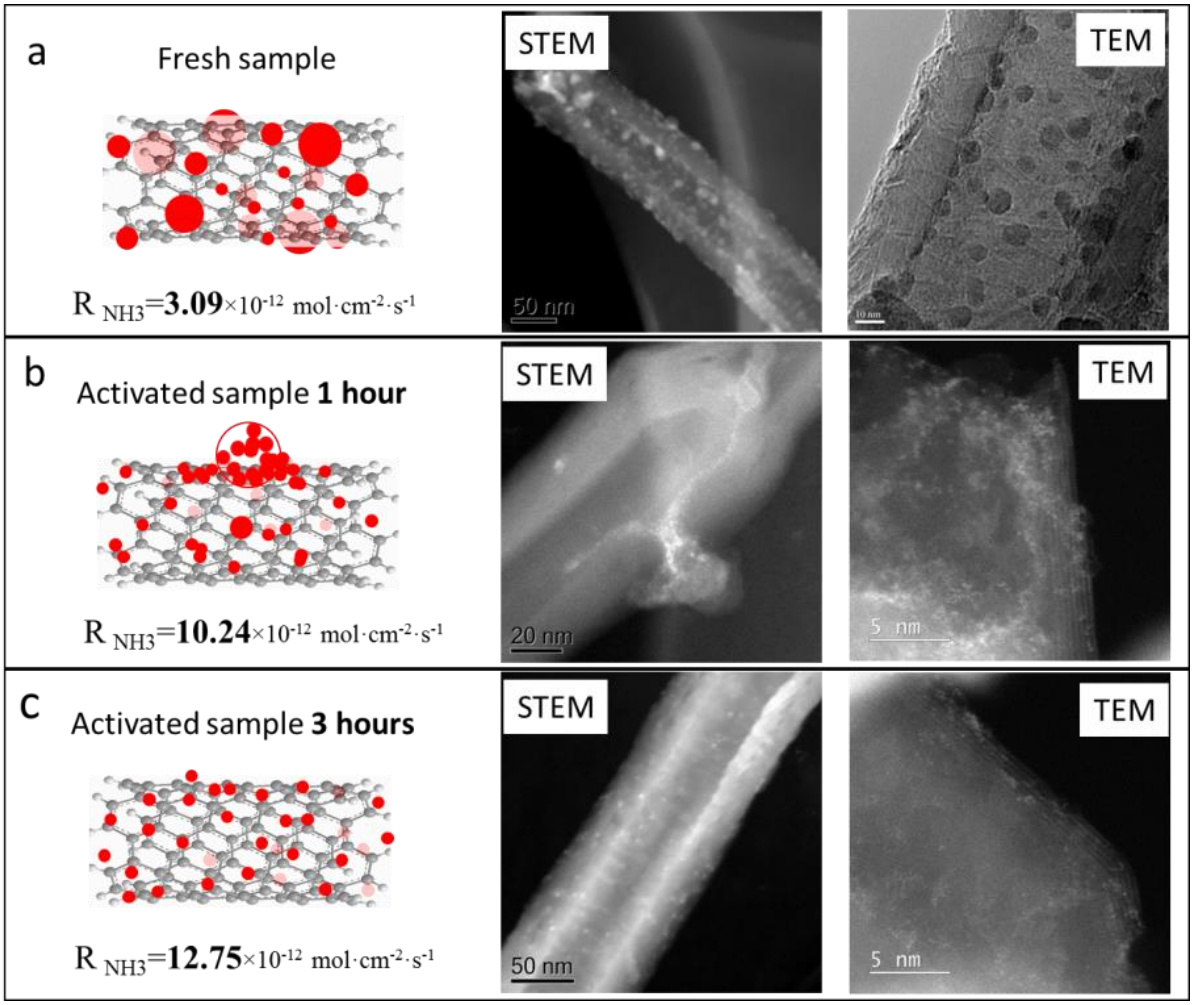

Figure 4-11. *HRTEM and STEM images of Fe_2O_3-CNT samples: a) fresh; b) after 1h of activation at -2.0 V vs Ag/AgCl. c) after 3h of activation at -2.0 V vs Ag/AgCl. And the corresponding reaction rate of ammonia formation.*

These small iron-oxide particles strongly interacted with CNT, showing significantly increased performance for ammonia synthesis compared to the bulk iron oxide. We may suggest that the activation of N_2 occurred at the surface of small iron oxide partials that were sitting at the defect sites or functional group of carbon (i.e. with charge density different from bulk iron oxide), as indicated by HRTEM images (***Figure 4-11c***). An in-

situ activation at -2.0V vs. Ag/AgCl for the Fe_2O_3-CNT, leading to the reconstruction of bulk iron-oxide particles and creating more defect site on CNTs, may enhance formation of the interface between iron-oxide nanoparticles and (defective) carbon, with a significant increase in the ammonia formation rate. However, the small iron-oxide species are not enough stable at this potential. A stabilization of the small iron-oxide nanoparticles is thus the crucial factor to improve the performances of these electrocatalysts in the ammonia electrocatalytic synthesis.

It is necessary to notice that, as shown ***in Figure 4-12***, in all the electrocatalysts tested a very less amount of Fe^0 was. This indicates that under the current experimental conditions used (applied voltage of -2.0V vs. Ag/AgCl) the iron oxide species were not reduced to metallic iron, the reconstruction process was dominate under the applied voltage.

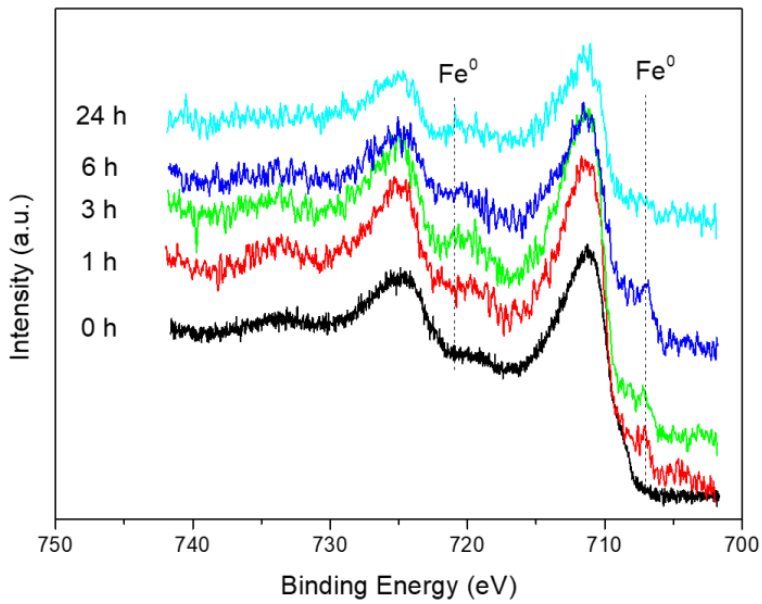

Figure 4-12. *Fe 2p XPS spectra of Fe_2O_3-CNT samples after different times of operations at a constant voltage of -2.0 V vs. Ag/AgCl.*

As shown in ***Figure 4-13***, a weak signal of N was detected in the fresh catalysts (0 hour) which might be from the incomplete removal of N from the $Fe(NO_3)_3$ used as precursor for the preparation of electrocatalysts. It was also observed the signal of N was not decreased after the reaction which indicates the ammonia produced was not from the trace amount of N detected in the fresh catalysts used. Additionally, N species in N-O structure was observed after the 3h of reaction. This might be due to the interaction of N_2 with O_2 during ex-situ XPS experiments.

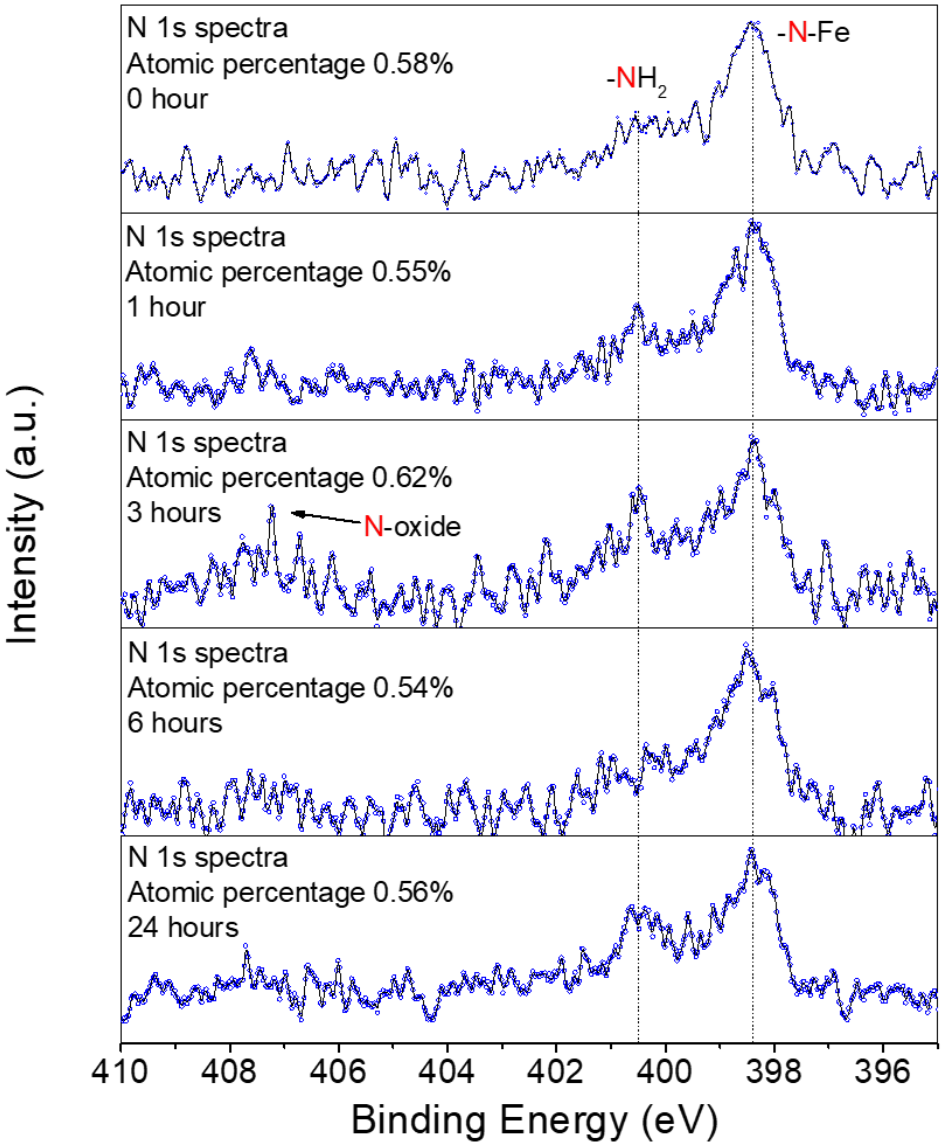

Figure 4-13. *N 1s XPS spectra of Fe_2O_3-CNT samples after different times of operations at a constant voltage of -2.0 V vs. Ag/AgCl. Conclusions*

4.5 Conclusion

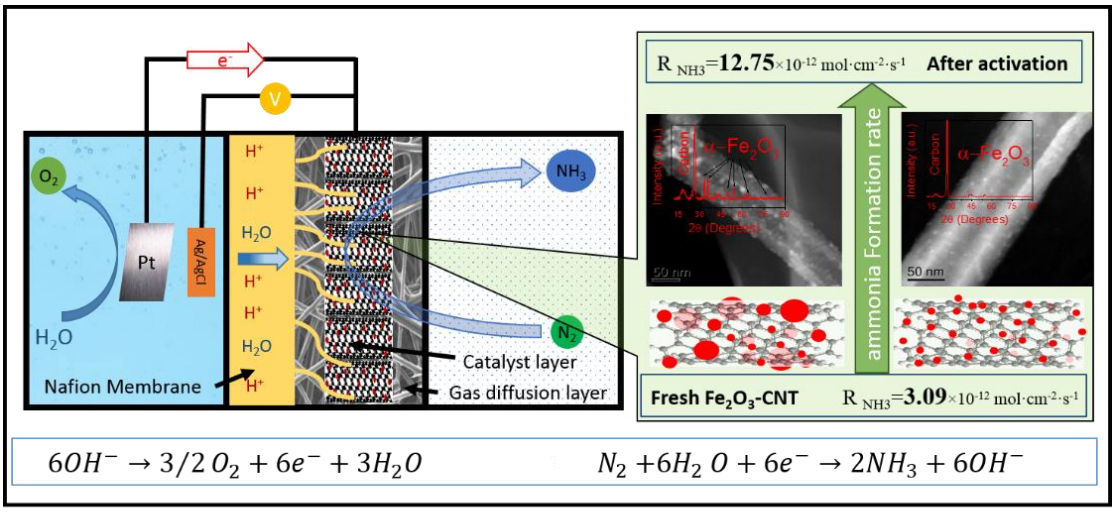

Figure 4-14 *graph of abstract of this chapter*

This chapter was conclude in **Figure 4-14**.The linear relationships between ammonia formation rate and the amount of O1(Fe-O-Fe) species detected by XPS, which are related to O^{2-} in Fe_2O_3 or FeOOH species, was confirmed by both chemical reduced samples (i.e. Fe-CNT, Fe_2N-CNT) and electrochemical activated Fe_2O_3-CNT (i.e. by in-situ activation at -2.0V vs. Ag/AgCl). This indicated that the O1 (Fe-O-Fe) species are associated with the active site for ammonia electrochemical synthesis. Furthermore, only small iron-oxide particles that strongly interacted with CNT, showed the significant increased ability for ammonia synthesis comparing to the bulk iron oxide. This is due to the small iron oxide partials that are sitting at the defect or functional groups of carbon (i.e. with charge density different from bulk iron oxide). An in-situ activation at -2.0V vs. Ag/AgCl for Fe_2O_3-CNT, leading to the reconstruction of bulk iron-oxide particles and creating more defect sites on CNT, give enhanced formation of the interface between iron-oxide nanoparticles and (defective) carbon, with a significant increase in the ammonia formation rate. These results thus provide new insights about the nature of the active sites for NH_3 synthesis from N_2 and H_2O at

ambient temperature/pressure, which are significantly different from the industrial Haber-Bosch catalysts.

4.6 Reference

1. Bazzanella A, Ausfelder F. Low carbon energy and feedstock for the European chemical industry, Dechema Pub.: 60486 Frankfurt am Main, Germany, June 2017.

2. Lanzafame P, Abate S, Ampelli C, Genovese C, Passalacqua R, Centi G, Perathoner S. Beyond Solar Fuels: Renewable Energy-Driven Chemistry. *ChemSusChem* 2017, **10**(22): 4409-44191.

3. Kyriakou V, Garagounis I, Vasileiou E, Vourros A, Stoukides M. Progress in the electrochemical synthesis of ammonia. *Catal. Today* 2017, **286**: 2-13.

4. Jewess M, Crabtree RH. Electrocatalytic Nitrogen Fixation for Distributed Fertilizer Production?. *ACS Sustainable Chem. Eng.* 2016, **4**(11): 5855–5858.

5. Shipman MA, Symes MD. Recent progress towards the electrosynthesis of ammonia from sustainable resources. *Catal. Today* 2017, **286**: 57-68.

6. Bao D, Zhang Q, Meng FL, Zhong HX, Shi MM, Zhang Y, *et al.* Electrochemical Reduction of N2 under Ambient Conditions for Artificial N_2 Fixation and Renewable Energy Storage Using N_2 /NH_3 Cycle. *Adv. Mater.* 2017, **29**(3): 1604799/1-5.

7. Montoya JH, Tsai C, Vojvodic A, Norskov JK. The Challenge of Electrochemical Ammonia Synthesis: A New Perspective on the Role of Nitrogen Scaling Relations. *ChemSusChem* 2015, **8**(13): 2180-2186.

8. Tanabe Y, Nishibayashi Y. Developing more sustainable processes for ammonia synthesis. *Coord. Chem. Rev*. 2013, **257**(17-18): 2551-2564.

9. Giddey S, Badwal SPS, Kulkarni A. Review of electrochemical ammonia production technologies and materials. *Int. J. Hydrog. Energy* 2013, **38**(34): 14576-14594.

10. Guo X, Zhu Y, Ma T. Lowering reaction temperature: Electrochemical ammonia synthesis by coupling

various electrolytes and catalysts. *J. Energy Chem*. 2017, **26**(6): 1107-1116

11. Chen S, Perathoner S, Ampelli C, Mebrahtu C, Su D, Centi G. Electrocatalytic Synthesis of Ammonia at Room Temperature and Atmospheric Pressure from Water and Nitrogen on a Carbon-Nanotube-Based Electrocatalyst. *Angew. Chemie Int. Ed*. 2017, **56**(10): 2699–2703.

12. Chen S, Perathoner S, Ampelli C, Mebrahtu Asmelash C, Su D, Centi G. Room Temperature Electrocatalytic Synthesis of NH_3 from H_2O and N_2 in a Gas-Liquid-Solid Three-phase Reactor. *ACS Sustainable Chem. & Eng*. 2017, **5**(8): 7393–7400.

13. Kandemir T, Schuster ME, Senyshyn A, Behrens M, Schlögl R. The Haber–Bosch process revisited: on the real structure and stability of "ammonia iron" under working conditions. *Angew. Chemie Int. Ed.* 2013, **52**(48): 12723-12726.

14. Garden AL, Skúlason E. The mechanism of industrial ammonia synthesis revisited: calculations of the role of the associative mechanism. *J. Phys. Chem*. C 2015, **119**(47): 26554-26559.

15. Ouzounidou M, Skodra A, Kokkofitis C, Stoukides M. Catalytic and electrocatalytic synthesis of NH_3 in a H^+ conducting cell by using an industrial Fe catalyst, *Solid State Ionics* 2007, **178**(1-2): 153-159

16. Abghoui Y, Skulason E. Onset potentials for different reaction mechanisms of nitrogen activation to ammonia on transition metal nitride electro-catalysts. *Catal. Today* 2017, **286**: 69-77.

17. Abghoui Y, Skúlason E. Electrochemical synthesis of ammonia via Mars-van Krevelen mechanism on the (111) facets of group III–VII transition metal mononitrides. *Catal. Today* 2017, **286**: 78-84.

18. Wilk B, Pelka R, Arabczyk W. Study of the Iron Catalyst for Ammonia Synthesis by Chemical Potential Programmed Reaction Method. *J. Phys. Chem. C* 2017, **121**(15): 8548-8556.

19. Hoffman BM, Lukoyanov D, Yang Z-Y, Dean DR, Seefeldt LC. Mechanism of nitrogen fixation by nitrogenase: The next stage, *Chem. Rev*. 2014, **114**(8): 4041-4062.

20. Hoffman BM, Lukoyanov D, Dean DR, Seefeldt LC. Nitrogenase: A Draft Mechanism, *Acc. Chem. Res.*

2013, 46(2): 587-595.

21. Arrigo R, Hävecker M, Wrabetz S, Blume R, Lerch M, McGregor J, *et al*. Tuning the acid/base properties of nanocarbons by functionalization via amination. *J. Am. Chem. Soc.* 2010, **132**(28): 9616-9630.

22. Su DS, Perathoner S, Centi G. Nanocarbons for the development of advanced catalysts. *Chem. Rev.* 2013, **113**(8): 5782-5816.

23. Su DS, Zhang J, Frank B, Thomas A, Wang X, Paraknowitsch J, et al. Metal-Free Heterogeneous Catalysis for Sustainable Chemistry. *ChemSusChem* 2010, **3**(2): 169-180.

CHAPTER 5

5. Synthesis and Characterization of Pincer Complexes for the catalytic NH_3 production

5.1 Introduction

The heterogeneously catalyzed ammonia synthesis (Haber Bosch process) has long been known and is well understood.[1] However, a major challenge for chemistry to move to a more sustainable, low-carbon future is to avoid the need of using fossil fuels to supply the energy to drive chemical processes, which accounts for the largest part of carbon dioxide emissions. Synthetic homogeneous catalysts designed for N_2 reduction provide well-defined molecular precatalysts and intermediates, which can be thoroughly characterized by diverse spectroscopic techniques and thereby provide opportunities for developing a new technology for ammonia production, and also a more determining mechanistic information about N_2 reduction to NH_3.[2] The reactivity of synthetic inorganic complexes offers insights into molecular reactivity and individual bondings pattern that contribute to the activation of the triple bond of N_2. Significant efforts have been made to prepare NH_3 catalytically under mild conditions using a transition metal complex, since the discovery of nitrogenase, along with a transition metal compound that contains N_2 bound to ruthenium.[3] A well-defined Mo-containing catalyst was reported for catalytic reduction of N_2 to NH_3 by H^+ and e^- (provided by electrode)[4] Eight of these proposed intermediates were prepared and characterized, which supported a mechanism involving the addition of $6H^+$ and $6e^-$ to the N_2 initially bound to a Mo^{3+} center. Other Mo pre-catalysts for reduction of N_2 using chemical reductants and an acid-a dimolybdenum-dinitrogen complex [5] and a molybdenum nitride [6] - were subsequently reported in 2011 and 2015, respectively. Fe complexes were also reported that catalyze reduction of N_2 to NH_3 using a strong reducing agent (KC_8) and a strong acid at 200 K.[7] In all cases, N_2 reduction is accompanied by production of H_2, this has been shown to involve a catalytic process,

with H^+ reduction competing with N_2 reduction. More work remains to move this field forward.

5.2 The scope of this chapter

Hölscher et al. have shown by means of DFT (Density Functional Theory) calculations that POP–Ru pincer complexes (POP = 2,5-bis(dimethylphosphanylmethyl)furan and 2,6-bis(dimethylphosphanylmethyl)-g-pyran) can be used to generate computationally derived closed catalytic cycles for the synthesis of NH_3 from N_2 and H_2 with appreciably low activation barriers. [8] In this chapter, the related complexes comprising similar structural with the calculated data were investigated. The data provided a possibility to compare the two technology roadmaps for sustainable ammonia synthesis. (Electrochemical ammonia synthesis; homogenous catalytic ammonia synthesis)

5.3 Complex synthesis and identify

General: All reactions were performed under Ar, H_2, or N_2 atmospheres using Schlenk or glove-box techniques. Solvents and substrates were purchased from Aldrich, Acros, and Strem and were purified according to standard procedures. [9]

Preparation of 2,6-Bis[(di-tert-butylphosphanyl)methyl]pyridine (1)

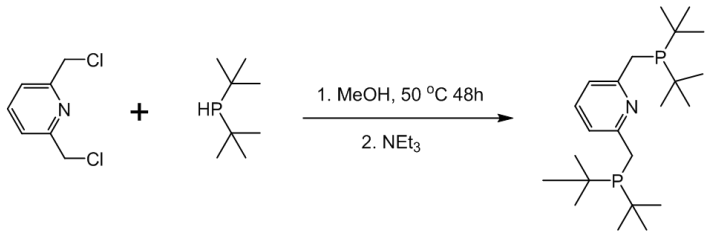

1

This reaction was performed in a schlenk bottle under Argon. Firstly, 2,6-bis(chloromethyl)-pyridine (440.1 mg, 2.5 mmol) was suspended in 5 mL of methanol; secondly, 913.8 mg of di-tert-butylphosphine (2.5 mmol) was added to the suspension

dropwise. The mixture was then heated to 50 ºC and kept at the temperature for 48 hours. After that, the mixture was cooled to room temperature. Then 1 mL of degased triethylamine (NEt_3) was added dropwise, and a white precipitant was observed. The precipitant was filtered and washed with degas water for two times, and MeCN for two times. After the purification process, the remaining solvent was evaporated under vacuum. The white powder was obtained and identified with NMR (300 MHz, in CD_2Cl_2, 25 ºC) .^{31}P NMR (122 MHz, in CD_2Cl_2, 25 ºC): δ = 35.60 ppm; the proton number and chemical shift were in accordance with values reported in the literature.[10]

Preparation of (OC-6-31)-[2,6-Bis[[bis(tert-butyl)phosphino-κP]methyl]pyridine-κN]trichloromolybdenum (2)

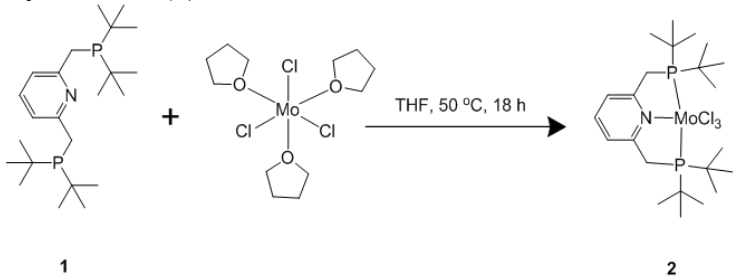

The reaction was performed in a schlenk bottle under argon. Firstly, 201 mg of molybdenum complex [$MoCl_3(thf)_3$] (0.480 mmol) was suspended in 6 mL of THF; then 200mg of **1** (0.506 mmol) was added to the mixture dropwise. The mixture was then heated to 50 ºC and kept for 18 hours. Then the mixture was cooled to room temperature. The solvent was evaporated under vacuum, and an orange precipitant was obtained. The precipitant was dissolved in 5 mL of methylene chloride (CH_2Cl_2), and 10 mL of hexane was slowly added to the solution to the extract the product. Orange crystal precipitated in the hexane layer. The precipitant was filtered and washed with ether (Et_2O) for two times. After the purification process, the remaining solvent was evaporated under vacuum. An orange powder was obtained, and identified with ^{1}H NMR (300 MHz, in CD_2Cl_2, 25 ºC) and ^{31}P NMR (122 MHz, in CD_2Cl_2, 25 ºC). Due the paramagnetism of this complex, the ^{1}H NMR spectrum cannot give any useful

information, but the ^{31}P NMR (122 MHz, in CD_2Cl_2, 25 °C) showed one single peakat a chemical shift of δ=66.47 ppm which is different from value of the free ligand (δ = 35.60 ppm), which is in accordance with a previous report [5].

^{31}P NMR (122 MHz, in CD_2Cl_2, 25 °C): δ = 66.47 ppm.

Preparation of [2, 6-Bis[[bis(tert-butyl)phosphino]methyl]pyridine]dichlororuthenium (3)

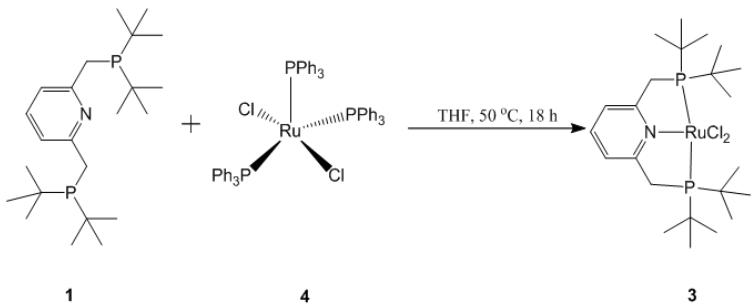

The reaction was performed in a schlenk bottle under Argon. Firstly, 300 mg of **1** was suspended with 15 mL of THF; secondly, 726 mg of $[RuCl_2(PPh_3)_3]$ (**4**) was added to the suspension. The mixture was then heated to 50 °C and kept for 12 hours. Then the mixture was cooled to room temperature. And the solvent was concentrated to 1 mL under vacuum, and 10 mL of hexane was slowly added to the solution to the extract the product. Orange crystal precipitation was formed in the hexane layer. The precipitant was filtered and washed with 5 mL Ether (Et_2O) for two times. After the purification process, the remaining solvent was evaporated under vacuum. An orange powder was obtained, and identified with ^{1}H NMR (300 MHz, in CD_2Cl_2, 25 °C) and ^{31}P NMR (122 MHz, in CD_2Cl_2, 25 °C). This results are in accordance with a previous report [11].

^{1}H NMR (300 MHz, in CD_2Cl_2, 25 °C): δ = 1.08 (s, 36H, 2×$P(C(CH_3)_3)_2$), δ = 4.12 (t, 4H, CH_2P), δ = 7.42 (d, 2H, pyridine-H3, 5), δ = 7.17 Hz, (t, 1H, pyridine-H4) ppm.

^{31}P NMR (122 MHz, in CD_2Cl_2, 25 °C): δ = 42.07 ppm.

Preparation of reduced [2, 6-Bis[[bis(tert-butyl)phosphino]methyl]pyridine]dichlororuthenium (5)

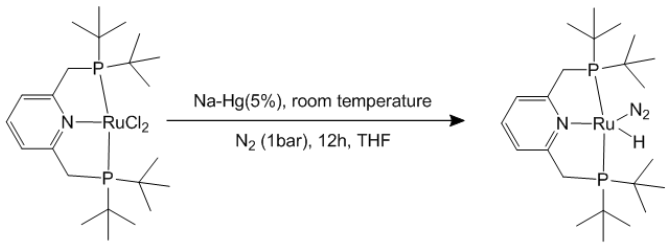

The reaction was performed in a schlenk bottle under argon. Firstly, an extra amount of Na–Hg (5 wt%, 440 mg, 0.44 mmol) was suspended in 3 mL of THF; secondly, 726 mg of **3** (50 mg, 0.088 mmol) were added to the suspension. The mixture was then stirred at room temperature for 24 h under N_2 (1 bar). Then the mixture was filtered with celite to remove the extra Na-Hg and the celite was washed with THF to collect the absorbed samples. All the filtrate was collected and the solvent was evaporated under vacuum. An orange powder was obtained and identified and ^{31}P NMR (122 MHz, in CD_2Cl_2, 25 ^oC) show single intense peak on the chemical shift of δ = 73.32 ppm, which is different from the value of the free ligand (δ = 35.60 ppm) and the free ligand that after treatment with H_2O_2 (δ = 61.56 ppm).

^{31}P NMR (122 MHz, in CD_2Cl_2, 25 ^oC): δ = 73.32 ppm.

Preparation of [2, 6-Bis[[bis(tert-butyl)phosphino]methyl]pyridine]dichloro osmium (6)

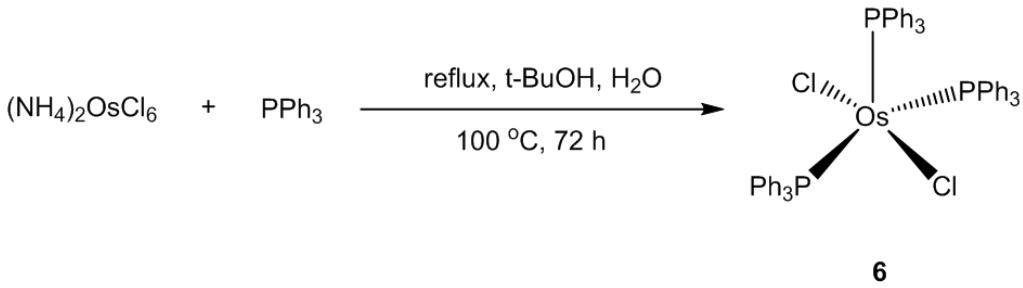

The reaction was performed in 1 L round-bottomed flask equipped with a Graham condenser. 1.0 g of ammonium hexachloroosmate(IV) [$(NH_4)_2OsCl_6$] was dissolved in 300 mL t-BuOH and water ($V_{t\text{-}BuOH}$:V_{H2O} =1:1). The mixture was heated to 100 °C and kept for 72 hours. After the reaction, the mixture was cooled to room temperature, and a green solid was obtained. The precipitant was filtered and washed with 20 mL degased water for three times, 20 mL of MeOH for three times and 20 mL of hexane for three times. After the purification process, the remaining solvent was evaporated under vacuum. A green powder was obtained ^{31}P NMR (122 MHz, in CD_2Cl_2, 25 ºC) which showed an intense peak at a chemical shift of δ= -3.88 ppm, (compare with the free ligand PPh_3 δ = -5.58 ppm). According to the NMR spectra, there was still around 12.5% free PPh_3 in the mixture. This can be removed by prolonged stirring under hexane at room temperature. This results are in accordance with a previous report [12].

^{31}P NMR (122 MHz, in CD_2Cl_2, 25 ºC): δ = -3.88 ppm.

Commercial available complexes were tested for ammonia synthesis.

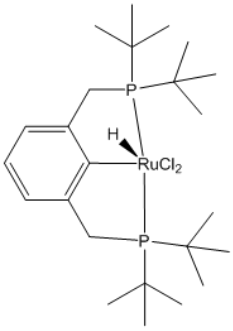

7

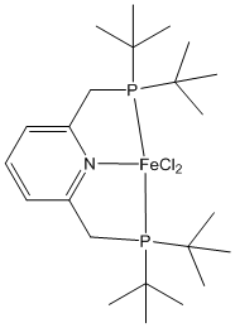

8

5.4 Performance test for ammonia synthesis of homogenous catalysts

5.4.1.Reaction condition and ammonia detection

Reaction condition: A 10 mL autoclave which can withstand a maximum pressure of 250 bar at 100 ºC was used for the catalytic performance test. The reaction was performed using the following procedures: firstly, 0.01 mmol of catalyst was added into

the tube for the autoclave in the glove box; secondly, the autoclave was closed and taken out from the glove box; thirdly, the autoclave was connected with pressured nitrogen line; fourthly, the N_2 pressure was increased to 3 bar and then released. This gas charge and release cycle was repeated for 3 times in order to remove the Argon in the autoclave; fifthly, the solvent and co-catalyst were injected under the protection of N_2; sixthly, the autoclave was pressured with nitrogen and hydrogen till the total pressure of 50 bar (the percentage of nitrogen and hydrogen was optimized); seventhly, the autoclave was heated to 100 °C for 24 hours; eighthly, the autoclave was cooled to room temperature for ammonia detection.

Ammonia detection: First of all, the pressured gas mixture was smoothly released to an absorber with fixed volume of dilute H_2SO_4; secondly, the inside tube was taken out smoothly after the autoclave was de-pressured to atmosphere; thirdly, an extra amount of sodium hydroxide was added into the tube; Fourthly, a rubber stopper was used to close the tube, and Argon was introduce though the tube, cold trap and finally arrive the absorber as shown in Scheme 1 ; Fifthly, the tube was heated slowly to avoid the significant pressure change in the system; finally, the ammonia in both of the absorber was quantified with spectrophotometry with salicylic acid methods, as described in **chapter 2.**

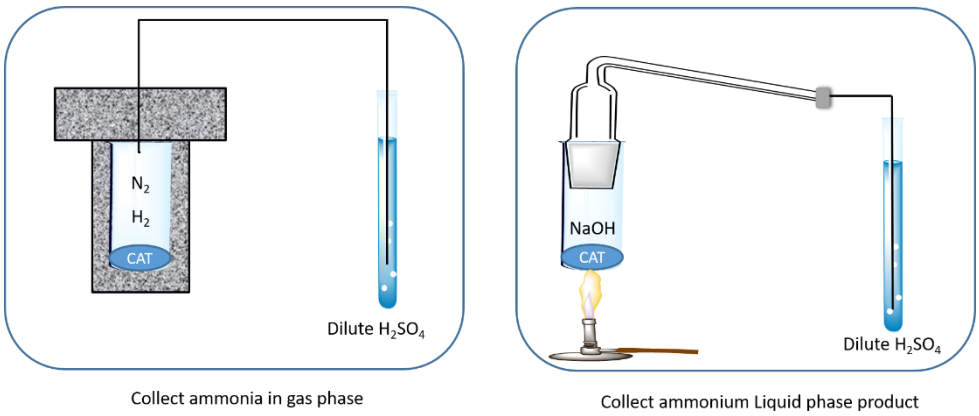

Scheme1. *Scheme view of collection of as-produced ammonia*

5.4.2. Reaction results

Blank tests were performed four independent times under the same conditions, as shown in ***Table 4.*** The average ammonia production was 0.169×10^{-3} mmol, and its standard deviation was 0.0091. This indicated that the system for ammonia synthesis was reliable and the data was reproducible. **Complex 3** was tested in various condtions. In the beginning, 0.01mmol of **3** was tested without solvent, there was 1.75×10^{-3} mmol of ammonia detected, which was about 10 times higher than the blank test. It means that **3** could accelerate the reaction of nitrogen and hydrogen to ammonia. Howerer, the conversion of H_2 was only 0.033%. Toluene, THF, and MeOH were added to the system as solvent to increase the dispersion of the catalysts. The best result was observed when MeOH was used as the solvent. This might be related to the fact that MeOH can provide hydrogen for the reaction. Next, the composition of the gas mixture was optimized. The total gas pressure was 50 bar, and three independent reactions with P_{N2}: P_{H2}=4:1, P_{N2}: P_{H2}=1:1 and P_{N2}: P_{H2}=1:4 were tested. The best result was observed with P_{N2}: P_{H2}=4:1. It is necessary to notice that almost the ammonia production was almost same with the blank test when the gas composition was N_2 10bar H_2 40bar, it indicates that the activation of hydrogen was not the rate limitating step for the reaction when **3** was used as catalyst. Acetic acid was used as co-catalyst for this reaction; 10 μL, 50 μL,100 μL and 500 μL of acetic acid were added to the reaction mixture at the same time with the solvent. It was found that when 10 μL acetic acid were added, the amount of ammonia formed was almost not affected; when 50 μL acetic acid was added, the amount of ammonia formed was increased by 40% compared to the result with no acetic acid; when the amount of acetic acid was increased futher, the ammonia formation decreased repidly. Futhermore, the **4** was tested in the same conditions, and the rate of ammonia formation was similar with **3**, which further confirmed the hypothesis that the activation of hydrogen was not the rate limitating step. Some other commercial complexes, such as **7** and **4** were also tested with the same conditions, and lower amount of ammonia

formed compared to **3**.

Table 4: *Catalytic performance summary with various homogenous catalysts*

Catalyst	**Solvent**	**N_2 (bar)**	**H_2 (bar)**	**Co-catalyst**	**Ammonia ($\times 10^{-3}$ mmol)**
Blank	-	40	10	-	0.178
	-	40	10	-	0.169
	-	40	10	-	0.156
	-	40	10	-	0.170
Complex 2	Toluene	40	10	-	0.55
	Toluene	25	25	$CoCp_2$	0.95
	Toluene	50	2,6-Lutidinium triflate (0.1 mol)	$CoCp_2$	0.83
Complex 3	-	40	10	-	1.75
	Toluene	40	10	-	1.46
	Toluene	25	25	-	1.43
	Toluene	10	40	-	0.15
	Toluene	40	10	AcOH 10µL	1.35
	Toluene	40	10	AcOH 50µL	2.05
	Toluene	40	10	AcOH 100µL	0.32
	Toluene	40	10	AcOH 500µL	0.01
	THF	40	10	-	1.39
	MeOH	40	10	-	1.78
Complex 4	Toluene	40	10	-	1.05
Complex 5	Toluene	40	10	-	1.38
Complex 6	Toluene	40	10	-	0.38
Complex 7	Toluene	40	10	-	0.78
Complex 8	Toluene	40	10	-	0.43
Catalyst loading: 0.01 mmol; **Reaction temperature:** 100°C; **Reaction time:** 20 hours; **Solvent volume:** 1 mL; **Autoclave volume:** 10 mL; 10 bar ≈ 4 mmol					

5.5 Conclusion

This is a preliminary study of the ammonia synthesis with homogenous catalysts. Some simple complexes were synthesized and identified. The reaction procedure and product detection methods were developed and optimized. A series of ruthenium complexes, were tested using the same conditions. **Ru(PNP)Cl_2** (PNP: 2,6-Bis[(di-tert-butylphosphanyl)methyl]pyridine) was found to be the best catalyts for ammonia synthesis among this series complex. It was also tested using different conditions, it was found that suitable amounts of acetic acid can incease its catalytic performance. Comparing different compositions of nitrogen and hydrogen loading, it was found that the ammonia formation rate increases with increasing nitrogen loading, from which we can deduce that activation of hydrogen was not the rate limitation step in this conditions.

Compared to electrochemical ammonia synthesis, the ammonia formation rate was around 1-2 magnitude orders of higher using homegenous catalyst. However, the reaction was performed with hydrogen pressure at 100 ^{o}C, instead of water at room termperature for electrochemical ammonia synthesis. Even though the price–performance ratio was lower using homogenous catalyst, it provides intersting possibility to study the mechanism of nitrogen activation.

5.6 Reference

1. Schlögl, R. (2003). Catalytic Synthesis of Ammonia—A “Never-Ending Story”?. *Angewandte Chemie International Edition*, *42*(18), 2004-2008.
2. Haggin, J. (1993). Chemists seek greater recognition for catalysis. Chemical and Engineering News;(United States), 71(22).
3. Allen, A. D., & Senoff, C. V. (1965). Nitrogenopentammineruthenium (II) complexes. *Chemical Communications (London)*, (24), 621-622.
4. Yandulov, D. V., & Schrock, R. R. (2003). Catalytic reduction of dinitrogen to ammonia at a single molybdenum center. *Science*, *301*(5629), 76-78.

5. Arashiba, K., Miyake, Y., & Nishibayashi, Y. (2011). A molybdenum complex bearing PNP-type pincer ligands leads to the catalytic reduction of dinitrogen into ammonia. *Nature chemistry*, *3*(2), 120-125.
6. Arashiba, K., Kinoshita, E., Kuriyama, S., Eizawa, A., Nakajima, K., Tanaka, H., Yoshizawa, K. & Nishibayashi, Y. (2015). Catalytic reduction of dinitrogen to ammonia by use of molybdenum–nitride complexes bearing a tridentate triphosphine as catalysts. *Journal of the American Chemical Society*, *137*(17), 5666-5669.
7. Anderson, J. S., Rittle, J., & Peters, J. C. (2013). Catalytic conversion of nitrogen to ammonia by an iron model complex. *Nature*, *501*(7465), 84.
8. Hölscher, M., Prechtl, M. H., & Leitner, W. (2007). Can [M(H)2(H2)(PXP)] pincer complexes (M= Fe, Ru, Os; X= N, O, S) serve as catalyst lead structures for NH3 synthesis from N_2 and H_2?. Chemistry–A European Journal, 13(23), 6636-6643.]
9. D. D. Perrin, W. L. F. Armarego, Purification of Laboratory Chemicals, Pergamon Press, London.
10. Kawatsura, M., & Hartwig, J. F. (2001). Transition metal-catalyzed addition of amines to acrylic acid derivatives. A high-throughput method for evaluating hydroamination of primary and secondary alkylamines. *Organometallics*, *20*(10), 1960-1964.
11. Zhang, J., Gandelman, M., Shimon, L. J., Rozenberg, H., & Milstein, D. (2004). Electron-rich, bulky ruthenium PNP-type complexes. Acceptorless catalytic alcohol dehydrogenation. *Organometallics*, *23*(17), 4026-4033.
12. Hoffman, P. R., & Caulton, K. G. (1975). Solution structure and dynamics of five-coordinate d6 complexes. *Journal of the American Chemical Society*, *97*(15), 4221-4228.

CHAPTER 6

General conclusion and outlooks

The present Ph.D thesis was focused on the development of advanced technic for ammonia synthesis with sustainable methods. Ammonia synthesis is the largest-scale chemical process with the higher impact on greenhouse gas emissions, about 350 Mt CO_2 emissions worldwide. This value could be decreased by over 90% in a direct electrocatalytic process using N_2, H_2O and renewable energy as input sources. In fact, CO_2 emissions are 1.83 t_{CO2}/t_{NH3} in the actual ammonia production scheme (via natural gas steam reforming followed by NH_3 synthesis), while the total footprint of the direct electrocatalytic route could be estimated in 0.12 t_{CO2eq}/t_{NH3}. Implementing this technology will thus result in a breakthrough change towards a sustainable, low-carbon chemical production based on the use of renewable energy sources. There is thus a rising interest in fossil-fuel-free direct ammonia synthesis.

In **Chapter 2**, we have shown here the possibility to realize the synthesis of ammonia under very mild conditions (room temperature and ambient pressure) starting from H_2O and N_2, and using electrical energy which could be provided from renewable energy sources, fully in line with the requirement to move to a "solar-driven chemistry" not based on the use of fossil fuels, with consequent decrease of the greenhouse gases emissions. Present data represent a breakthrough on the type of electrocatalysts used, but also contain the elements to indicate an expected further progress. We thus believe that these results could open a new direction in the development of systems for the electrocatalytic synthesis of ammonia from H_2O and N_2.

In **Chapter 3**, present data evidence that 30% Fe_2O_3-CNT is the best electrocatalyst among iron based catalysts supported on carbon nanotubes. The performances greatly depend on the cell design, where the possibility of ammonia crossover through the membrane has to be inhibited. The reaction conditions also play a significant role. When an acid is used as electrolyte, the current density is determined by proton concentration but if a base is used as electrolyte, the water transport determines the current density. The electrolyte (type, pH, concentration) plays a critical role on the selectivity of ammonia, but does not influences greatly the ammonia formation rate. A complex effect

of the applied voltage was observed. An excellent stability was found for an applied voltage -1.0 V vs. Ag/AgCl. At higher negative applied voltages, the ammonia formation rate and Faradaic selectivity are higher, but with a change of the catalytic performances, although the current densities remain constant for at least 24h of experiments. This effect is interpreted in terms of reduction of the iron-oxide species above a negative voltage threshold, which enhances the side reaction of H^+/e^- recombination to generate H_2 rather than their use to reduce activated N_2 species, possibly located at the interface between iron-oxide and functionalized CNT.

In **Chapter 4,** the linear relationships between ammonia formation rate and the amount of O1(Fe-O-Fe) species detected by XPS, which are related to O^{2-} in Fe_2O_3 or FeOOH species, was confirmed by both chemical reduced samples (i.e. Fe-CNT, Fe_2N-CNT) and electrochemical activated Fe_2O_3-CNT (i.e. by in-situ activation at -2.0V vs. Ag/AgCl vs. Ag/AgCl). This indicated that the O1 (Fe-O-Fe) species are associated with the active site for ammonia electrochemical synthesis. Furthermore, only small iron-oxide particles that strongly interacted with CNT, showed the significant increased ability for ammonia synthesis comparing to the bulk iron oxide. This is due to the small iron oxide partials that are sitting at the defect or functional groups of carbon (i.e. with charge density different from bulk iron oxide). An in-situ activation at -2.0V vs. Ag/AgCl for Fe_2O_3-CNT, leading to the reconstruction of bulk iron-oxide particles and creating more defect sites on CNT, give enhanced formation of the interface between iron-oxide nanoparticles and (defective) carbon, with a significant increase in the ammonia formation rate. These results thus provide new insights about the nature of the active sites for NH_3 synthesis from N_2 and H_2O at ambient temperature/pressure, which are significantly different from the industrial Haber-Bosch catalysts.

In **Chapter 5**, preliminary studies of the ammonia synthesis with homogenous catalysts were conducted. Some simple complexes were synthesized and characterized. The reaction procedure and product detection methods were developed and optimized. A series of ruthenium complexes were tested under the same condition. **Ru(PNP)Cl_2** (PNP: 2,6-Bis[(di-tert-butylphosphanyl)methyl]pyridine) was found to be the best catalyst for ammonia synthesis among this series complexes. It was also tested with

different conditions, it was found that a suitable amount of acetic acid can increase its catalytic performance. Comparing different compositions of nitrogen and hydrogen pressure, it was found that the ammonia formation increases with increasing nitrogen pressure, from which we can deduce that activation of hydrogen was not the rate limiting step under this conditions.

Comparing with electrochemical ammonia synthesis, the ammonia formation rate was around 1-2 magnitude orders of higher with the homogenous catalysts. However, the reaction was performed with hydrogen pressure at 100 ^{o}C, instead of water at room temperature for electrochemical ammonia synthesis, the price–performance ratio was lower. The reaction with homogenous catalyst provides interesting possibilities to study the mechanism of nitrogen activation.

PERSONAL INFORMATION

Shiming Chen

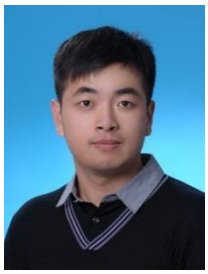

Ingegneria e Chimica dei Materiali e delle Costruzioni

+39 3426192115 +86-18642011966

schen@unime.it
kxxmaqq@gmail.com

Sex Male | Date of birth 24/12/1989 | Nationality Chinese

EDUCATION AND TRAINING

November 2015 - Present

Ph.D. (SINCHEM-Erasmus Mundus Joint Doctorate Program) at:

Dep't of Engineering University of Messina: Home University

ITMC RWTH Aachen University: Host University

2012-2015

Master Degree

Institute of Metal Research, Chinese Academy of Science

- Thesis Title *'The Research of Carbon-based Solid Base Catalyst '*, which is part of the national natural foundation project *' Controlled Synthesis, Structure and Application of Carbon Nanomaterials '* .
- Grasp the skills of digging problems in the whole experimental process, then do the research about current scientific situation in related field and finally solve the problems.
- Gain more experimental skills and be able to conduct the research under tutor's guidance

2008-2012

Bachelor of Science in Chemistry

Jilin University in China

- Basic theory of Math, Physics
- Inorganic Chemistry, Analytical Chemistry (including Instrumental Analysis), Organic Chemistry, Physical Chemistry (including Structural Chemistry), Chemistry Engineering
- A good command of basic experimental skills and basic theory of chemical engineering cartography

PUBLICATIONS

1. **Chen, S.,** Perathoner, S., Ampelli, C., Mebrahtu, C., Su, D., & Centi, G. (2017). Electrocatalytic Synthesis of Ammonia at Room Temperature and Atmospheric Pressure from Water and Nitrogen on a Carbon-Nanotube-Based Electrocatalyst. *Angewandte Chemie International Edition*, *56*(10), 2699-2703.
2. **Chen, S.,** Perathoner, S., Ampelli, C., Mebrahtu, C., Su, D., & Centi, G. (2017). Room-Temperature Electrocatalytic Synthesis of NH3 from H2O and N2 in a Gas–Liquid–Solid Three-Phase

Reactor. *ACS Sustainable Chemistry & Engineering*, *5*(8), 7393-7400.

3.**Chen, S.,** Perathoner, S., Ampelli, C., Mebrahtu Asmelash, C., Su, D., & Centi, G Active species and their dynamic during the electrocatalytic ambient temperature/pressure direct synthesis of ammonia from N2 and H2O over iron nanoparticles on CNTs (To be submitted)

4. Perathoner, S., Ampelli, C., **Chen, S**., Passalacqua, R., Su, D., & Centi, G. (2017). Photoactive materials based on semiconducting nanocarbons–a challenge opening new possibilities for photocatalysis. *Journal of energy chemistry*, *26*(2), 207-218.

5.Mebrahtu, C., Abate, S., Perathoner, **S., Chen,** S., & Centi, G. (2018). CO2 methanation over Ni catalysts based on ternary and quaternary mixed oxide: A comparison and analysis of the structure-activity relationships. *Catalysis Today*, *304*, 181-189.

6.Mebrahtu, C., Abate, S., **Chen, S.,** Sierra Salazar, A. F., Perathoner, S., Krebs, F., ... & Centi, G. (2018). Enhanced Catalytic Activity of Iron-Promoted Nickel on γ-Al2O3 Nanosheets for Carbon Dioxide Methanation. *Energy Technology*, *6*(6), 1196-1207.

7. (book Chapter) Chen, S., Perathoner, S., Ampelli, C., Mebrahtu Asmelash, C., Su, D., & Centi, G Horizons in Sustainable Industrial Chemistry and Catalysis, Chapter 2: Electrochemical Nitrogen activation.

Conference and Seminars

1.3rd SINCHEM Winter School, February,15h–17th,2016, Bologna, Italy. (**oral presentation**)

2.Carbon for Catalysis: CarboCat-VII Symposium, June 12th to June 16th, 2016 Strasbourg, France.(**Poster**)

3.4th International Conference Tailor-Made Fuels from Biomass, June 21st – 23rd, 2016, Aachen, German.

4.16th International Congress on Catalysis, 03 July 2016 to 08 July 2016, Beijing，China. (**Poster**)

5.SINCHEM Autumn School, November 30th- December 1st, 2016 Lyon, France. (**oral presentation**)

6.Green Chemistry Horizon Programme - SINCHEM Winter School, February, 2nd–3rd, 2017, Aachen, German. (**oral presentation)**

7.25th North American Catalysis Society Meeting, June 4th - 9th, 2017. Denver, CO, the USA. (**Oral presentation**)

8.13th European Catalysis Congress, August 27th -31st, 2017. Florence, Italy. (**oral presentation**)

9.SINCHEM Autumn School, November 22th-24th, 2017 Turin, Italy. (**oral presentation**)

10.4th International Symposium on Chemistry for Energy Conversion and Storage (CHEMENER 2018), January 28th-31st, 2018, Berlin, Germany.

11.The SINCHEM & PHOTOTRAIN WINTER SCHOOL, February 12th-14th, 2018, Bologna, Italy. (**oral presentation**)